The Effect of Tether Groups on the Spin State of Iron(II) Bis[2,6-Di(pyrazolyl)pyridine] Complexes

Izar Capel Berdiell[a,b], Victor García-López[c], Mark J. Howard,[a]
Miguel Clemente-León[c] and Malcolm A. Halcrow*,[a]

[a]*School of Chemistry, University of Leeds, Woodhouse Lane, Leeds LS2 9JT, United Kingdom.*
E-mail: m.a.halcrow@leeds.ac.uk

[b]*Current address: Institute of Electronic Structure and Laser, Foundation for Research and Technology - Hellas, P.O. Box 1527, GR-711 10 Heraklion, Greece.*

[c]*Instituto de Ciencia Molecular, Universidad de Valencia, Catedrático José Beltrán 2, 46980, Spain.*

Supporting Information

Ligand synthesis

The precursors 2,6-di(pyrazol-1-yl)pyridine-4-carboxylic acid[1] and 4-hydroxymethyl-2,6-di(pyrazol-1-yl)pyridine[2] were synthesised by the literature procedures. Other reagents were purchased commercially and used as supplied.

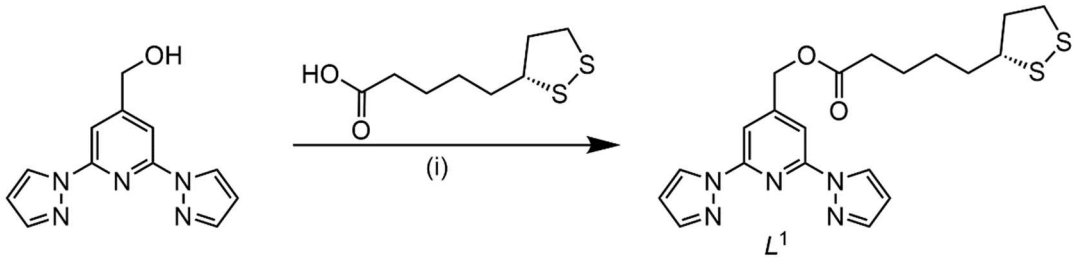

Scheme S1 Synthesis of L^1. Reagents and conditions: (i) 4-dimethylaminopyridine, *N*,*N*-dicyclohexyl carbodiimide, dichloromethane, 0 °C → room temperature.

Synthesis of [2,6-di(pyrazol-1-yl)pyrid-4-yl]methyl (*R*)-lipoate (L^1). 4-Hydroxymethyl-2,6-di(pyrazol-1-yl)pyridine (0.23 g, 1.0 mmol), (*R*)-lipoic acid (0.30 g, 1.4 mmol) and 4-dimethylamino-pyridine (0.044 g, 0.28 mmol) were mixed in dry dichloromethane (70 cm^3) at 0 °C. A solution of *N*,*N*-dicyclohexyl carbodiimide (0.44 g, 2.1 mmol) in dry dichloromethane (15 cm^3) was added dropwise to the cooled suspension over a period of 30 mins. After stirring for a further 30 mins at 0 °C, the mixture was warmed to room temperature and stirred for a further 18 hrs. The suspension was filtered, and the liquid phase was evaporated to dryness yielding a pale yellow solid. The purified by flash silica column chromatography silica (1:1 hexane:ethyl acetate eluent, R_f 0.68). Yield 0.34 g, 82 %. Mp 62-63 °C. Found: C, 55.9; H, 5.59; N, 16.2 %. Calcd for $C_{20}H_{23}N_5O_2S_2$ C, 55.9; H, 5.40; N, 16.3. ES-MS *m/z* 430.1386 (calcd for $[HL^3]^+$ 430.1371), 452.1191 (calcd for $[NaL^3]^+$ 452.1185), 881.2484 (calcd for $[Na(L^3)_2]^+$ 881.2479). ^{1}H NMR ($CDCl_3$) δ 1.51 (m, 2H), 1.71 (m, 4H), 1.89 (m, 1H), 2.45 (m, 3H), 3.13 (m, 2H – all lipoate CH_2), 3.57 (m, 1H, lipoate C*H*), 5.23 (s, 2H, CH_2O), 6.49 (dd, 1.7 and 2.5 Hz, 2H, pz H^4), 7.76 (d, 1.7 Hz, 2H, pz H^3), 7.81 (s, 2H, py $H^{3/5}$), 8.55 (d, 2.5 Hz, 2H, pz H^5) ppm. ^{13}C NMR ($CDCl_3$) δ 24.6, 28.7, 33.8, 34.5, 38.4, 40.1 (all 1C, lipoate CH_2), 56.2 (1C, lipoate *C*H), 64.1 (1C, CH_2O), 107.3 (2C, py $C^{3/5}$), 108.1 (2C, pz C^4), 127.1 (2C, pz C^5), 142.4 (2C, pz C^3), 150.3 (2C, py $C^{2/6}$), 151.3 (1C, py C^4), 172.8 (1C, CO_2) ppm.

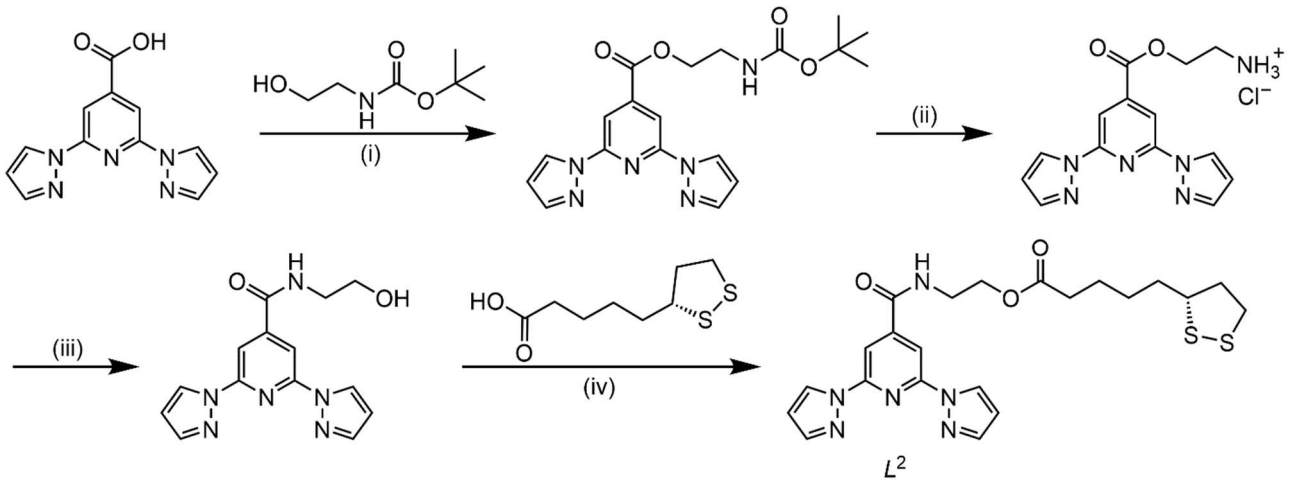

Scheme S2 Synthesis of L^2. Reagents and conditions: (iv) 4-dimethylaminopyridine, *N*,*N*-dicyclohexyl carbodiimide, dichloromethane, 0 °C → room temperature→reflux; (ii) acyl chloride, methanol, 0 °C → room temperature; (iii) water, dmso, reflux then Na_2CO_3, room temperature; (iv) 4-dimethyl-aminopyridine, *N*,*N*-dicyclohexyl carbodiimide, dichloromethane, 0 °C → room temperature.

Synthesis of *N*-BOC-2-aminoethyl [2,6-di(pyrazol-1-yl)pyrid-4-yl]carboxylate. 4-Dimethylamino-pyridine (0.27 g, 1.8 mmol), *N*-BOC-2-ethanolamine (1.60 g, 9.93 mmol) and 2,6-di(pyrazol-1-yl)pyridine-4-carboxylic acid (2.00 g, 7.84 mmol) were mixed in dry dichloromethane (150 cm^3). and the mixture was stirred at 0 °C for 5 minutes. A solution of *N*,*N*-dicyclohexyl carbodiimide (2.39 g, 11.6 mmol) dissolved in dry dichloromethane (100 cm^3) was then added dropwise. The resultant mixture was stirred for 30 mins at 0 °C, then for 6 hrs at room temperature, then for 3 hrs under reflux. The cooled suspension was filtered and the filtrate was evaporated to dryness. The residue was purified by flash silica column chromatography (1:4 hexane:ethyl acetate eluent, R_f 0.9). Yield 2.0 g, 65 %. Mp 146-147 °C. ES-MS *m/z* 421.1596 (calcd for $[NaL]^+$ 421.1600), 819.3298 (calcd for $[NaL_2]^+$ 819.3303). ^{1}H NMR ($CDCl_3$) δ 1.45 (s, 9H, C{C*H*$_3$}$_3$), 3.58 (pseudo-q, 5.2 Hz, 2H, C*H*$_2$N), 4.48 (t, J = 6.4 Hz, 2H, C*H*$_2$O), 4.98 (br s, 1H, N*H*), 6.54 (pseudo-t, 1.9 Hz, 2H, pz *H*^{4}), 7.81 (s, 2H, pz *H*^{3}), 8.39 (s, 2H, py *H*$^{3/5}$), 8.58 (d, 2.6 Hz, 2H, pz *H*^{5}) ppm. ^{13}C NMR ($CDCl_3$) δ 28.4 (3C, C{*C*H$_3$}$_3$), 39.6 (*C*H$_2$N), 65.6 (*C*H$_2$O), 79.8 (1C, *C*{CH$_3$}$_3$), 108.5 (2C, pz *C*^{4}), 109.2 (2C, py *C*$^{3/5}$), 127.2 (2C, pz *C*^{5}), 142.9 (2C, pz *C*^{3}), 143.0 (1C, py *C*^{4}), 150.8 (2C, py *C*$^{2/6}$), 155.8 (N*C*O$_2$), 163.9 (py*C*O$_2$) ppm.

Synthesis of 2-aminoethyl [2,6-di(pyrazol-1-yl)pyrid-4-yl]carboxylate hydrochloride. Acyl chloride, (14 cm^3) was added dropwise to methanol (140 cm^3) at 0 °C, and the mixture was then stirred for 50 min. *N*-BOC-2-aminoethyl [2,6-di(pyrazol-1-yl)pyrid-4-yl]carboxylate (1.60 g, 4.02 mmol) was then added, and the mixture was for 16 hrs at room temperature. The resultant white precipitate was collected by filtration, dried and analysed without further purification. Yield 1.3 g, 98 %. ES-MS *m/z* 299.1268 (calcd for $[HL]^+$ 299.1256). ^{1}H NMR ({CD$_3$}$_2$SO) δ 3.29 (m, 2H, C*H*$_2$N), 4.61 (t, 6.2 Hz, 2H, C*H*$_2$O), 6.69 (dd, 1.8 and 2.6 Hz, 2H, pz *H*^{4}), 7.94 (d, 1.8 Hz, 2H, pz *H*^{3}), 8.29 (s, 2H, py *H*$^{3/5}$), 8.40 (br s, 3H, N*H*^{3}), 9.03 (d, 2.6 Hz, 2H, pz *H*^{5}) ppm. ^{13}C NMR ({CD$_3$}$_2$SO) δ 37.7 (1C, *C*H$_2$N), 62.7 (1C, *C*H$_2$O), 108.3 (2C, pz *C*^{4}), 109.0 (2C, py *C*$^{3/5}$), 128.5 (2C, pz *C*^{5}), 142.9 (1C, py *C*^{4}), 143.3 (2C, pz *C*^{3}), 150.3 (2C, py *C*$^{2/6}$), 163.6 (1C, *C*O$_2$) ppm.

Synthesis of 2-hydroxyethyl [2,6-di(pyrazol-1-yl)pyrid-4-yl]carboxamide. 2-Aminoethyl [2,6-di(pyrazol-1-yl)pyrid-4-yl]carboxylate hydrochloride (1.50 g, 4.48 mmol) was suspended in water (100 cm^3) and dimethyl sulfoxide (5 cm^3). The mixture was refluxed for 15 mins until the solid had dissolved to form a yellow solution, then cooled. The solution was neutralised with solid Na_2CO_3, then stirred for a further 1hr at room temperature. A white solid precipitated which was collected by filtration, and dried *in vacuo*. No further purification was required. Yield 0.85 g, 59 % yield. Mp 196-197 °C. ES-MS *m/z* 299.1259 (calcd for $[HL]^+$ 299.1256), 321.1078 (calcd for $[NaL]^+$ 321.1076), 619.2243 (calcd for $[NaL_2]^+$ 619.2254). ^{1}H NMR ({CD$_3$}$_2$SO) δ 3.38, 3.56 (both roofed m, 2H, C*H*$_2$N and C*H*$_2$O), 4.79 (t, 5.7 Hz, 1H, O*H*), 6.67 (dd, 1.7 and 2.6 Hz, 2H, pz *H*^{4}), 7.91 (d, 1.7 Hz, 2H, pz *H*^{3}), 8.22 (s, 2H, py *H*$^{3/5}$), 8.99 (d, 2.6 Hz, 2H, pz *H*^{5}), 9.09 (t, 5.4 Hz, 1H, N*H*) ppm. ^{13}C NMR ({CD$_3$}$_2$SO) δ 42.5 (1C, *C*H$_2$N), 59.4 (1C, *C*H$_2$O), 106.9 (2C, py *C*$^{3/5}$), 108.7 (2C, pz *C*^{4}), 128.3 (2C, pz *C*^{5}), 142.9 (2C, pz *C*^{3}), 147.9 (1C, py *C*^{4}), 150.1 (2C, py *C*$^{2/6}$), 163.5 (1C, *C*ONH) ppm.

Synthesis of 2-[(2,6-di(pyrazol-1-yl)pyridine)-4-carboxamido]ethyl (*R*)-lipoate (*L*^{2}). 2-Hydroxyethyl [2,6-di(pyrazol-1-yl)pyrid-4-yl]carboxamide (0.66 g, 2.2 mmol), (*R*)-lipoic acid (0.46 g, 2.2 mmol) and 4-dimethylaminopyridine (0.067 g, 0.45 mmol) were mixed in dry dichloromethane (75 cm^3) at 0 °C. *N*,*N*-dicyclohexyl carbodiimide (0.53 g, 2.6 mmol) in dry dichloromethane solution (22 cm^3) was added drop by drop to the cooled suspension over half hour. After half hour stirring, the ice bath was removed and the mixture was left stirring overnight at room temperature. The suspension was filtered and the liquid phase was concentrated under vacuum yielding a pale yellow solid. The compound was isolated by eluting through silica gel in 1:1, hexane/ethyl acetate, R_f 0.45 as a pale brown powder. Yield 0.84 g, 77 %. Mp: 124-125 °C. Found: C, 54.5; H, 5.45; N, 17.3 %. Calcd for $C_{22}H_{26}N_6O_3S_2$ C, 54.3; H, 5.39; N, 17.3 %. ES-MS *m/z* 487.1600 (calcd for $[HL^4]^+$ 487.1586), 509.1412 (calcd for $[NaL^4]^+$ 509.1406), 973.3096 (calcd for $[H(L^4)_2]^+$ 973.3094), 995.2920 (calcd for $[Na(L^4)_2]^+$ 995.2913). ^{1}H NMR ($CDCl_3$) δ 1.46 (m, 2H), 1.69 (m, 4H), 1.86 (m, 1H), 2.40 (m, 3H), 3.07 (td, 6.9 and 11.3 Hz, 1H), 3.13 (ddd, 5.4, 7.0 and 11.3 Hz, 1H – all lipoate C*H*$_2$), 3.53 (m, 1H, lipoate C*H*), 3.77 (dd, 5.6 and 10.7 Hz, 2H, C*H*$_2$NH), 4.32 (m, 2H, C*H*$_2$O), 6.51 (dd, 1.7 and 2.5 Hz, 2H, pz *H*^{4}), 6.94 (m, 1H, N*H*), 7.77 (d, 1.7 Hz, 2H, pz *H*^{3}), 8.12 (s, 2H, py *H*$^{3/5}$), 8.52 (d, 2.5 Hz, 2H, pz *H*^{5}) ppm. ^{13}C NMR ($CDCl_3$) δ 24.5, 28.7, 33.9, 34.5, 38.4, 40.1 (all 1C, lipoate *C*H$_2$), 39.7 (1C, *C*H$_2$NH), 56.2 (1C, lipoate *C*H), 62.8 (1C, *C*H$_2$O), 107.0 (2C, py *C*$^{3/5}$), 108.4 (2C, pz *C*^{4}), 127.2 (2C, pz *C*^{5}), 142.8 (2C, pz *C*^{3}), 147.4(1C, py *C*^{4}), 150.7 (2C, py *C*$^{2/6}$), 164.7 (1C, *C*ONH), 173.6 (1C, *C*O$_2$) ppm.

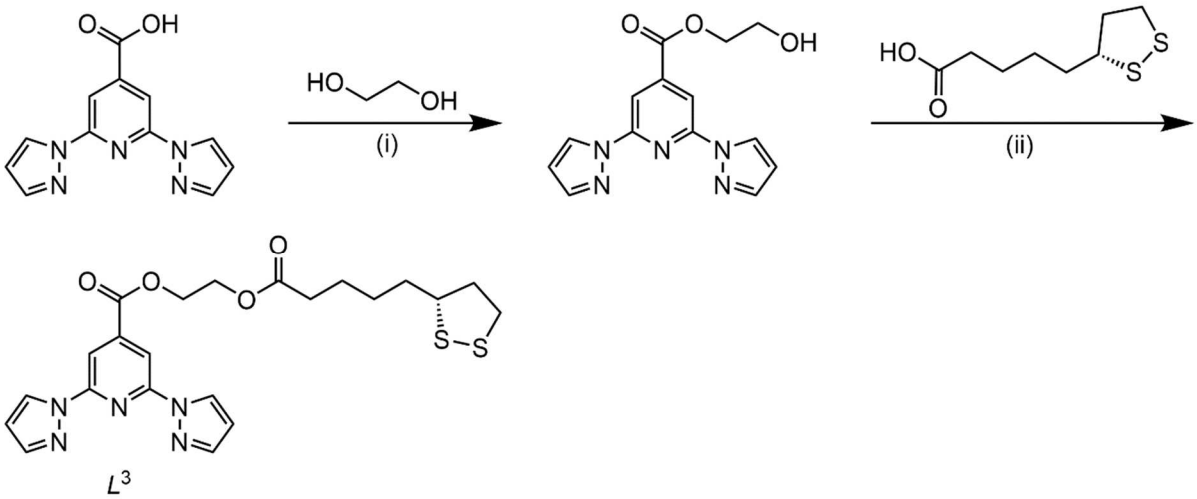

Scheme S3 Synthesis of L^3. Reagents and conditions: (i) cat H_2SO_4, 120 °C; (ii) 4-dimethylamino-pyridine, *N*,*N*-dicyclohexyl carbodiimide, dichloromethane, 0 °C → room temperature.

Synthesis of 2-hydroxyethyl [2,6-di(pyrazol-1-yl)pyrid-4-yl]carboxylate. 2,6-Di(pyrazol-1-yl)-pyridine-4-carboxylic acid (1.00 g, 3.92 mmol) was dissolved in ethylene glycol (150 cm^3) at 120 °C. A catalytic amount of concentrated sulfuric acid H_2SO_4 (0.1 cm^3) was added and the mixture was stirred for 3 h. The mixture was then cooled to room temperature, giving a white precipitate. This was collected by filtration, dried *in vacuo* and analysed without further purification. Yield 0.77 g, 64 %. Mp 158-159 °C. ES-MS *m/z* 300.1084 (calcd for $[HL]^+$ 300.1091), 322.0906 (calcd for $[HL]^+$ 322.0911). ^{1}H NMR ($CDCl_3$) δ 4.04 (t, 6.8 Hz, 2H, CH_2OH), 4.57 (6.8 Hz, 2H, CH_2OCO), 6.55 (pseudo-t, 1.7 Hz, 2H, pz H^4), 7.82 (d, 1.5 Hz, 2H, pz H^3), 8.40 (s, 2H, py $H^{3/5}$), 8.56 (d, 2.6 Hz, 2H, pz H^5) ppm. ^{13}C NMR ($CDCl_3$) δ 60.9 (1C, CH$_2$OH), 67.7 (1C, CH$_2$OCO), 108.5 (2C, pz C^4), 109.2 (2C, py $C^{3/5}$), 127.3 (2C, pz C^5), 142.9 (2C, pz C^3), 143.0 (1C, py C^4), 150.8 (2C, py $C^{2/6}$), 164.2 (1C, CO$_2$) ppm.

Synthesis of 2-[(2,6-di(pyrazol-1-yl)pyridine)-4-carboxy]ethyl (*R*)-lipoate (L^3). 2-Hydroxyethyl [2,6-di(pyrazol-1-yl)pyrid-4-yl]carboxylate (0.56 g, 1.9 mmol), (*R*)-lipoic acid (0.39 g, 1.9 mmol) and 4-dimethylaminopyridine (0.056 g, 0.37 mmol) were mixed in dry dichloromethane (50 cm^3) at 0 °C. A solution of *N*,*N*-dicyclohexyl carbodiimide (0.44 g, 2.2 mmol) in dry dichloromethane (25 cm^3) was then added dropwise to the cooled suspension during 30 mins. After stirring at 0 °C for an additional 30 mins, the solution was stirring at room temperature for 16 hrs. The mixture was filtered and the supernatant was concentrated under vacuum to give a yellow solid. The pale yellow product was purified by flash silica column chromatography (eluent 1:4 hexane:ethyl acetate, R_f 0.88) as a pale yellow powder. Yield 0.56 g, 66 %. Mp: 104-105 °C. Found: C, 54.3; H, 5.27; N, 14.2 %. Calcd for $C_{22}H_{25}N_5O_4S_2$ C, 54.2; H, 5.17; N, 14.4 %. ES-MS *m/z* 488.1427 (calcd for $[HL^5]^+$ 488.1426), 510.1240 (calcd for $[NaL^5]^+$ 510.1246). ^{1}H NMR ($CDCl_3$) δ 1.47 (m, 2H), 1.69 (m, 4H), 1.87 (m, 1H), 2.41 (m, 3H), 3.12 (m, 2H – all lipoate CH_2), 3.53 (m, 1H, lipoate CH), 4.39, 4.55 (roofed m, both 2H, CH_2O), 6.54 (pseudo-t, 2.0 Hz, 2H, pz H^4), 7.82 (d, 1.8 Hz, 2H, pz H^3), 8.40 (s, 2H, py $H^{3/5}$), 8.58 (d, 2.6 Hz, 2H, pz H^5) ppm. ^{13}C NMR ($CDCl_3$) δ 24.6, 28.7, 33.9, 34.5, 38.4 and 40.2 (all 1C, lipoate CH$_2$), 58.3 (1C, lipoate CH), 61.8, 63.8 (both 1C, CH$_2$O), 108.5 (2C, pz C^4), 109.2 (py $C^{3/5}$), 127.2 (2C, pz C^5), 142.9 (3C, py C^4 + pz C^3), 150.9 (2C, py $C^{2/6}$), 163.8 (1C, py$C$O$_2$), 173.2 (1C, CH$_2C$O$_2$) ppm.

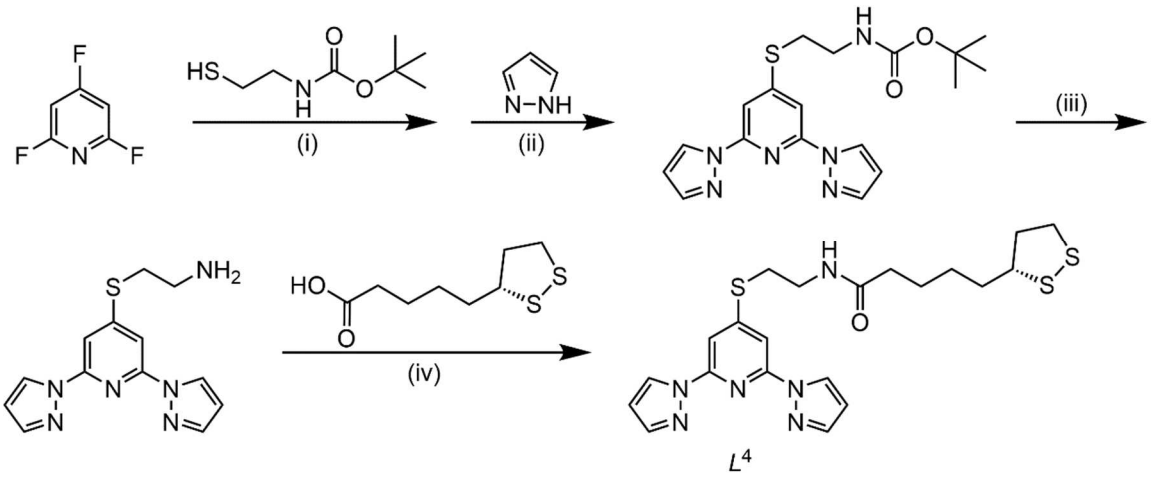

L^4

Scheme S4 Synthesis of L^4. Reagents and conditions: (i) NaH, thf, room temperature; (ii) NaH, thf, room temperature, then water; (iii) acyl chloride, methanol, 0 °C → room temperature then water, Na_2CO_3; (iv) 4-dimethylaminopyridine, *N*,*N*-dicyclohexyl carbodiimide, dichloromethane, 0 °C → room temperature.

Synthesis of *N*-BOC-4-(2-aminoethylsulfanyl)-2,6-di(pyrazol-1-yl)pyridine. 2,4,6-Trifluoropyridine (1.50 g, 11.3 mmol) was added to a suspension of BOC-cysteamine (2.19 g, 12.4 mmol) and NaH (60 wt % in mineral oil; 0.051 g 11.3 mmol) in tetrahydrofuran (50 cm^3), and the mixture was stirred at room temperature for 10 min. Solid pyrazole (1.62 g, 23.7 mmol) and NaH (60 wt % in mineral oil; 0.93 g, 23.3 mmol) were then added, which led to an immediate thickening of the solution. The mixture slowly clarified upon stirring at room temperature for 6 hrs. The solvent was then removed *in vacuo* and the residue was suspended in water (30 cm^3). The mixture was extracted with chloroform (3x 100 cm^3), dried over magnesium sulfate then evaporated to dryness. The product was purified by flash silica column chromatography (4:1 hexane:ethyl acetate eluent, R_f 0.25). Yield 1.5 g, 34 %. Mp 118-119 °C. ES-MS *m/z* 387.1598 (calcd for $[HL]^+$ 387.1598), 409.1426 (calcd for $[NaL]^+$ 409.1417), 795.2954 (calcd for $[NaL_2]^+$ 795.2942). ^{1}H NMR ($CDCl_3$) δ 1.43 (s, 9H, C{CH_3}$_3$), 3.25 (t, 6.2 Hz, 2H, CH_2S), 3.47 (m, 2H, CH_2NH), 5.11 (br s, 1H, N*H*), 6.45 (pseudo-t, 1.8 Hz, 2H, pz H^4), 7.67 (s, 2H, py $H^{3/5}$), 7.72 (br s, 2H, pz H^3), 8.49 (d, 2.5 Hz, 2H, pz H^5) ppm. ^{13}C NMR ($CDCl_3$) δ 28.3 (3C, C{*C*H$_3$}$_3$), 31.3 (1C, *C*H$_2$S), 39.1 (1C, *C*H$_2$NH), 79.6 (1C, *C*{CH$_3$}$_3$), 105.8 (2C, py $C^{3/5}$), 107.9 (2C, pz C^4), 127.2 (2C, pz C^5), 142.3 (2C, pz C^3), 149.8 (2C, py $C^{2/6}$), 154.9 (1C, py C^4), 155.6 (1C, N*C*O$_2$) ppm.

Synthesis of 4-(2-aminoethylsulfanyl)-2,6-di(pyrazol-1-yl)pyridine. Acyl chloride (3.5 cm^3) was added dropwise to methanol (40 cm^3) at 0 ºC, and the mixture was stirred for 30 min. *N*-BOC-4-(2-aminoethyl-sulfanyl)-2,6-di(pyrazol-1-yl)pyridine (1.39 g, 3.60 mmol) was added to the solution, and the mixture was stirred for 18 hrs at room temperature. The resultant white precipitate (the hydrochloride salt of the product) was collected by filtration and air-dried. The precipitate was redissolved in water (65 cm^3) and the solution was first neutralised to *p*H 7 with solid Na_2CO_3, then stirred overnight at room temperature leading to a white precipitate. The product was extracted with chloroform (3 x 100 cm^3) and the dried organic fractions were evaporated to dryness, yielding the pure compound without further purification. Yield 0.97 g, 92 %. Mp: 84-85 °C. ES-MS *m/z* 287.1089 (calcd for $[HL]^+$ 287.1079). ^{1}H NMR ($CDCl_3$) δ 3.10 (m, 2H, CH_2NH$_2$), 3.24 (t, 6.4 Hz, 2H, CH_2S), 6.49 (pseudo-t, 2.2 Hz, 2H, pz H^4), 7.74 (s, 2H, py $H^{3/5}$), 7.75 (d, 1.8 Hz, 2H, pz H^3), 8.54 (d, 2.6 Hz, 2H, pz H^5) ppm. ^{13}C NMR ($CDCl_3$) δ 35.2 (1C, *C*H$_2$S), 40.7 (1C, *C*H$_2$NH$_2$), 106.0 (2C, py $C^{3/5}$), 108.0 (2C, pz C^4), 127.2 (2C, pz C^5), 142.4 (2C, pz C^3), 149.9 (2C, py $C^{2/6}$), 154.9 (1C, py C^4) ppm.

Synthesis of *N*-([2,6-di(pyrazol-1-yl)pyrid-4-ylsulfanyl]-2-aminoethyl (*R*)-lipoamide (L^4). 4-(2-Aminoethylsulfanyl)-2,6-di(pyrazol-1-yl)pyridine (0.78 g, 2.7 mmol), (*R*)-lipoic acid (0.62 g, 3.0 mmol) and 4-dimethylaminopyridine (0.083 g, 0.54 mmol) were mixed in dry dichloromethane (50 cm^3) at 0 °C. A solution of *N*,*N*-dicyclohexyl carbodiimide (673 mg, 3.25 mmol) in dry dichloromethane (25 cm^3) was added dropwise to the cooled suspension during 30 mins. After an additional 30 min stirring, the ice bath was removed and the mixture was stirred overnight at room temperature. The suspension was filtered and the liquid phase was concentrated under vacuum yielding a pale yellow solid. The pale yellow solid product was isolated by elution through silica gel in ethyl acetate (R_f 0.51). Yield 0.99 g, 77% yield. Mp 117-118 °C.

Found: C, 53.1; H, 5.61; N, 17.7 %. Calcd for $C_{21}H_{26}N_6OS_3$ C, 53.1; H, 5.52; N, 17.7 %. ES-MS *m/z* 475.1658 (calcd for $[HL^6]^+$ 475.1409), 497.1581 (calcd for $[NaL^6]^+$ 497.1228), 971.3308 (calcd for $[Na(L^6)_2]^+$ 971.2558). ^{1}H NMR ($CDCl_3$) δ 1.46 (m, 2H), 1.67 (m, 4H), 1.90 (m, 1H), 2.19 (m, 2H), 2.45 (m, 1H), 3.14 (m, 2H − all lipoate CH_2), 3.32 (t, 6.4 Hz, 2H, CH_2S), 3.55 (m, 1H, lipoate C*H*), 3.63 (pseudo-q, 6.1 Hz, 2H, CH_2NH), 5.95 (br s, 1H, N*H*), 6.5 (pseudo-t, 2.0 Hz, 2H, pz H^4), 7.73 (s, 2H, py $H^{3/5}$), 7.76 (s, 2H, pz H^3), 8.55 (d, 2.7 Hz, 2H, pz H^5) ppm. ^{13}C NMR ($CDCl_3$) δ 25.2, 28.8, 34.6, 36.3, 38.4, 40.2 (all 1C, lipoate CH_2), 31.0 (CH_2S), 38.0 (1C, CH_2NH), 56.3 (1C, lipoate *C*H), 38.0 (1C, CH_2NH), 105.9 (2C, py $C^{3/5}$), 108.1 (2C, pz C^4), 127.3 (2C, pz C^4), 142.5 (2C, pz C^3), 150.0 (2C, py $C^{2/6}$), 154.0 (1C, py C^4), 172.9 (1C, *C*ONH) ppm.

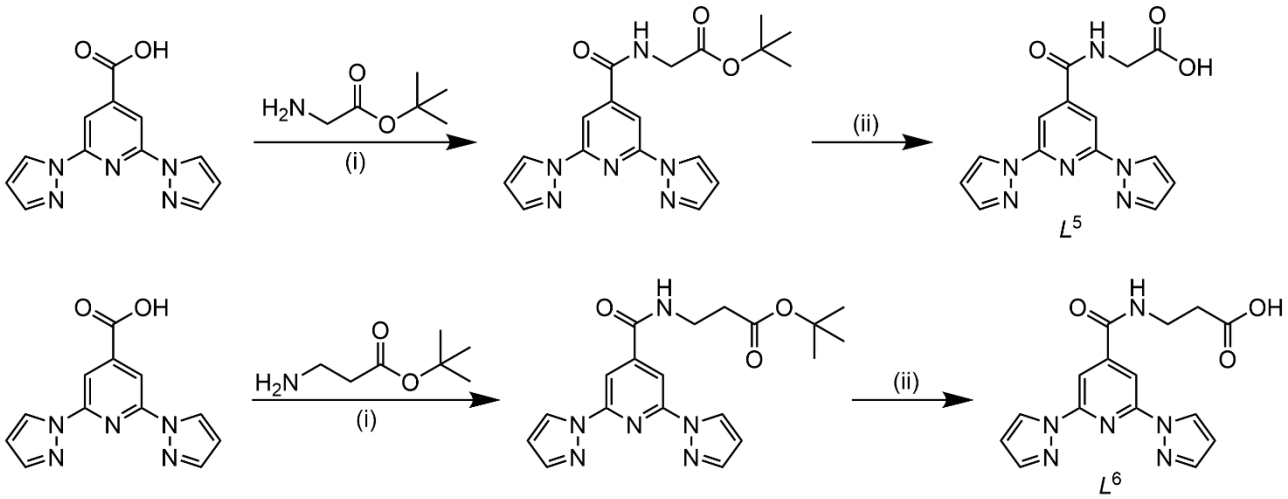

Scheme S5 Synthesis of L^5 and L^6. Reagents and conditions: (iv) 4-dimethylaminopyridine, *N*,*N*-dicyclohexyl carbodiimide, dichloromethane, 0 °C →room temperature; (ii) trifluoroacetic acid, dichloromethane, room temperature.

Synthesis of *tert*butyl 2-[(2,6-di(pyrazol-1-yl)pyridine)-4-carboxamido]acetate. 4-Dimethylamino-pyridine (0.36 g, 2.4 mmol), *tert*butyl aminoacetate (1.63 g, 12.4 mmol) and 2,6-di(pyrazol-1-yl)pyridine-4-carboxylic acid (3.01 g, 11.8 mmol) were mixed in dry dichloromethane (cm^3), and the mixture was stirred for 5 mins at 0 °C. A solution of *N*,*N*-dicyclohexyl carbodiimide (2.78 g, 13.5 mmol) in dichloromethane (cm^3) was added dropwise to the reaction, after which the mixture was stirred at 0 °C for 30 mins, and allowed to warm to room temperature and stirred for a further 16 hrs. The suspension was filtered and the filtrate was evaporated to dryness. The residue was purified by silica column chromatography (1:4 hexane:ethyl acetate →ethyl acetate eluent, R_f 0.63→0.87. Yield 3.5 g, 79 %. Mp 151-152 °C. ES-MS *m/z* 369.1500 (calcd for $[HL]^+$ 369.1675), 391.1514 (calcd for $[NaL]^+$ 391.1495), 759.3092 (calcd for $[NaL_2]^+$ 759.3091). ^{1}H NMR ($CDCl_3$) δ 1.52 (s, 9H, C{CH_3}$_3$), 4.18 (d, 5.0 Hz, 2H, CH_2), 6.51 (pseudo-t, 1.8 Hz, 2H, pz H^4), 6.96 (br s, 1H, N*H*), 7.78 (d, 1.6 Hz, 2H, pz H^3), 8.20 (s, 2H, py $H^{3/5}$), 8.55 (d, 2.4 Hz, 2H, pz H^5) ppm. ^{13}C NMR ($CDCl_3$) δ 28.1 (3C, C{*C*H$_3$}$_3$), 42.6 (1C, CH_2), 82.8 (1C, *C*{CH$_3$}$_3$), 107.2 (2C, py $C^{3/5}$), 108.4 (2C, pz C^4), 127.2 (2C, pz C^5), 142.8 (2C, pz C^3), 147.0 (2C, py $C^{2/6}$), 150.8 (1C, py C^4), 164.4 (1C, *C*ONH), 168.6 (1C, CO_2) ppm.

Synthesis of 2-[(2,6-di(pyrazol-1-yl)pyridine)-4-carboxamido]acetic acid (L^5). Trifluoroacetic acid (10 cm^3) was carefully added to a solution of *tert*butyl 2-[(2,6-di(pyrazol-1-yl)pyridine)-4-carboxamido]acetate (1.0 g, 0.027 mmol) in dichloromethane (50 cm^3). The mixture was stirred at room temperature for 1 hr, then concentrated until the product precipitated as a white solid. Yield 0.71 g, 84 %. Mp 272-273 °C. Found: C, 53.7; H, 3.59; N, 26.8 %. Calcd for $C_{14}H_{12}N_6O_3$ C, 53.9; H, 3.87; N, 26.9 %. ES-MS *m/z* 313.1044 (calcd for $[HL^7]^+$ 313.1044), 335.0859 (calcd for $[NaL^7]^+$ 335.0863). NMR ({CD_3}$_2$SO) δ 3.98 (d, 5.9 Hz, 2H, CH_2), 6.67 (dd, 1.5 and 2.6 Hz, 2H, pz H^4), 7.92 (d, 1.6 Hz, 2H, pz H^3), 8.23 (s, 2H, py $H^{3/5}$), 9.00 (d, 2.6 Hz, 2H, pz H^5), 9.51 (t, 5.9 Hz, 1H, N*H*) ppm. ^{13}C NMR ({CD_3}$_2$SO) δ 41.3 (1C, CH_2), 106.8 (2C, py $C^{3/5}$), 108.8 (2C, pz C^4), 128.4 (2C, pz C^5), 143.0 (2C, pz C^3), 147.2 (2C, py $C^{2/6}$), 150.2 (1C, py C^4), 163.8 (1C, *C*ONH), 170.8 (1C, CO_2) ppm.

Synthesis of *tert*butyl 2-[(2,6-di(pyrazol-1-yl)pyridine)-4-carboxamido]propionate. Method as for *tert*butyl 2-[(2,6-di(pyrazol-1-yl)pyridine)-4-carboxamido]acetate, using *tert*butyl 2-aminopropionate (1.80 g, 12.4 mmol). The crude product was purified by flash silica column chromatography (1:4 hexane:ethyl acetate→ethyl acetate eluent, R_f 0.69→0.90. Yield 2.3 g, 44 %. Mp 132-133 °C. ES-MS *m/z* 383.1542 (calcd for $[HL]^+$ 383.1826), 405.1603 (calcd for $[NaL]^+$ 405.1646), 787.3416 (calcd for $[NaL_2]^+$ 787.3399). ^{1}H NMR ($CDCl_3$) δ 1.48 (s, 9H, C{CH_3}$_3$), 2.60 (t, 6.1 Hz, 2H, CH_2CO$_2$), 3.73 (pseudo-q, 6.0 Hz, 2H, CH_2NH), 6.52 (dd, 1.7 and 2.4 Hz, 2H, pz H^4), 7.05 (br s, 1H, N*H*), 7.78 (d, 1.7 Hz, 2H, pz H^3), 8.15 (s, 2H, py $H^{3/5}$), 8.55 (d, 2.4 Hz, 2H, pz H^5) ppm. ^{13}C NMR ($CDCl_3$) δ 28.1 (3C, C{*C*H$_3$}$_3$), 34.9, 35.8 (both 1C, *C*H$_2$), 81.5 (1C, *C*{CH$_3$}$_3$), 107.1 (2C, py $C^{3/5}$), 108.3 (2C, pz C^4), 127.2 (2C, pz C^5), 142.7 (2C, pz C^3), 147.8 (2C, py $C^{2/6}$), 150.8 (1C, py C^4), 164.5 (1C, *C*ONH), 171.8 (1C, *C*O$_2$) ppm.

Synthesis of 2-[(2,6-di(pyrazol-1-yl)pyridine)-4-carboxamido]propionic acid (L^6). Method as for L^5, using *tert*butyl 2-[(2,6-di(pyrazol-1-yl)pyridine)-4-carboxamido]propionate (1.0 g, 0.026 mmol). The product is a white solid. Yield 0.65 g, 76 %. Mp 214-215 °C. Found: C, 55.4; H, 4.15; N, 25.6 %. Calcd for $C_{15}H_{14}N_6O_3$ C, 55.2; H, 4.32; N, 25.8 %. ES-MS *m/z* 327.1203 (calcd for $[HL^8]^+$ 327.1200), 349.1018 (calcd for $[NaL^8]^+$ 349.1020), 675.2131 (calcd for $[Na(L^8)_2]^+$ 675.2147). NMR ({CD$_3$}$_2$SO) δ 2.58 (t, 7.1 Hz, 2H, CH_2CO$_2$), 3.52 (pseudo-q, 6.0 Hz, 2H, CH_2NH), 6.52 (dd, 1.7 and 2.6 Hz, 2H, pz H^4), 7.91 (d, 1.7 Hz, 2H, pz H^3), 8.20 (s, 2H, py $H^{3/5}$), 8.98 (d, 2.4 Hz, 2H, pz H^5), 9.19 (t, 5.3 Hz, 1H, N*H*) ppm. ^{13}C NMR ({CD$_3$}$_2$SO) δ 33.3, 35.8 (both 1C, *C*H$_2$), 106.8 (2C, py $C^{3/5}$), 108.7 (2C, pz C^4), 128.4 (2C, pz C^5), 142.9 (2C, pz C^3), 147.7 (2C, py $C^{2/6}$), 150.1 (1C, py C^4), 163.4 (1C, *C*ONH), 172.7 (1C, *C*O$_2$) ppm.

Single Crystal Structure Analyses

Diffraction data for L^3 were recorded at station I19 of the Diamond synchrotron (λ = 0.6889 Å). All other crystallographic data were measured with an Agilent Supernova dual-source diffractometer using monochromated Cu-K_α (λ = 1.5418 Å) radiation. The diffractometer was fitted with an Oxford Cryostream low-temperature device. Experimental details of the structure determinations in this study are given in Tables S1-S2. All the structures were solved by direct methods *(SHELXS97*[1]), and developed by full least-squares refinement on F^2 (*SHELXL97*[1]). Crystallographic figures were prepared using *XSEED*,[2] and octahedral coordination volumes (V_{Oh}) were calculated with *Olex2*.[3]

Unless otherwise stated, all fully occupied non-H atoms in these refinements were refined anisotropically. Disordered anions were modelled with refined Cl–O and O···O distance restraints; and, disordered solvent was also modelled using fixed bond length and angle restraints. All H atoms were placed in calculated positions and refined using a riding model.

CCDC deposition numbers for each structure are listed in Tables S1 and S2.

Structure refinement of L^1. There are two unique molecules in the asymmetric unit. A CH_2S moiety in the dithiocyclopentyl ring of molecule N(1)-C(29) is disordered over two sites, whose occupancy ratio refined to 0.75:0.25. A C_2H_4S moiety in the dithiocyclopentyl ring of the other molecule, N(30)-C(58), is also disordered over two sites, whose with refined occupancies of 0.60:0.40. This disorder was treated with the following fixed restraints: C–C = 1.51(2), C–S = 1.82(2), S–S = 2.08(2) and 1,3-C···C = 2.47(2) Å. All fully occupied non-H atoms, plus the 0.6-occupied partial S atom S(56A), were refined anisotropically.

ADSYMM highlights pseudo-inversion symmetry in the lattice, which could imply a transformation to the more common centrosymmetric space group *C*2/*c*. However, an attempted refinement in that space group was clearly inferior [R_1 = 0.152, wR_2 = 0.496 with several non-positive definite atoms], and the essentially zero Flack parameter of the C_2 refinement confirms that choice of space group.

Structure refinement of L^2. No disorder is present in the model, and no restraints were applied to the refinement.

Structure refinement of L^3. There are two unique molecules in the asymmetric unit, both of whose lipoate substituents are disordered over three [molecule N(1)-C(33)] or two [molecule N(34)-C(66)] sites. These were refined using the following fixed restraints: C–C = 1.51(2), C–S = 1.82(2), S–S = 2.08(2), 1,3-C···C = 2.47(2) and 1,3-C···S = 2.80(2) Å. The displacement ellipsoids of each orientation of the three-fold-disordered ligand were also constrained to be similar with *SHELXL* SIMU restraints. Partial atoms C(29B) and C(32A), and wholly occupied S(64), are each shared between two different disorder orientations in the final model. While the groups around C(29B) and C(32A) deviate somewhat from tetrahedrality, attempts to

split these atoms into separate sites for each disorder orientation were unsatisfactory. All fully occupied non-H atoms, plus the half-occupied S atoms, were refined anisotropically.

Structure refinement of *tert*butyl 2-[(2,6-di(pyrazol-1-yl)pyridine)-4-carboxamido]acetate. No disorder is present in the model, and no restraints were applied to the refinement. All H atoms were located in the Fourier map and allowed to refine, with U_{iso} = 1.2x U_{eq}{C} [aromatic C−H], 1.2x U_{eq}{N} [carboxamido N−H] or 1.5x U_{eq}{C} [methyl C−H].

Structure refinement of [Fe(L^5)$_2$][ClO$_4$]$_2$·MeCN. Two datasets were collected from the same crystal, at 120 K and at 330 K (in that order). The plate crystal diffracted more weakly along its short axis at the higher temperature, but the refinement is still reasonably precise.

Both anions exhibit minor disorder over two orientations at 120 K, which refined to occupancy ratios of 0.87:0.13 and 0.90:0.10; in the latter case, these share a common wholly occupied Cl atom. An antibumping restraint was required to prevent one of the minor anion sites refining too close to a carboxamido O atom (which is disordered in the higher temperature structure). All non-H atoms except the minor anion disorder sites were refined anisotropically. The highest residual Fourier peak of +1.6 eÅ^{-3} is within one of the disordered anions.

At 330 K the anion disorder is more pronounced, and each anion was modelled over three equally occupied sites using SIMU displacement ellipsoid restraints, as well as the refined distance restraints mentioned previously. The carboxamido O atom O(42) also had an enlarged displacement ellipsoid, and was modelled over two orientations in a 0.67:0.33 ratio using the fixed restraint C=O = 1.22(1) Å. The MeCN molecule did not show obvious signs of disorder or reduced occupancy at this high temperature.

Structure refinement of [Fe(L^5)$_2$][ClO$_4$]$_2$·*n*MeCN (*n* ≈ 1.5). These needle morphology crystals co-crystallised with [Fe(L^5)$_2$][ClO$_4$]$_2$·MeCN (described above). The crystals diffracted relatively weakly, such that data were only obtained to 2θ = 135.4°. A preliminary structure solution showed substantial disorder in the complex cation, anions and solvent which limited the quality of the refinement. This may reflect the influence of a 2D network of channels in the lattice, which contain the anions and solvent molecules.

Experimental details for this solvatomorph are included in Table S2, but the structure has not been deposited with the CCDC.

Structure refinement of [Fe(L^6)$_2$][ClO$_4$]$_2$·2MeCN.
Two datasets were collected from the same crystal, at 120 K and at 290 K (in that order). The asymmetric unit contains three formula units of the compound, that is: three complex dications; six perchlorate anions; and six acetonitrile molecules.

At 120 K, two of the anions are disordered over two orientations, whose occupancy ratios both refined to 0.67:0.33. Residual Fourier peaks in the region of the carboxamido substituents in complex molecule B also indicated the presence of disorder in those groups. This disorder reflects the presence of two different hydrogen-bond acceptors in the vicinity of the carboxide groups in each side-chain. It was modelled over two sites, using the fixed restraints C−C = 1.51(2), C(O)−N = 1.30(2), CH$_2$−N = 1.46(2), C=O = 1.22(2), C−O = 1.28(2), carboxylic O···O = 2.20(2) and carboxamide N···O = 2.26(2) Å. The disorder sites of side-chain C(42B)-O(49B) share two common, wholly occupied C atoms C(46B) and C(47B). The occupancy of the ligand disorder orientations refined to 0.70:0.30 for C(18B)-O(25B), and 0.84:0.16 for C(42B)-O(49B).

All wholly occupied non-H atoms, the major Cl atom from each disordered anion, and the major ligand disorder orientations were refined anisotropically. An exception is C(42B), which was left isotropic since U_{iso} for its counterpart C(42D) became unacceptably large when C(42B) was refined anisotropically. H atoms were placed in calculated positions and refined using a riding model. The highest residual Fourier peak of +1.1 eÅ^{-3} is 0.9 Å from Fe(1B).

The crystal diffracted more weakly at 290 K, with only 56 % observed data to θ = 73.6°. All the anions were clearly disordered, and were treated over two half-occupied sites. There is also evidence of disorder in several carboxamidopropionic substituents and solvent molecules, but this was not modelled to preserve the observed data:parameter ratio in the refinement.

CCDC-2074276−2074283 contain the supplementary crystallographic data for this paper (Tables S1 and S2). These data can be obtained free of charge from The Cambridge Crystallographic Data Centre via www.ccdc.cam.ac.uk/data_request/cif.

Table S1 Experimental data for the organic ligand crystal structure determinations.

	L^1	L^2	L^3	*tert*butyl 2-[(2,6-di(pyrazol-1-yl)pyridine)-4-carboxamido]acetate
molecular formula	$C_{20}H_{23}N_5O_2S_2$	$C_{22}H_{26}N_6O_3S_2$	$C_{22}H_{25}N_5O_4S_2$	$C_{18}H_{20}N_6O_3$
M_r	429.55	486.61	487.59	368.40
crystal class	monoclinic	orthorhombic	monoclinic	orthorhombic
space group	$C2$	$P2_12_12_1$	$P2_1$	$Pbca$
a / Å	38.6148(7)	5.0813(1)	7.1017(1)	12.2001(2)
b / Å	5.2928(1)	12.2490(4)	17.0738(1)	10.0229(2)
c / Å	20.9507(3)	36.8728(9)	18.7947(2)	30.9937(4)
α / °	–	–	–	–
β / °	105.394(2)	–	91.382(1)	–
γ / °	–	–	–	–
V / Å^3	4128.29(12)	2294.99(10)	2278.25(4)	3789.93(10)
Z	8	4	4	8
T / K	120(2)	120(2)	100(2)	150(2)
μ / mm^{-1}	2.563[c]	2.420[c]	0.274[d]	0.756[c]
D_c / gcm^{-3}	1.382	1.408	1.422	1.291
measured reflections	8327	5883	24658	9262
independent reflections	5960	3894	9365	3726
R_{int}	0.023	0.032	0.068	0.021
parameters	538	298	616	304
restraints	19	0	121	0
R_1 [$F_0 > 4\sigma(F_0)$][a]	0.032	0.037	0.080	0.040
wR_2, all data[b]	0.082	0.089	0.235	0.111
goodness of fit	1.084	1.072	1.311	1.055
$\Delta\rho_{min/max}$ / eÅ^{-3}	–0.23/+0.32	–0.28/+0.36	–0.70/+0.62	–0.18/+0.25
Flack parameter	0.022(10)	−0.027(19)	0.05(6)	–
CCDC	2074276	2074277	2074278	2074279

[a] $R = \Sigma[\,|F_o| - |F_c|\,] / \Sigma|F_o|$ [b] $wR = [\Sigma w(F_o^2 - F_c^2) \;/\; \Sigma wF_o^4]^{1/2}$ [c] Collected with Cu-K_α radiation. [d] Collected with synchrotron radiation.

Table S2 Experimental data for the metal complex crystal structure determinations.

	$[Fe(L^5)_2][ClO_4]_2 \cdot MeCN$		$[Fe(L^5)_2][ClO_4]_2 \cdot n MeCN$ ($n \approx 1.5$)[a]	$[Fe(L^6)_2][ClO_4]_2 \cdot 2MeCN$	
molecular formula	$C_{30}H_{27}Cl_2FeN_{13}O_{14}$		$C_{31}H_{28.5}Cl_2FeN_{13.5}O_{14}$	$C_{34}H_{34}Cl_2FeN_{14}O_{14}$	
M_r	920.39		940.92	989.50	
crystal class	monoclinic		triclinic	triclinic	
space group	$P2_1/n$		$P\bar{1}$	$P\bar{1}$	
a / Å	13.7327(2)	13.8756(4)	8.2783(3)	13.6232(3)	13.6682(3)
b / Å	16.1080(2)	16.2798(7)	13.1029(5)	17.8150(3)	17.9378(5)
c / Å	16.7324(3)	17.2477(10)	18.9841(8)	26.3257(4)	26.8890(8)
α / °	–	–	92.414(3)	78.8771(15)	78.756(3)
β / °	94.0283(14)	95.073(3)	100.938(3)	83.7423(15)	84.199(2)
γ / °	–	–	93.223(3)	78.8440(16)	79.817(2)
V / Å^3	3692.16(9)	3880.9(3)	2015.68(14)	6133.6(2)	6349.0(3)
Z	4	4	2	6	6
T / K	120(2)	330(2)	120(2)	120(2)	290(2)
μ{Cu-K_α} / mm^{-1}	5.384	5.123	4.942	4.914	4.748
D_c / gcm^{-3}	1.656	1.575	1.533	1.607	1.553
measured reflections	14682	11526	–	52042	54085
independent reflections	7220	6591	–	23091	23886
R_{int}	0.028	0.023	–	0.026	0.053
parameters	579	572	–	1814	1733
restraints	41	181	–	80	114
R_1 [$F_0 > 4\sigma(F_0)$][a]	0.068	0.076	–	0.057	0.098
wR_2, all data[b]	0.208	0.253	–	0.148	0.333
goodness of fit	1.045	1.088	–	1.037	1.059
$\Delta\rho_{min/max}$ / eÅ^{-3}	−0.74/+1.57	−0.54/+0.48	–	−0.79/+1.12	−1.09/+0.87
CCDC	2074280	2074281	–	2074282	2074283

[a]A preliminary structure solution confirmed the identity of this material and its low-spin state at 120 K, but showed extensive disorder in the complex molecule and other residues which could not be modelled to a publishable standard (Figure S25). The preliminary solution was also used for the simulated powder pattern of this pseudopolymorph in Figure S36.

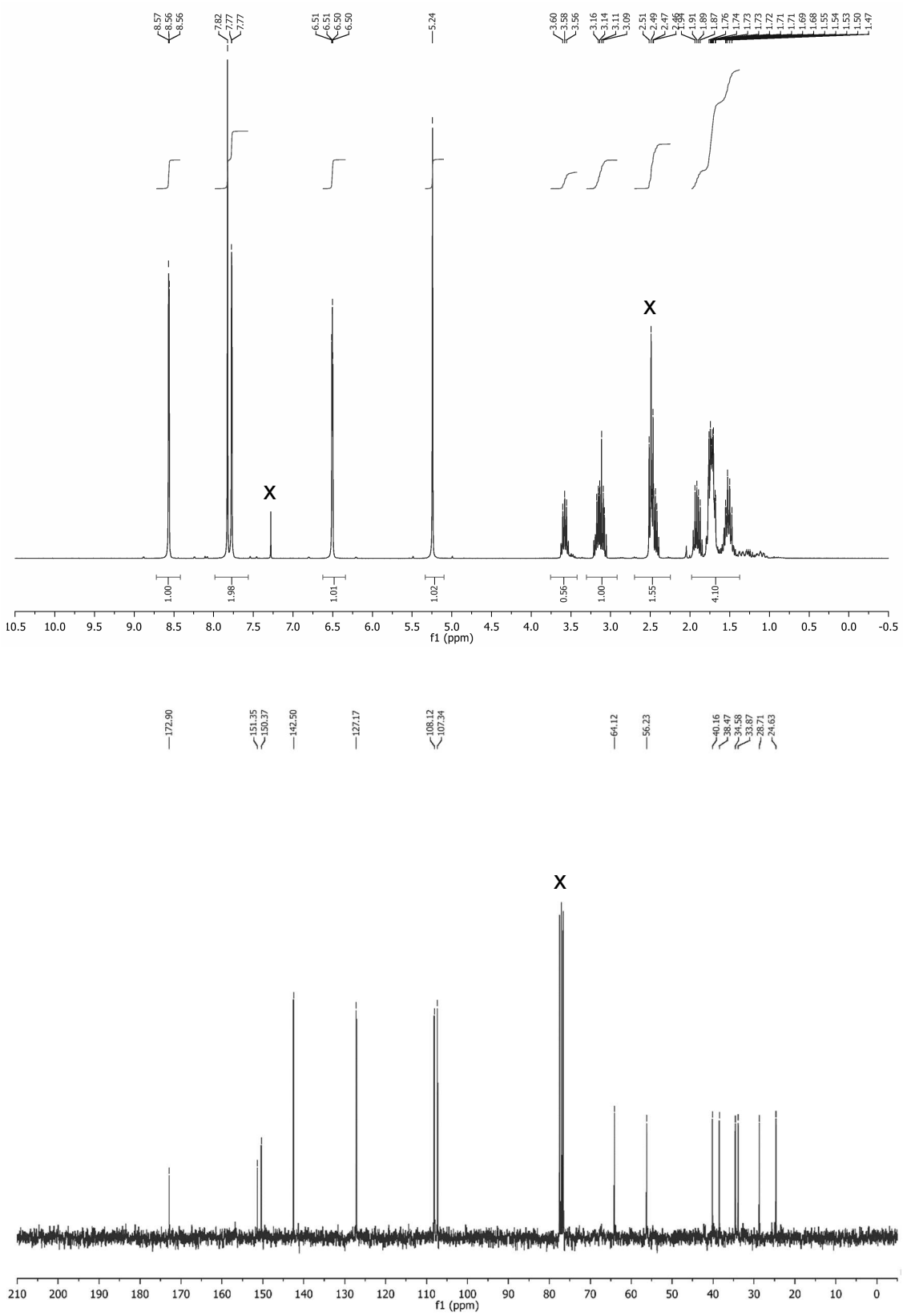

Figure S2 ^{1}H (top) and ^{13}C (bottom) NMR spectra of L^1 ($CDCl_3$).

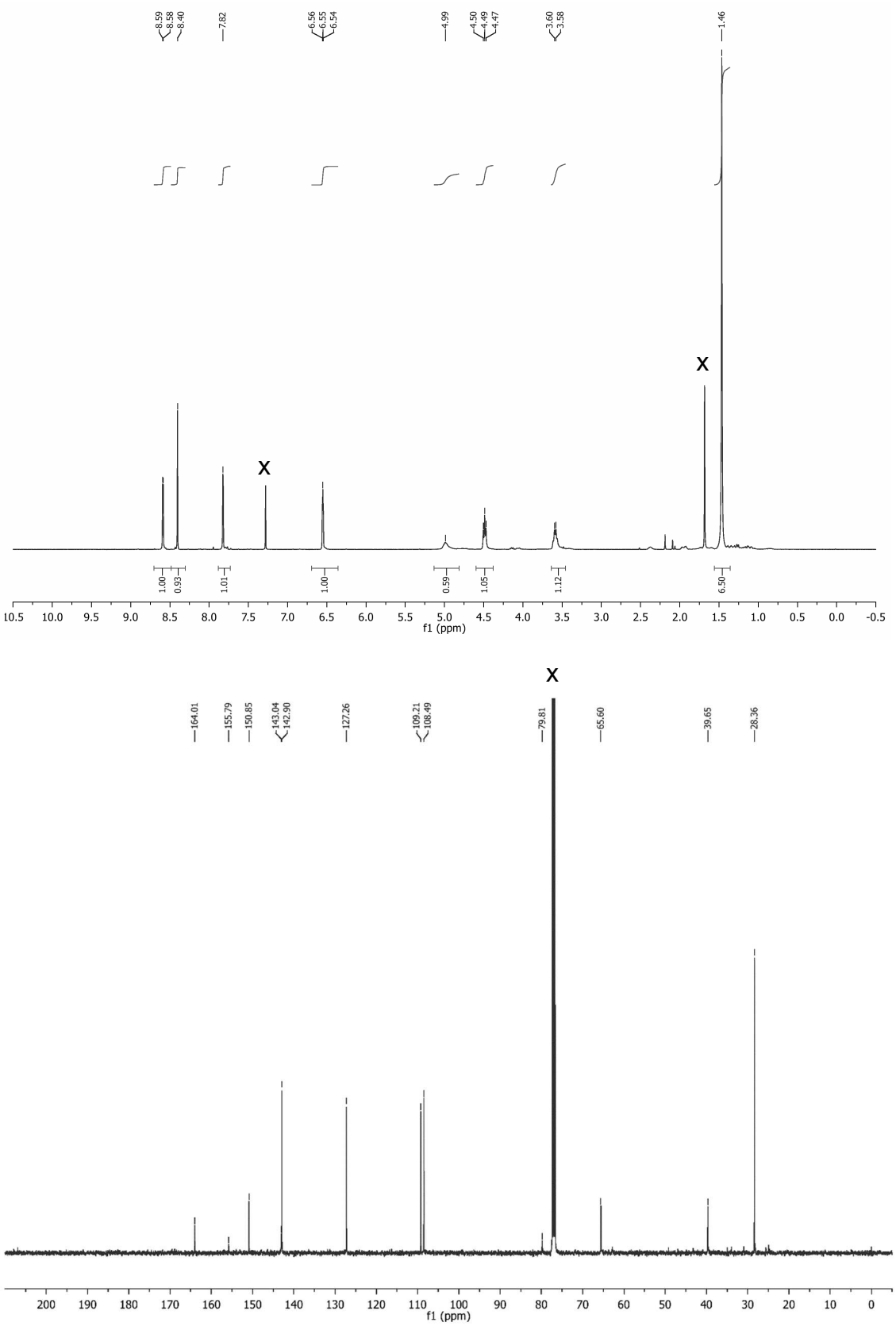

Figure S3 ^{1}H (top) and ^{13}C (bottom) NMR spectra of *N*-BOC-2-aminoethyl [2,6-di(pyrazol-1-yl)pyrid-4-yl]-carboxylate ($CDCl_3$).

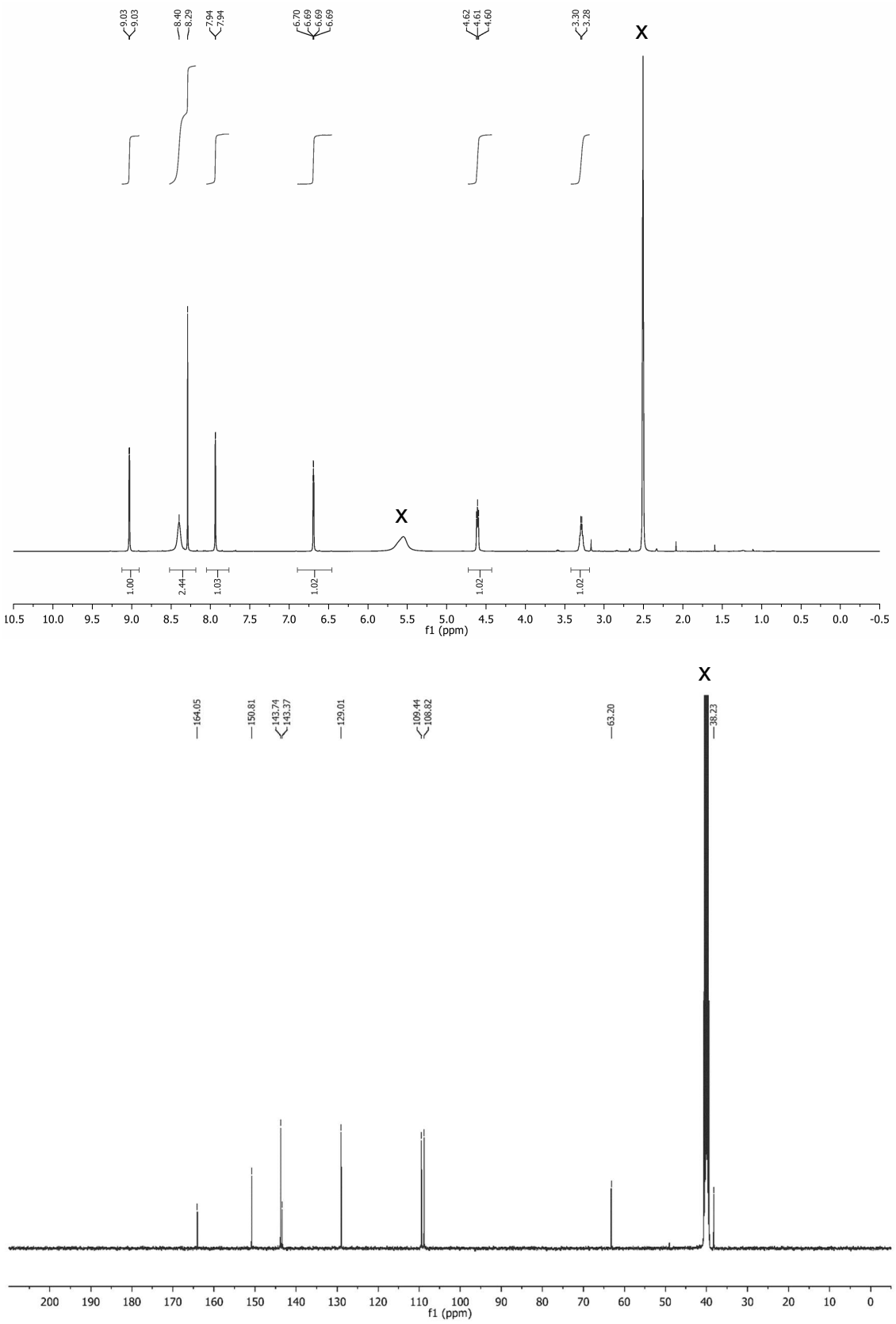

Figure S4 ^{1}H (top) and ^{13}C (bottom) NMR spectra of 2-aminoethyl [2,6-di(pyrazol-1-yl)pyrid-4-yl]carboxylate hydrochloride ($\{CD_3\}_2SO$).

X

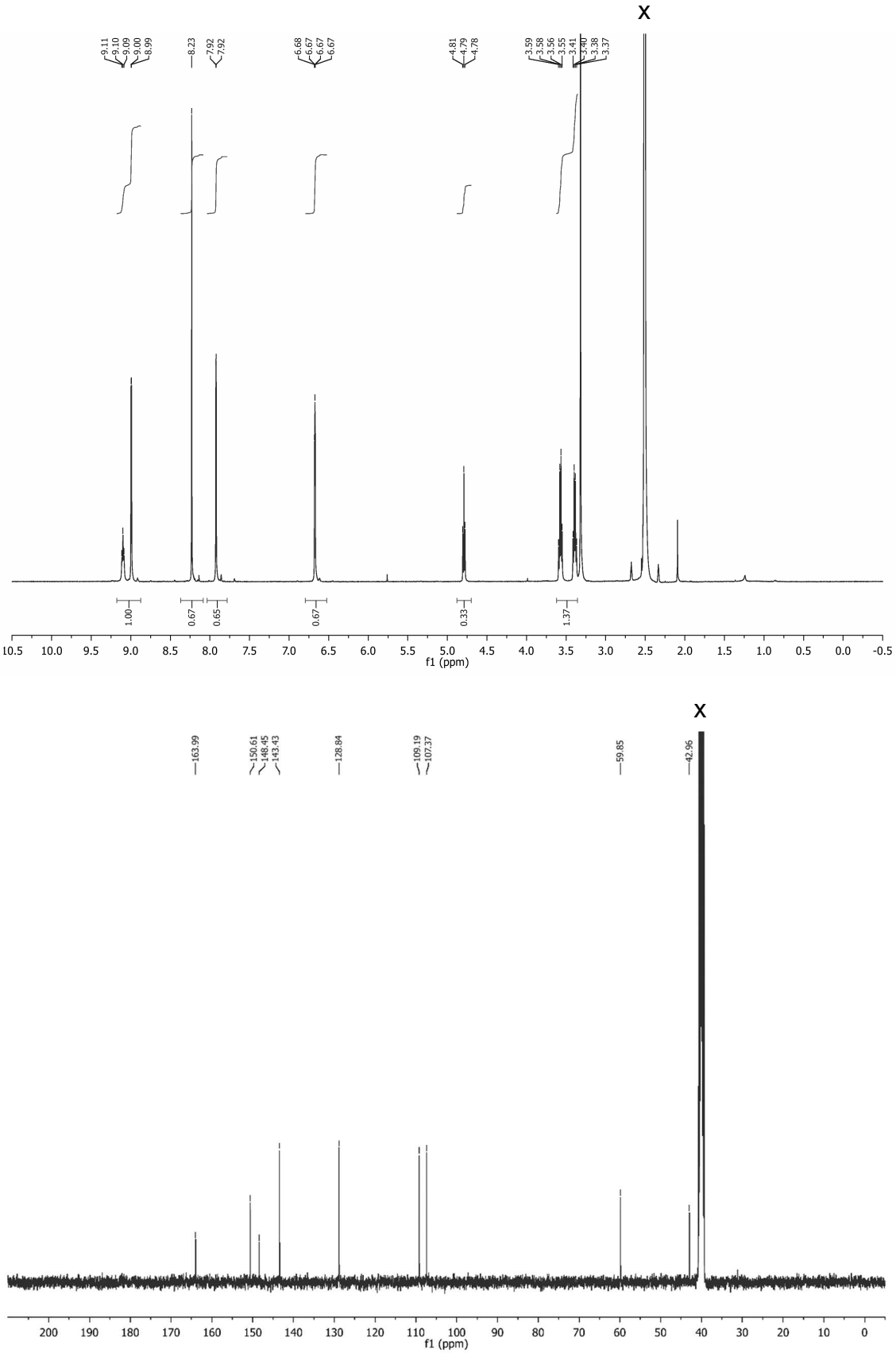

Figure S5 ^{1}H (top) and ^{13}C (bottom) NMR spectra of 2-hydroxyethyl [2,6-di(pyrazol-1-yl)pyrid-4-yl]-carboxamide ($\{CD_3\}_2SO$).

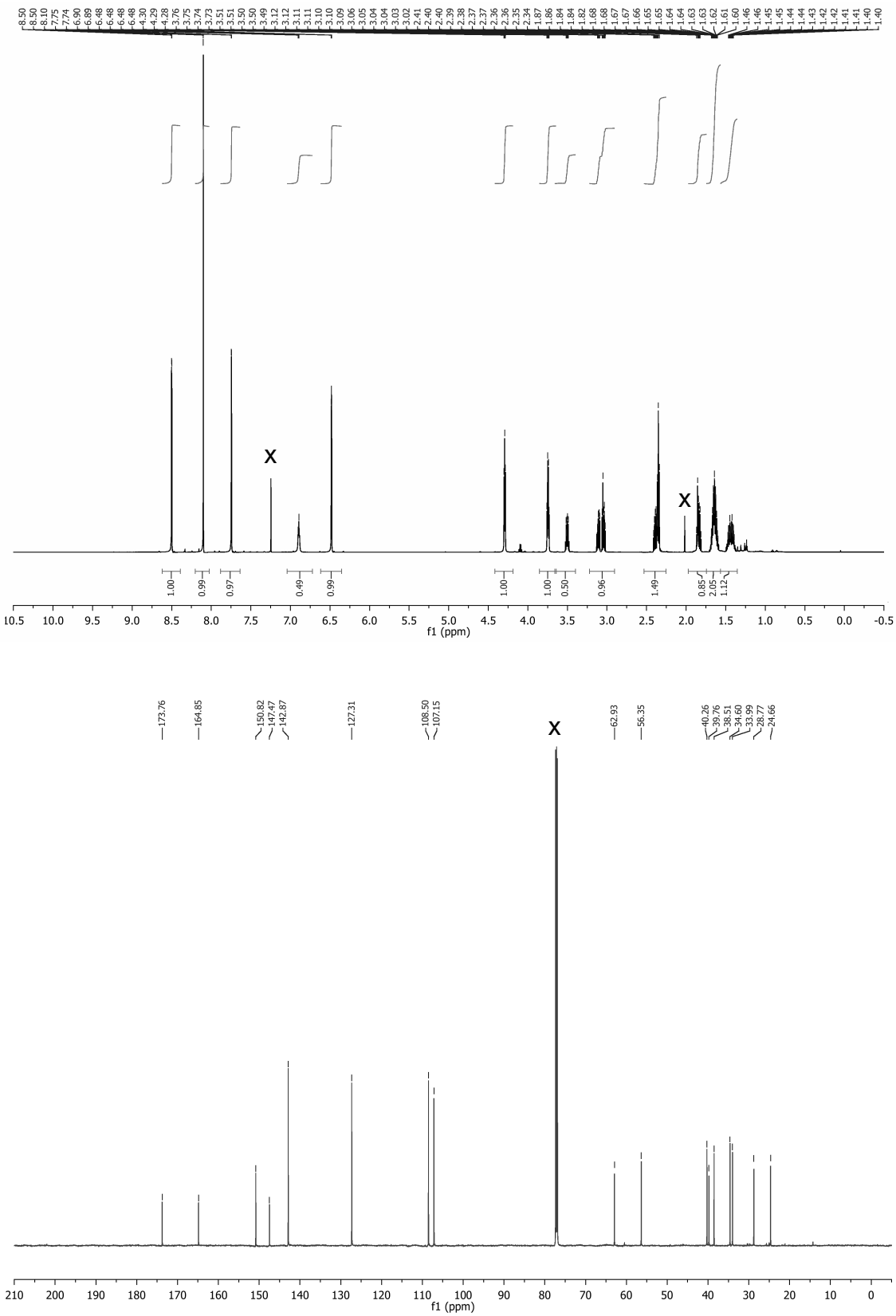

Figure S6 ^{1}H (top) and ^{13}C (bottom) NMR spectra of L^2 ($CDCl_3$).

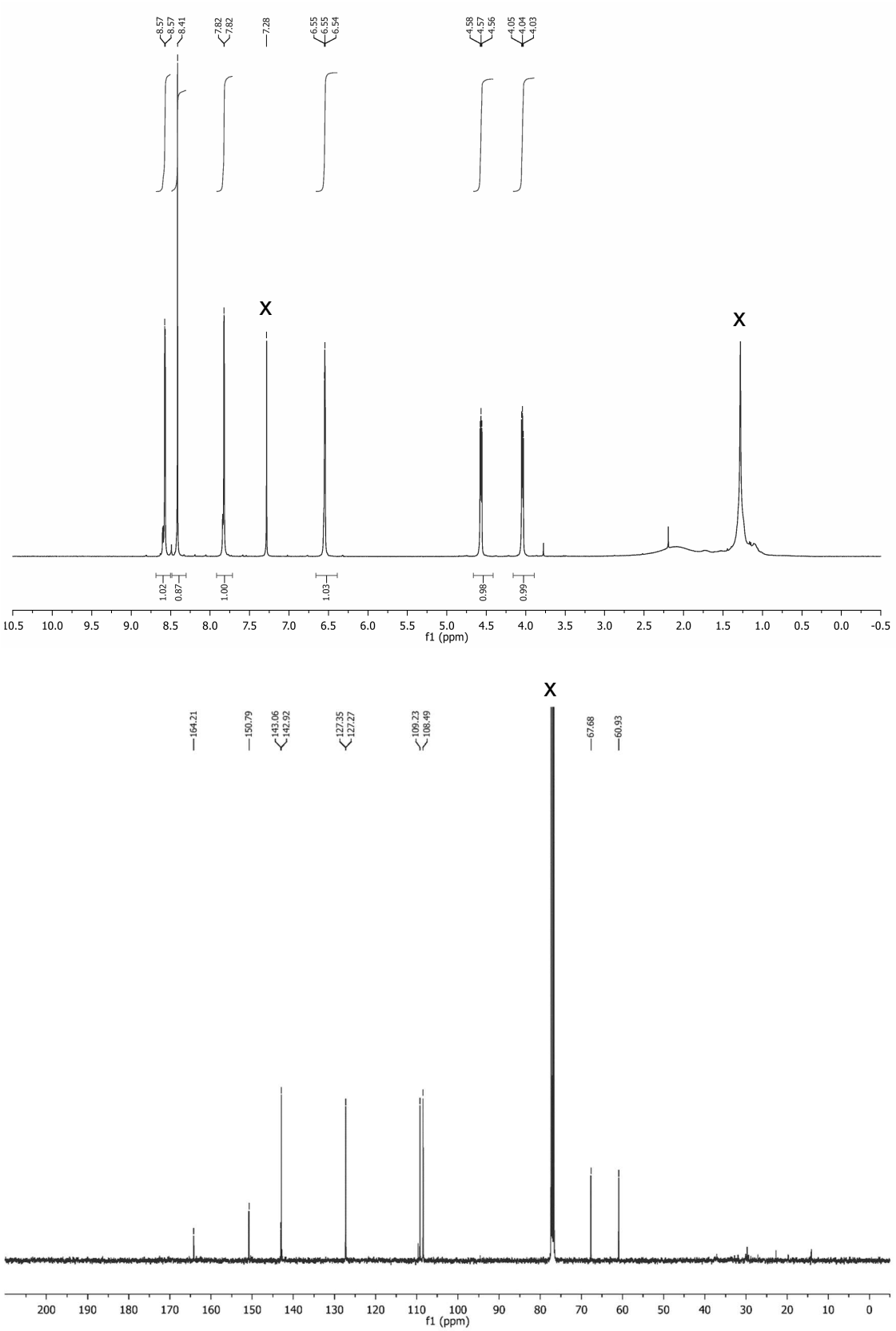

Figure S7 ^{1}H (top) and ^{13}C (bottom) NMR spectra of 2-hydroxyethyl [2,6-di(pyrazol-1-yl)pyrid-4-yl]-carboxylate ($CDCl_3$).

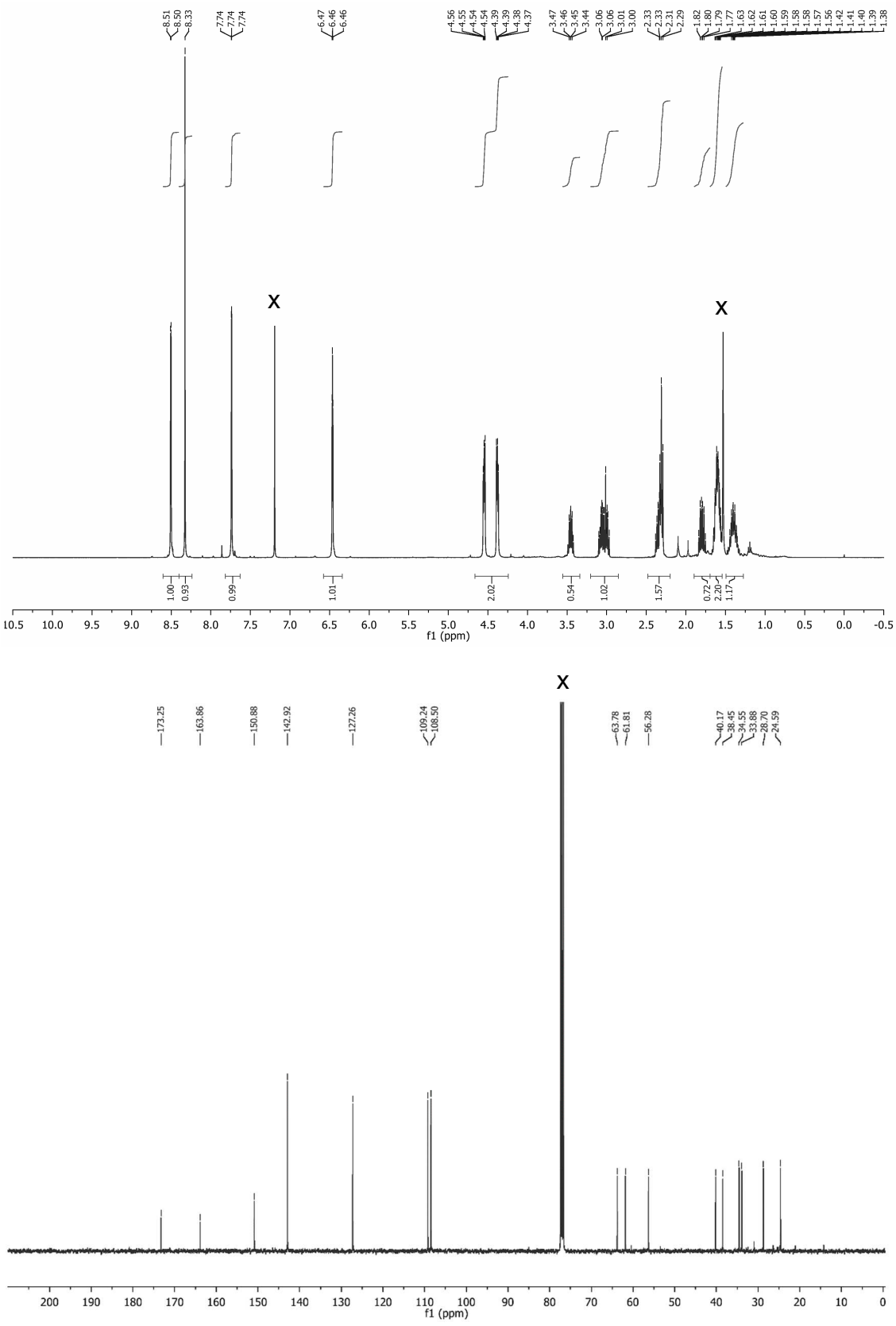

Figure S8 ^{1}H (top) and ^{13}C (bottom) NMR spectra of L^3 ($CDCl_3$).

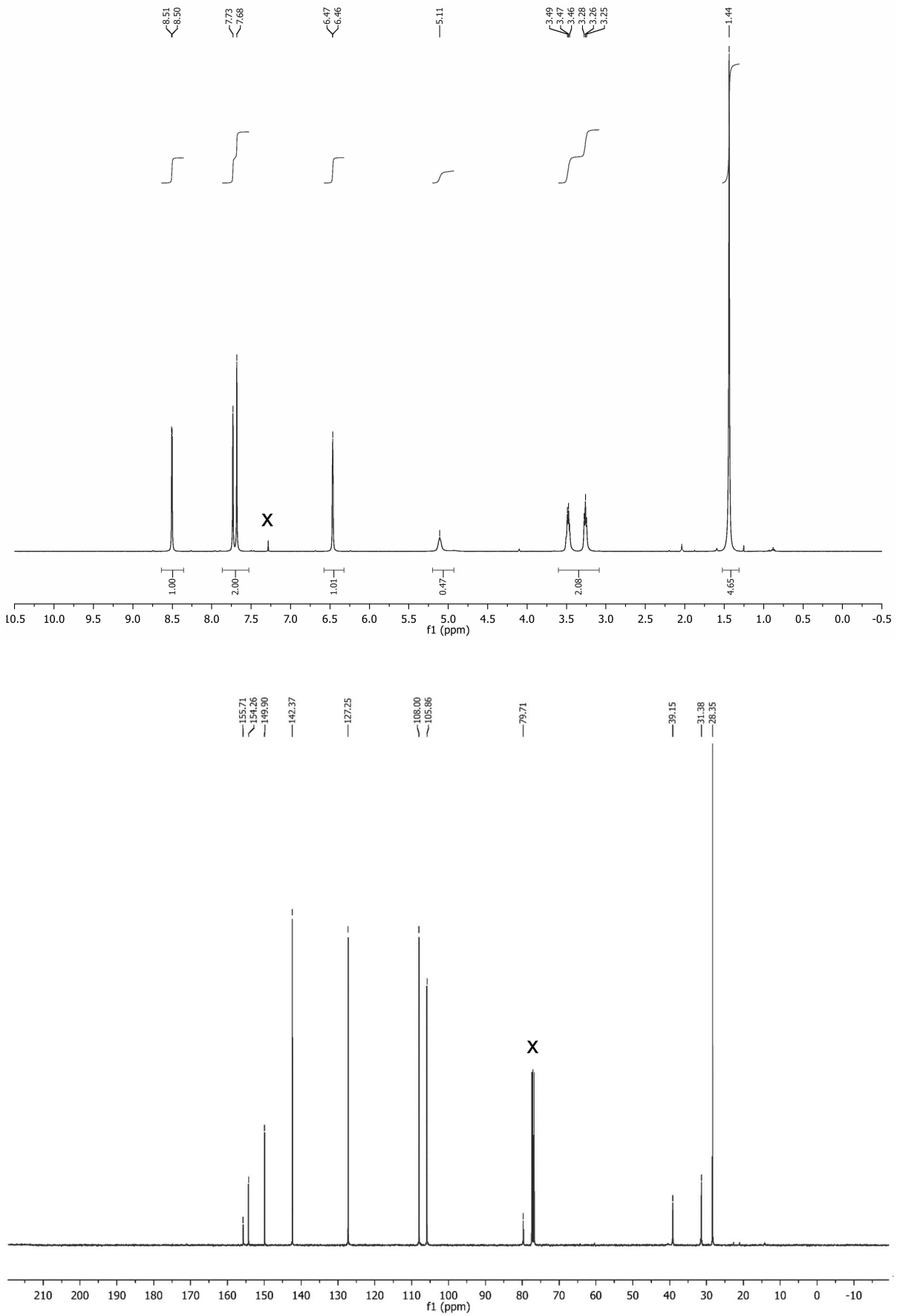

Figure S9 ^{1}H (top) and ^{13}C (bottom) NMR spectra of *N*-BOC-4-(2-aminoethylsulfanyl)-2,6-di(pyrazol-1-yl)pyridine ($CDCl_3$).

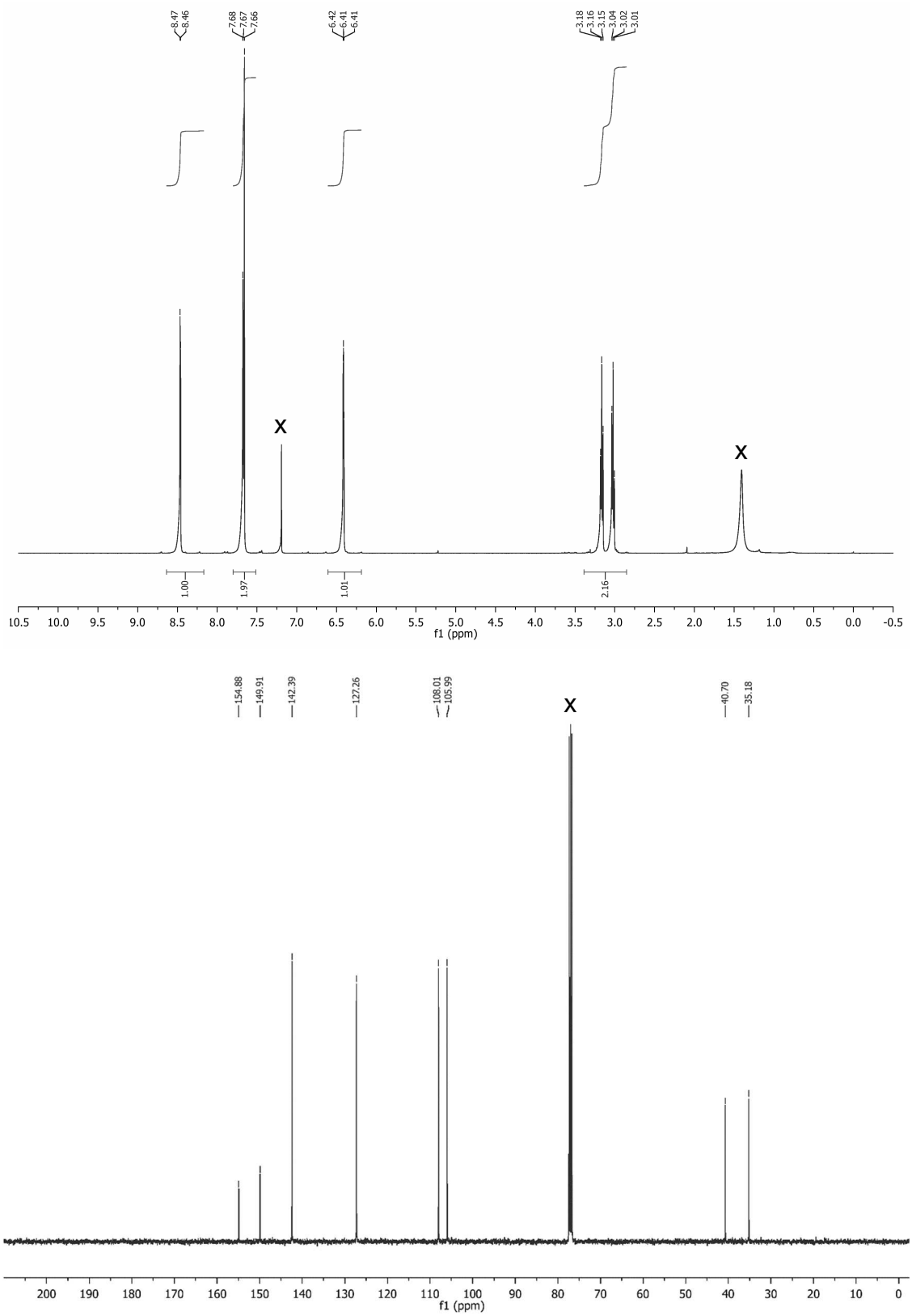

Figure S10 ^{1}H (top) and ^{13}C (bottom) NMR spectra of 4-(2-aminoethylsulfanyl)-2,6-di(pyrazol-1-yl)pyridine ($CDCl_3$).

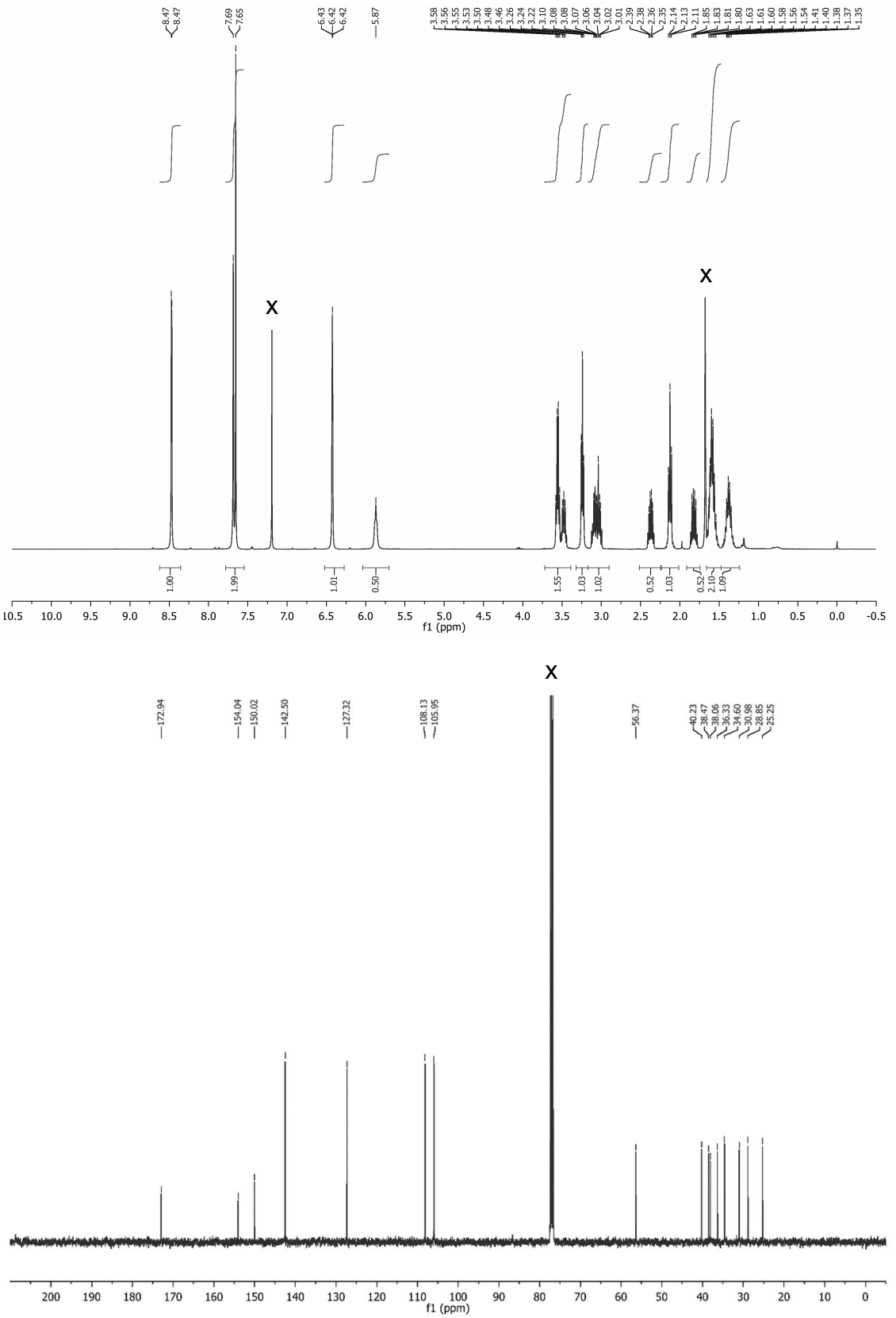

Figure S11 ^{1}H (top) and ^{13}C (bottom) NMR spectra of L^4 ($CDCl_3$).

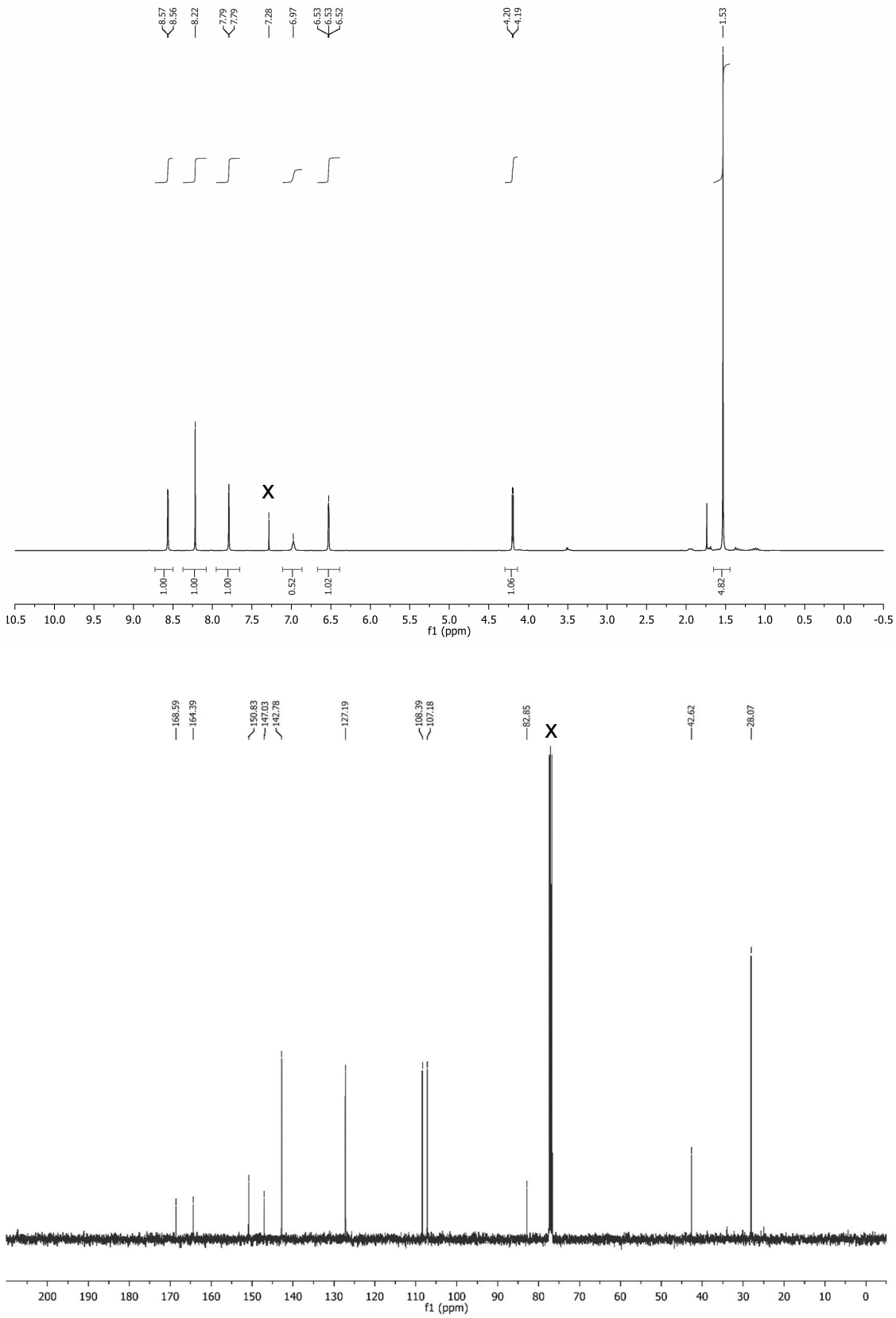

Figure S12 ^{1}H (top) and ^{13}C (bottom) NMR spectra of *tert*butyl 2-[(2,6-di(pyrazol-1-yl)pyridine)-4-carboxamido]acetate ($CDCl_3$).

X

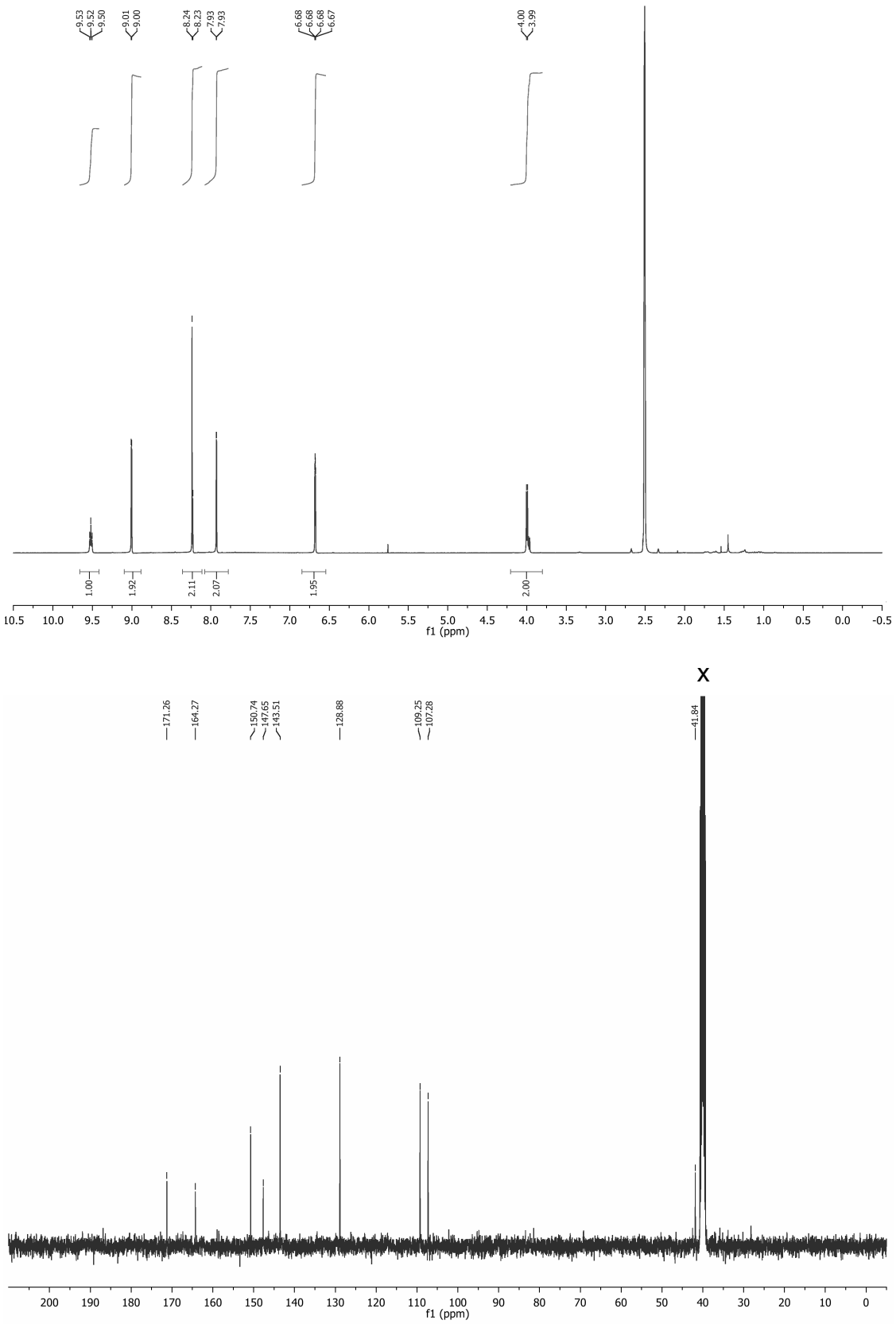

Figure S13 ^{1}H (top) and ^{13}C (bottom) NMR spectra of L^5 ({CD_3}$_2$SO).

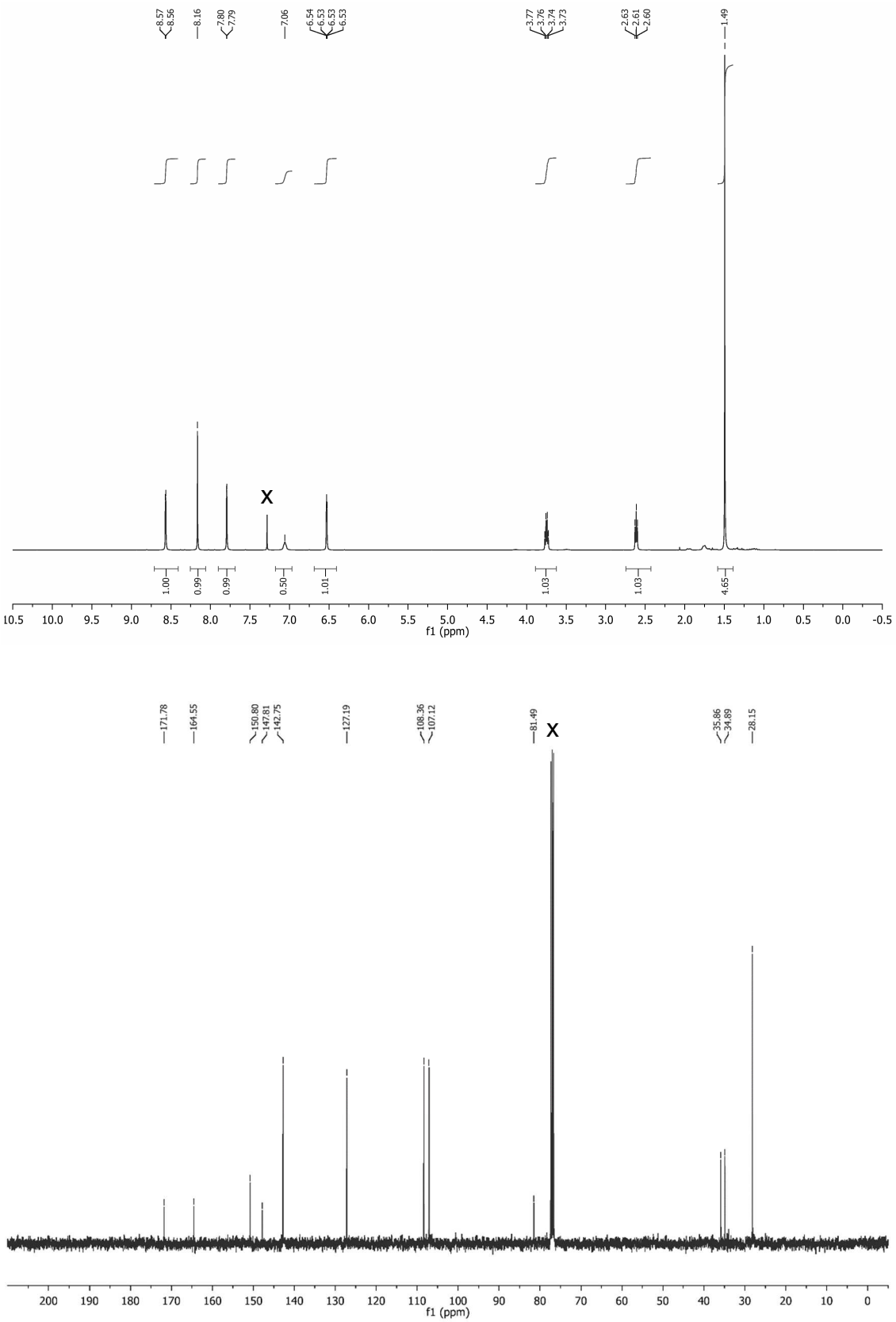

Figure S14 ^{1}H (top) and ^{13}C (bottom) NMR spectra of *tert*butyl 2-[(2,6-di(pyrazol-1-yl)pyridine)-4-carboxamido]propionate ($CDCl_3$).

X X

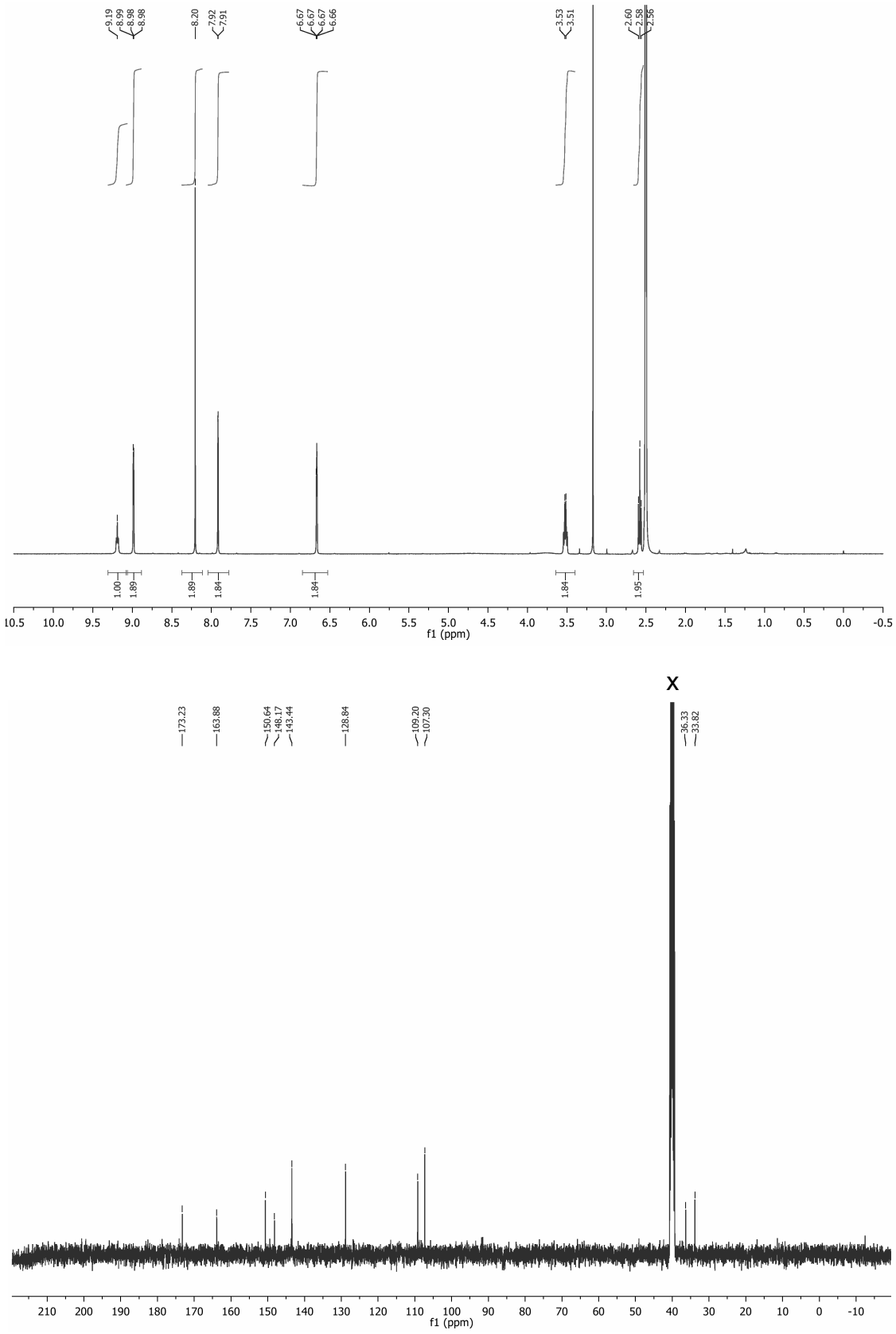

Figure S15 ^{1}H (top) and ^{13}C (bottom) NMR spectra of L^6 ({CD_3}$_2$SO).

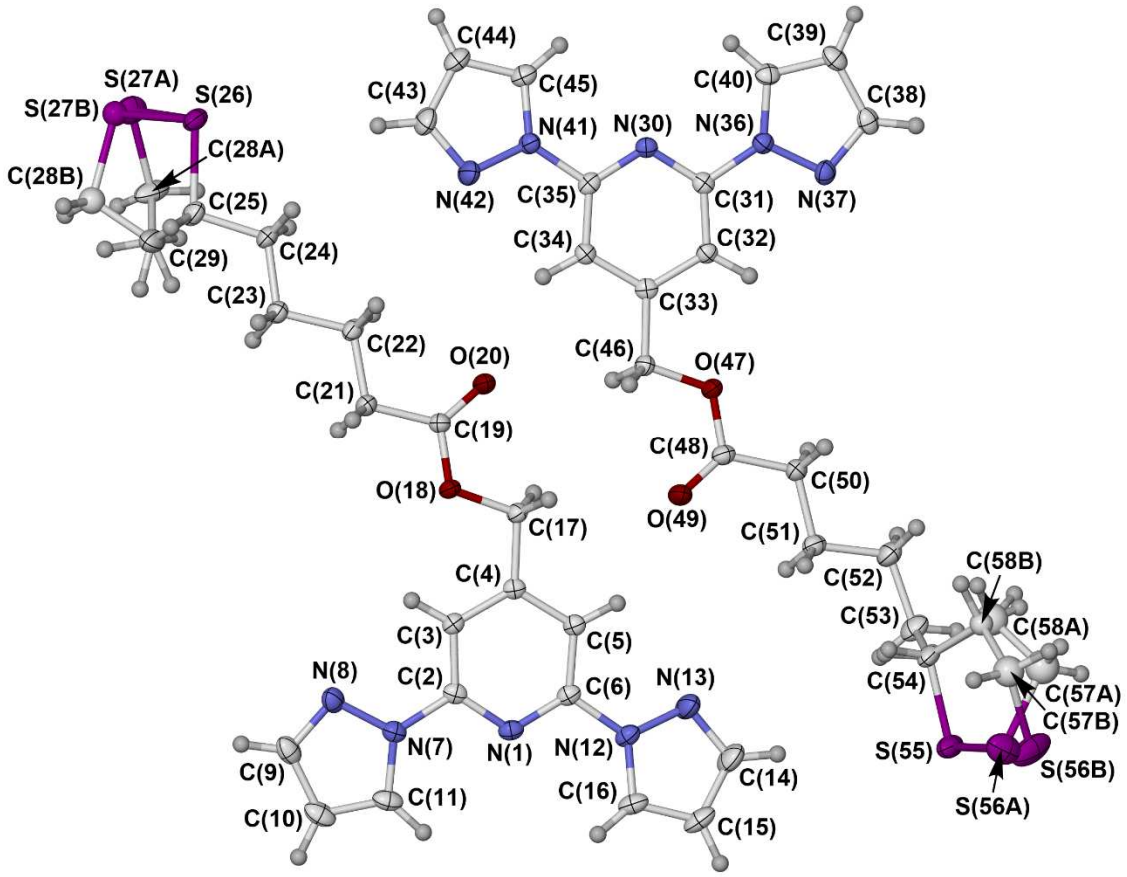

Figure S16 The asymmetric unit of L^1 showing the atom numbering scheme. Displacement ellipsoids are plotted at the 50 % probability level.

Colour code: C, white; H, pale grey; N, blue; O, red; S, purple.

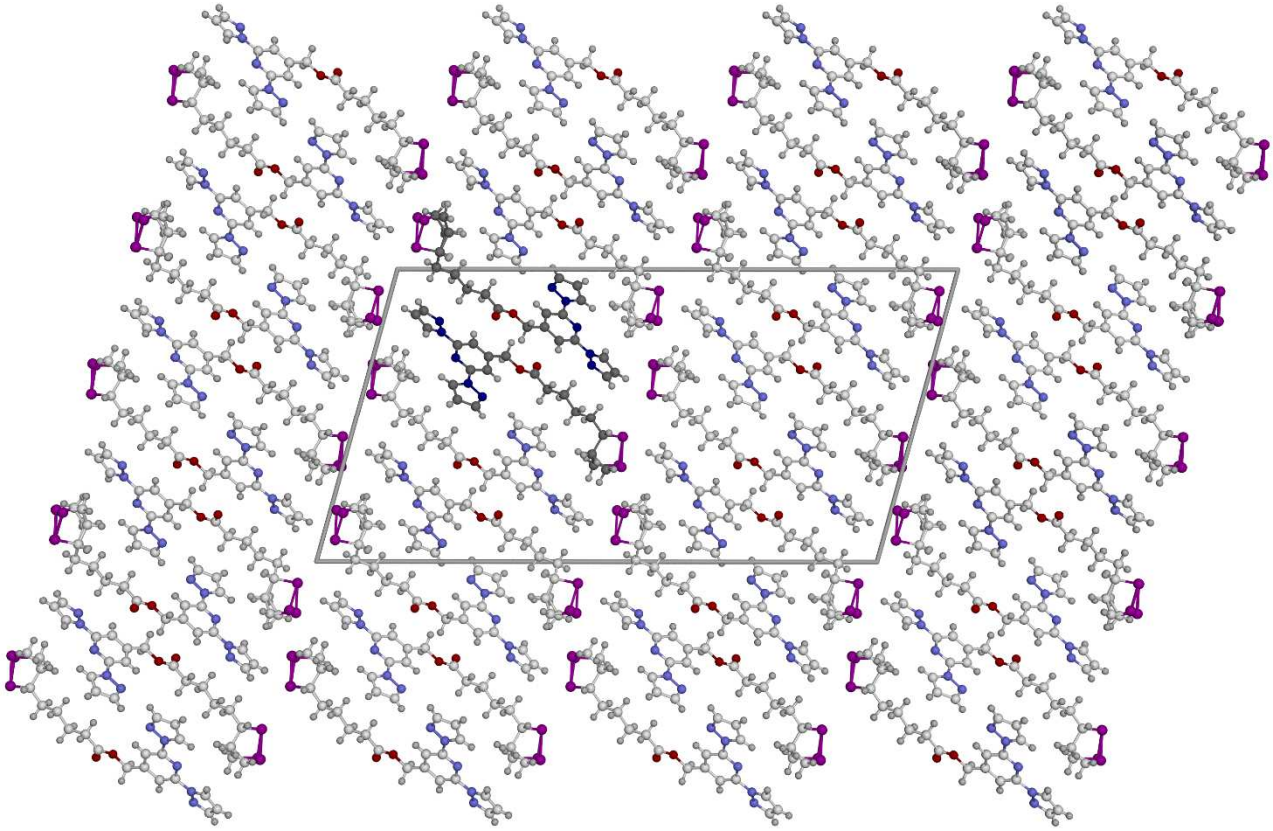

Figure S17 Packing diagram of L^1, viewed parallel to the [010] crystal vector with the unit cell *a* axis horizontal. Both orientations of the disordered dithiacyclopentyl group are included in the diagram.

One molecule from each environment in the asymmetric unit is highlighted with dark colouration.

Colour code: C, white or dark grey; H, pale grey; N, pale or dark blue; O, red; S, purple.

Molecules [N(1)-C(29)] and [N(30)-C(58)] are arranged separately into canted stacks, by translation along *b*. Adjacent molecules in the stacks are horizontally offset so there is no direct $\pi\cdots\pi$ overlap between their heterocyclic rings.

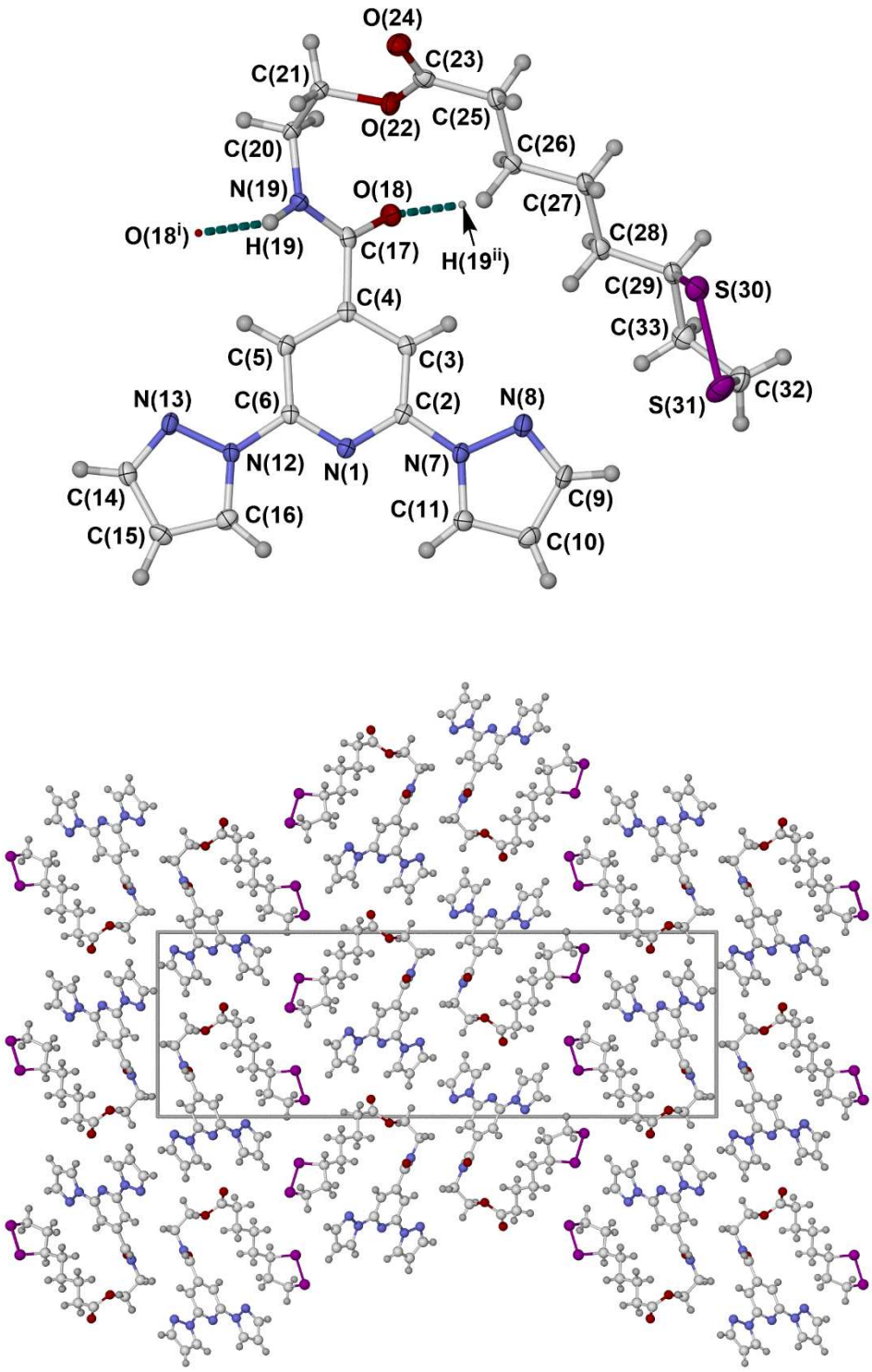

Figure S18 Top: the asymmetric unit of L^2showing the atom numbering scheme. Displacement ellipsoids are plotted at the 50 % probability level. Bottom: Packing diagram of L^2, viewed parallel to the [100] crystal vector with *c* horizontal. The top view is the same as in Figure 1 of the main article. Symmetry codes: (i) 1+*x*, *y*, *z*; (ii) −1+*x*, *y*, *z*.

Colour code: C, white; H, pale grey; N, blue; O, red; S, purple.

The molecules associate into hydrogen bonded chains by translation along *a*. These chains are oriented perpendicular to the plane of the packing diagram.

The dimensions of the intermolecular hydrogen bond are N(19)−H(19) = 0.88 Å, H(19)···O(18^{i}) = 2.06 Å, N(19)···O(18^{i}) = 2.892(3) Å and N(19)−H(19)···O(18^{i}) = 158.2°.

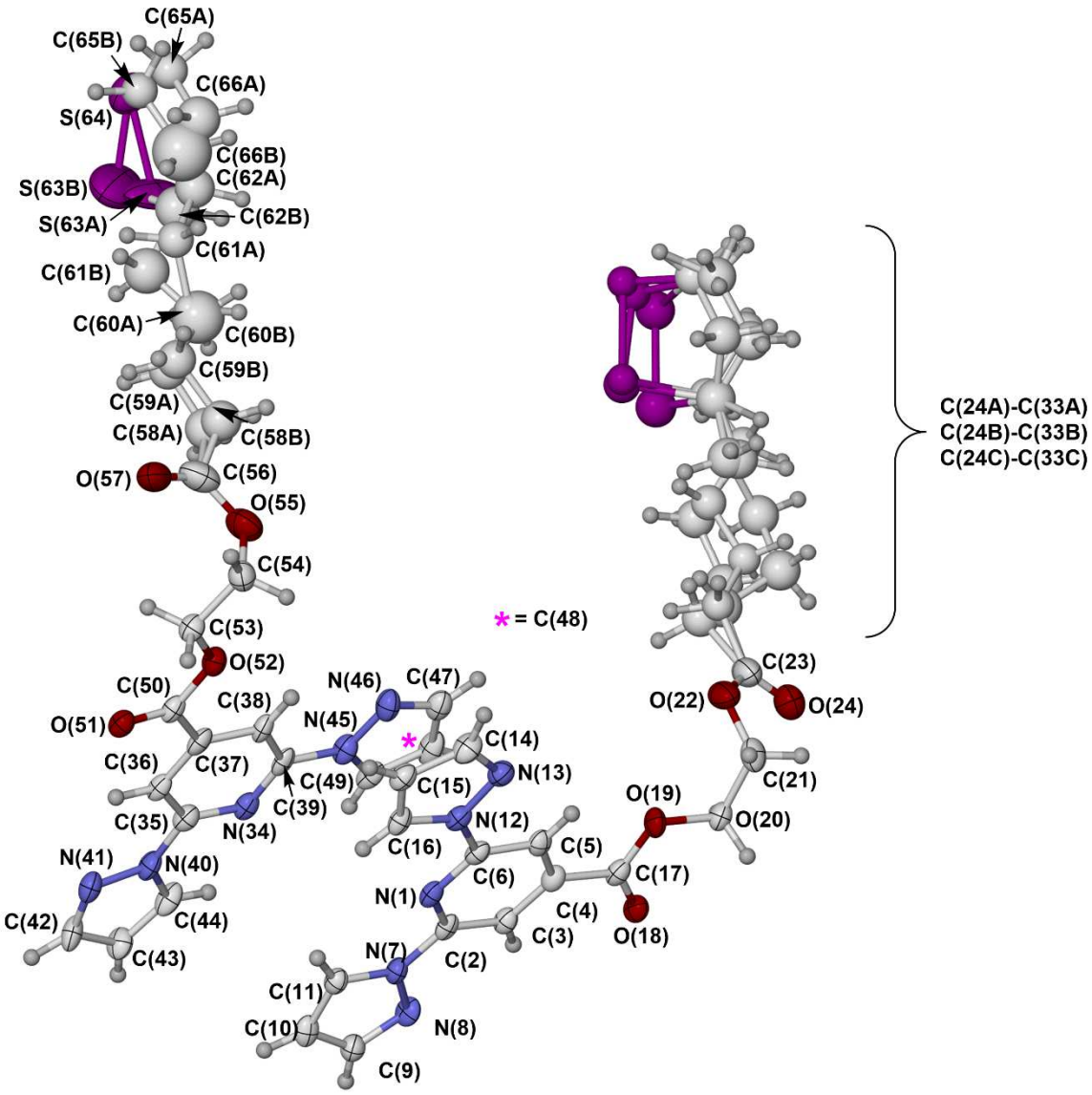

Figure S19 The asymmetric unit of L^3 showing the atom numbering scheme. Displacement ellipsoids are plotted at the 50 % probability level.

Colour code: C, white; H, pale grey; N, blue; O, red; S, purple.

The lipoate chains are disordered over three [molecule N(1)-C(33)] or two [molecule N(34)-C(66)] orientations. Individual atom labels are not given for the three-fold disordered atoms.

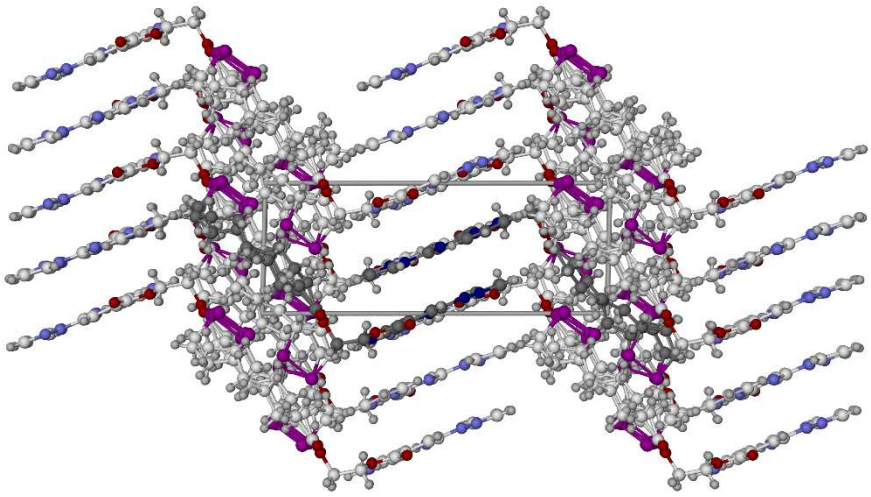

Figure S20 Packing diagram of L^3, showing its lipid bilayer-like crystal packing. The views is parallel to the [010] crystal vector, with *c* horizontal. All orientations of the disordered lipoate residues are included in the diagrams.

One molecule from each environment in the asymmetric unit is highlighted with dark colouration.

Colour code: C, white or dark grey; H, pale grey; N, pale or dark blue; O, red; S, purple.

An alternative view of this crystal packing is in Figure 2 of the main article.

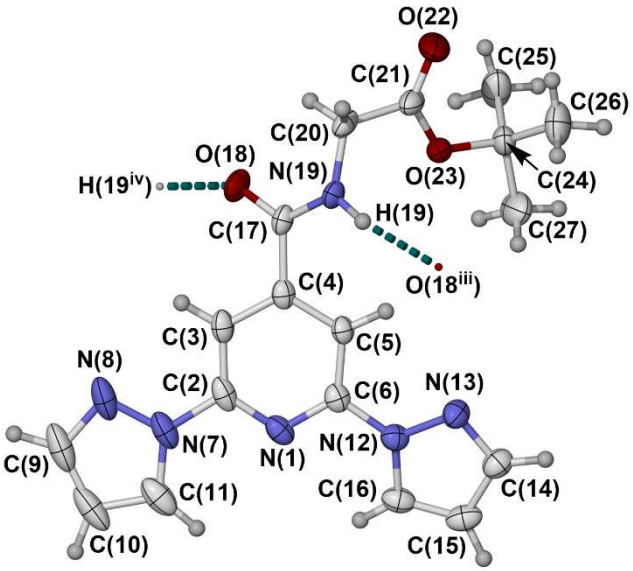

Figure S21 The asymmetric unit of *tert*butyl 2-[(2,6-di(pyrazol-1-yl)-pyridine)-4-carboxamido]acetate, showing the atom numbering scheme. Displacement ellipsoids are plotted at the 50 % probability level. Symmetry codes: (iii) ½−*x*, ½+*y*, *z*; (iv) ½−*x*, −½+*y*, *z*.

Colour code: C, white; H, pale grey; N, blue; O, red.

The dimensions of the intermolecular hydrogen bond are: N(19)−H(19) = 0.869(19) Å; H(19)···O(18^{iii}) = 2.052(19) Å; N(19)···O(18^{iii}) = 2.9083(14) Å; and N(19)−H(19)···O(18^{iii}) = 168.3(16)°.

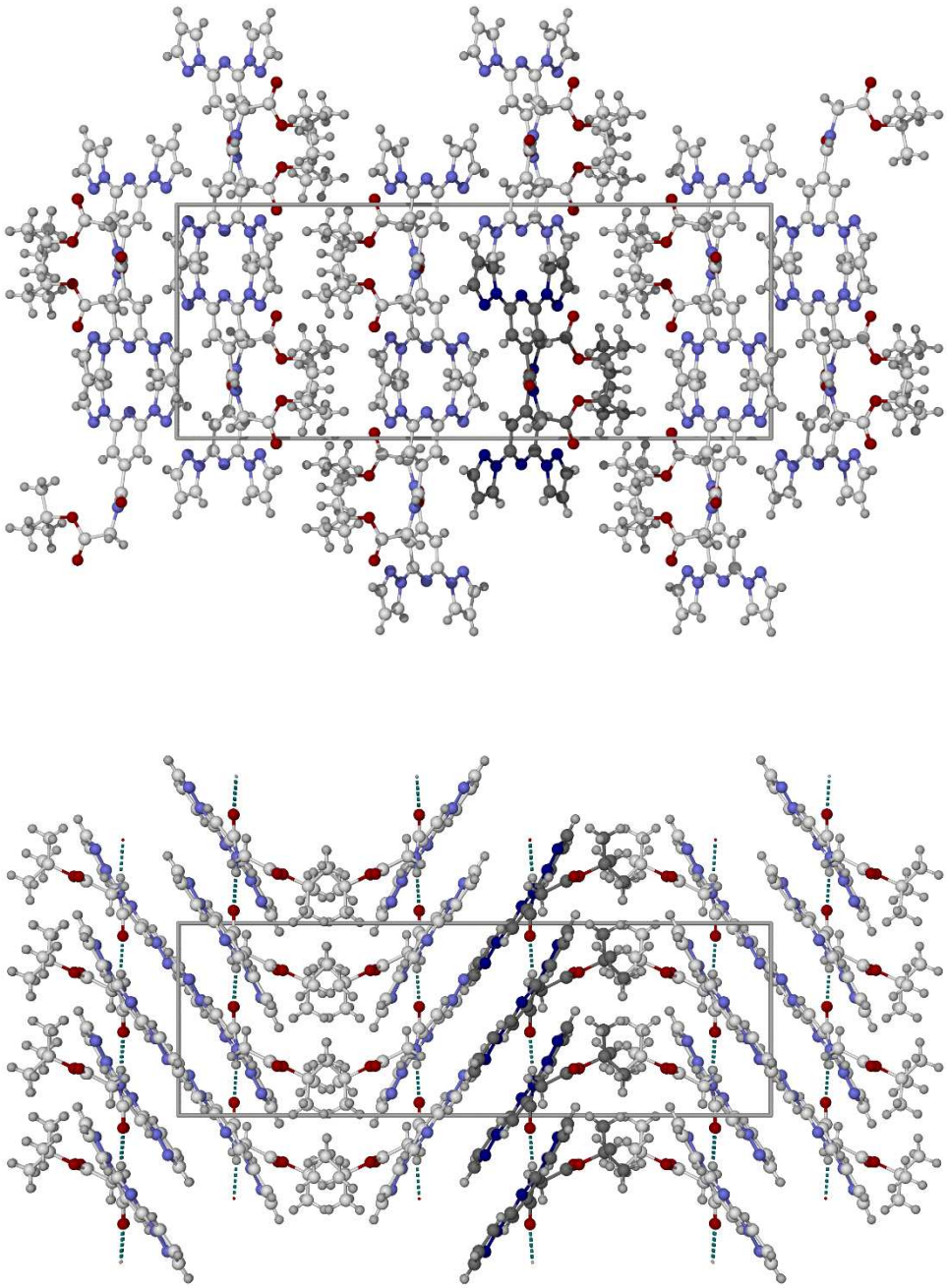

Figure S22 Packing diagrams of *tert*butyl 2-[(2,6-di(pyrazol-1-yl)-pyridine)-4-carboxamido]acetate, viewed parallel to the [010] crystal vector with *c* horizontal (top), and the [100] crystal vector with *c* horizontal (bottom).

The molecules associate into zig-zag hydrogen bonded chains *via* the crystallographic *b* glide plane, which propagate along the *b* axis. One chain is highlighted with dark colouration in the Figures, for clarity.

The overall packing resembles a lipid bilayer, with the heterocyclic and *tert*butyl residues segregated into bilayers oriented in the (002) crystal plane.

Definitions of the structural parameters in Tables S3 and S6.

V_{Oh} is the volume (in Å^3) of the FeN_6 coordination octahedron in the complex,[3] which is typically <10 Å^3 in low-spin $[Fe(bpp)_2]^{2+}$ (bpp = 2,6-di{pyrazol-1-yl}pyridine) derivatives and ≥11.5 Å^3 in their high-spin form.[4]

Σ and Θ are defined as follows:

$$\Sigma = \sum_{i=1}^{12} |90 - \beta_i| \qquad \Theta = \sum_{j=1}^{24} |60 - \gamma_j|$$

where β_i are the twelve *cis*-N–Fe–N angles about the iron atom and γ_i are the 24 unique N–Fe–N angles measured on the projection of two triangular faces of the octahedron along their common pseudo-threefold axis (Scheme S6). Σ is a general measure of the deviation of a metal ion from an ideal octahedral geometry, while Θ more specifically indicates its distortion towards a trigonal prismatic structure. A perfectly octahedral complex gives $\Sigma = \Theta = 0$.[3,5]

Because the high-spin state of a complex has a much more plastic structure than the low-spin, this is reflected in Σ and Θ which are usually much larger in the high-spin state. The absolute values of these parameters depend on the metal/ligand combination in the compound under investigation, however. Typical values of these parameters for complexes related to $[FeL_2]^{2+}$ are given in refs. 6 and 7.

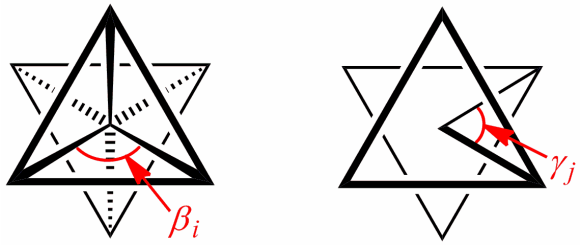

Scheme S6 Angles used in the definitions of the coordination distortion parameters Σ and Θ.

The parameters in Scheme S7 define the magnitude of an angular Jahn-Teller distortion, that is often observed in high-spin $[Fe(bpp)_2]^{2+}$ derivatives like $[FeL_2]^{2+}$ ($\theta \leq 90°$, $\phi \leq 180°$).[6-8] They are also a useful indicator of the molecular geometry, in defining the disposition of the two ligands around the metal ion. Spin-crossover can be inhibited if θ and ϕ deviate too strongly from their ideal values, because the associated rearrangement to a more regular low-spin coordination geometry ($\theta \approx 90°$, $\phi \approx 180°$) cannot be accommodated by a rigid solid lattice.[8,9] In less distorted examples, significant changes in θ and ϕ between the spin states can be associated with enhanced SCO cooperativity.[10]

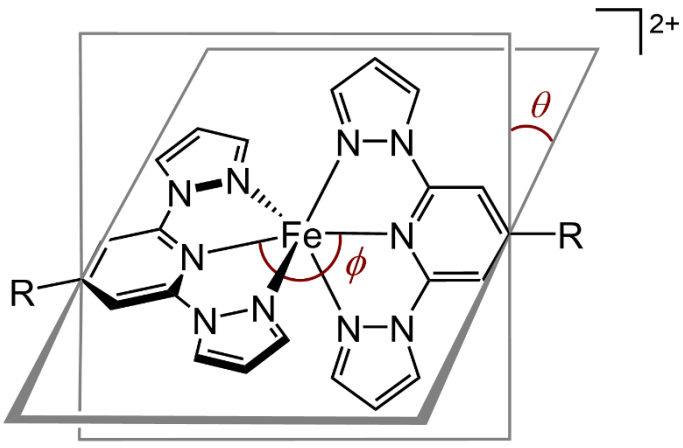

Scheme S7 θ and ϕ, used to discuss the structures of $[FeL_2]^{2+}$.

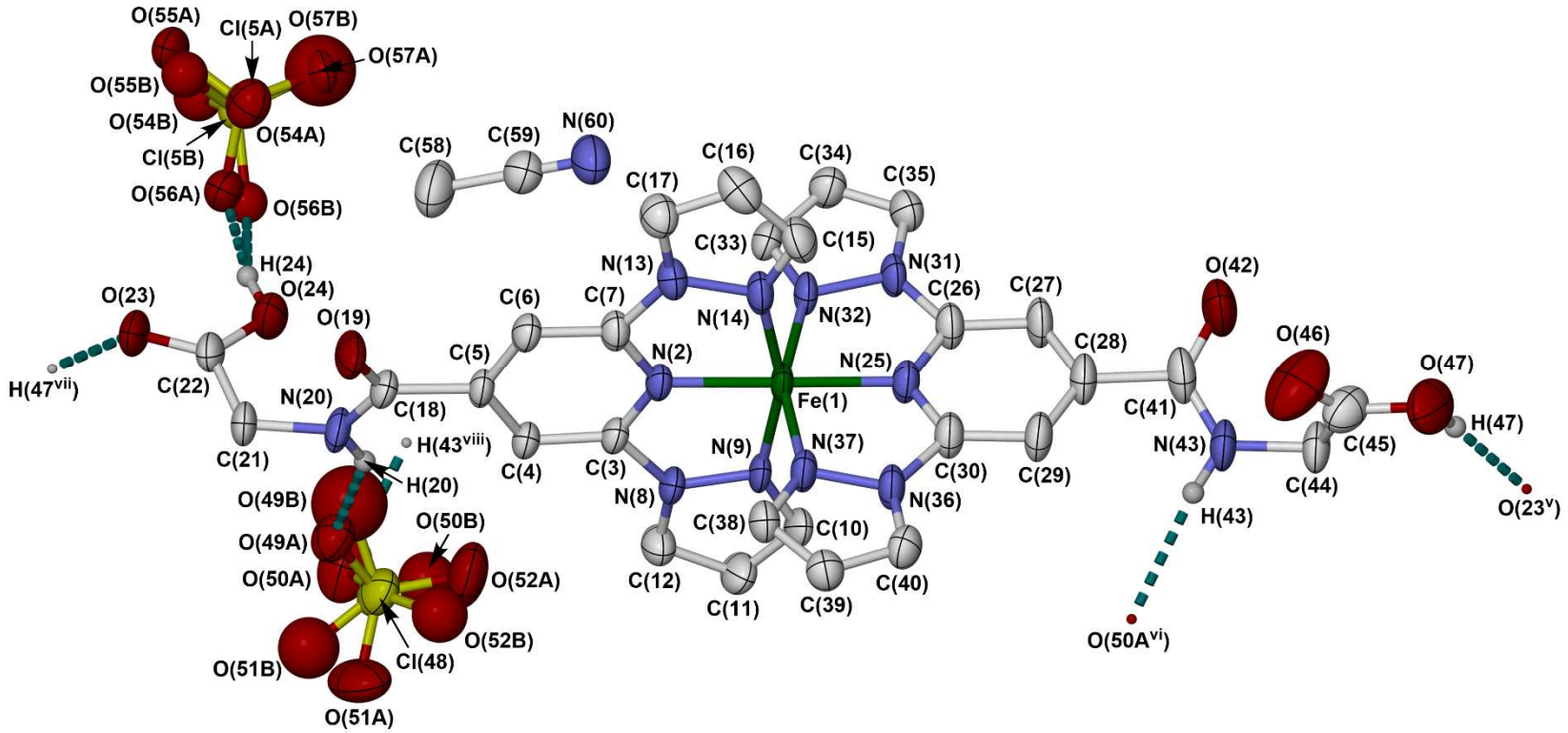

Figure S23 The asymmetric unit of the monoclinic pseudopolymorph $[Fe(L^5)_2][ClO_4]_2 \cdot MeCN$ at 120 K, with the full atom numbering scheme. Displacement ellipsoids are at the 50 % probability level, and C-bound H atoms are omitted. Symmetry codes: (v) $^3/_2+x$, $^3/_2-y$, $^1/_2+z$; (vi) $1+x$, y, z; (vii) $-^3/_2+x$, $^3/_2-y$, $-^1/_2+z$; (viii) $-1+x$, y, z.

Colour code: C, white; H, pale grey; Cl, yellow; Fe, green; N, blue; O, red.

Table S3 Selected bond lengths, angles and other structural parameters (Å , °, Å^3) for [Fe(L^5)$_2$][ClO$_4$]$_2$·MeCN. See Figure S23 for the atom numbering scheme, while definitions of V_{Oh}, Σ, Θ, φ and θ are given on page S33.

T / K	120 K	330 K		120 K	330 K
Fe(1)–N(2)	1.896(3)	2.051(4)	Fe(1)–N(25)	1.907(3)	2.051(4)
Fe(1)–N(9)	1.985(3)	2.097(5)	Fe(1)–N(32)	1.986(3)	2.113(5)
Fe(1)–N(14)	1.981(4)	2.109(6)	Fe(1)–N(37)	1.979(3)	2.113(5)
N(2)–Fe(1)–N(9)	80.08(12)	75.95(17)	N(9)–Fe(1)–N(37)	92.01(15)	93.5(2)
N(2)–Fe(1)–N(14)	80.20(13)	75.23(18)	N(14)–Fe(1)–N(25)	99.25(14)	107.28(18)
N(2)–Fe(1)–N(25)	179.44(15)	177.10(18)	N(14)–Fe(1)–N(32)	91.58(14)	94.58(19)
N(2)–Fe(1)–N(32)	100.57(12)	106.34(17)	N(14)–Fe(1)–N(37)	91.00(14)	92.4(2)
N(2)–Fe(1)–N(37)	99.82(13)	102.90(17)	N(25)–Fe(1)–N(32)	79.33(13)	75.10(17)
N(9)–Fe(1)–N(14)	160.28(12)	151.18(17)	N(25)–Fe(1)–N(37)	80.27(13)	75.71(16)
N(9)–Fe(1)–N(25)	100.48(13)	101.51(17)	N(32)–Fe(1)–N(37)	159.59(12)	150.76(16)
N(9)–Fe(1)–N(32)	92.35(14)	93.9(2)			
V_{Oh}	9.665(10)	11.375(17)	φ	179.44(15)	177.10(18)
Σ	87.2(5)	130.4(6)	θ	89.70(3)	88.92(6)
Θ	286	428			

Table S4 Hydrogen bond parameters (Å , °) for [Fe(L^5)$_2$][ClO$_4$]$_2$·MeCN. Symmetry codes: (v) $^3/_2+x$, $^3/_2-y$, $^1/_2+z$; (vi) $1+x$, y, z.

	X−H (X = N or O)	H···O	X···O	X−H···O
T = 120 K				
N(20)−H(20)···O(49A)/O(49B)	0.88	2.20/2.40	2.917(5)/3.12(4)	138.9/139.8
O(24)−H(24)···O(56A)/O(56B)	0.84	1.84/1.72	2.658(5)/2.48(2)	165.3/149.8
N(43)−H(43)···O(50A^{vi})	0.88	2.19	3.070(7)	173.6
O(47)−H(47)···O(23^{v})	0.84	1.86	2.674(6)	164.3
T = 330 K				
N(20)−H(20)···O(49A)/O(49B)/O(49C)	0.86	2.21/2.20/2.30	2.971(17)/2.955(16)/3.019(14)	147.2/147.0/141.2
O(24)−H(24)···O(56A)/O(56C)[a]	0.82	1.88/1.88	2.70(2)/2.668(16)	172.7/162.0
N(43)−H(43)···O(49A^{vi})[a]	0.86	2.38	3.22(2)	165.8
O(47)−H(47)···O(23^{v})	0.82	1.85	2.656(10)	166.8

[a]The other disorder sites of this anion do not lie within hydrogen bonding distance of this interaction.

Hydrogen bond parameters donated by the carboxylic acid groups should be interpreted with caution. The *SHELXL* AFIX 83 instruction for O−H groups imposes a 109.5 C−O−H bond angle, which is unrealistic for a carboxylic acid O−H group.

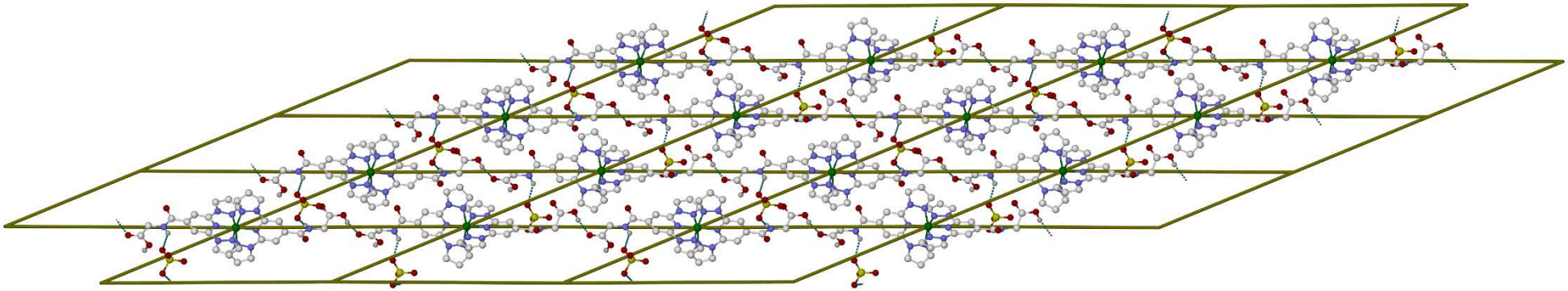

Figure S24 The 4^4 2D hydrogen bond network topology in monoclinic $[Fe(L^5)_2][ClO_4]_2 \cdot MeCN$ at 120 K. Anion Cl(53)-O(57) and the solvent molecule, which don't contribute to the network topology, are omitted from the plot as are all C-bound H atoms are omitted from the diagram. Network connections between molecules linked by hydrogen bonds are shown with a gold colouration. Colour code: C, white; H, pale grey; Cl, yellow; Fe, green; N, blue; O, red.

A full view of the hydrogen bond layers, without the connections marked, is in Figure 3 of the main article.

Table S5 Intermolecular $\pi\cdots\pi$ interaction parameters (Å , °) for $[Fe(L^5)_2][ClO_4]_2$·MeCN. Symmetry codes: (ix) $^3/_2-x$, $-^1/_2+y$, $^1/_2-z$.

	Dihedral angle	Interplanar distance	Horizontal offset
T = 120 K			
[N(13)–C(17)]···[N(36^{ix})–C(40^{ix})]	7.3(3)	3.277(17)	2.43
T = 330 K			
[N(13)–C(17)]···[N(36^{ix})–C(40^{ix})]	7.6(5)	3.29(3)	2.46

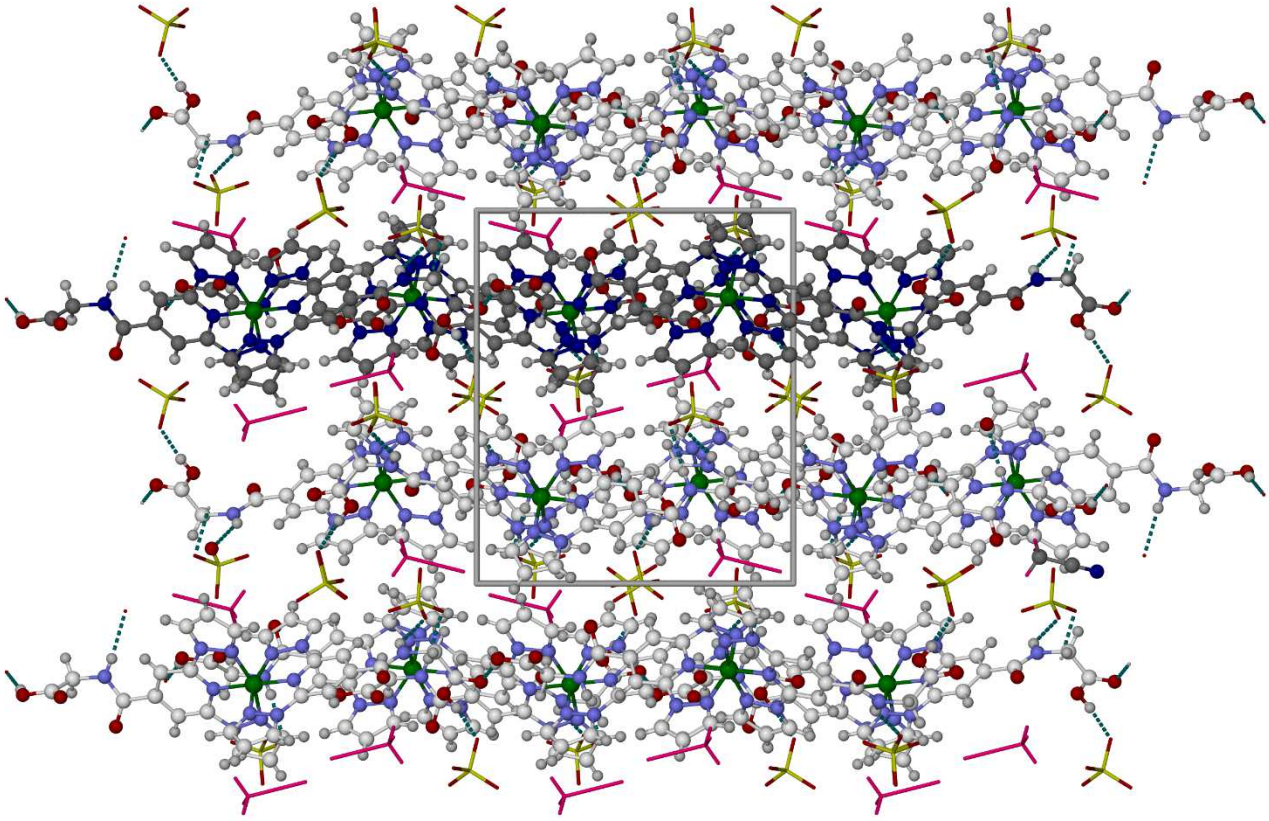

Figure S25 Packing diagram of monoclinic $[Fe(L^5)_2][ClO_4]_2$·MeCN at 120 K, viewed along the [001] crystal vector with *a* horizontal. One hydrogen bonded layer of molecules is highlighted with dark colouration (Figure 3, main article), and only the major orientation of the disordered anions is included. The anions and solvent are de-emphasised for clarity.

Colour code: C{complex}, white or dark grey; H, pale grey; Cl, yellow; Fe, green; N{complex}, pale or dark blue; O, red; MeCN, purple.

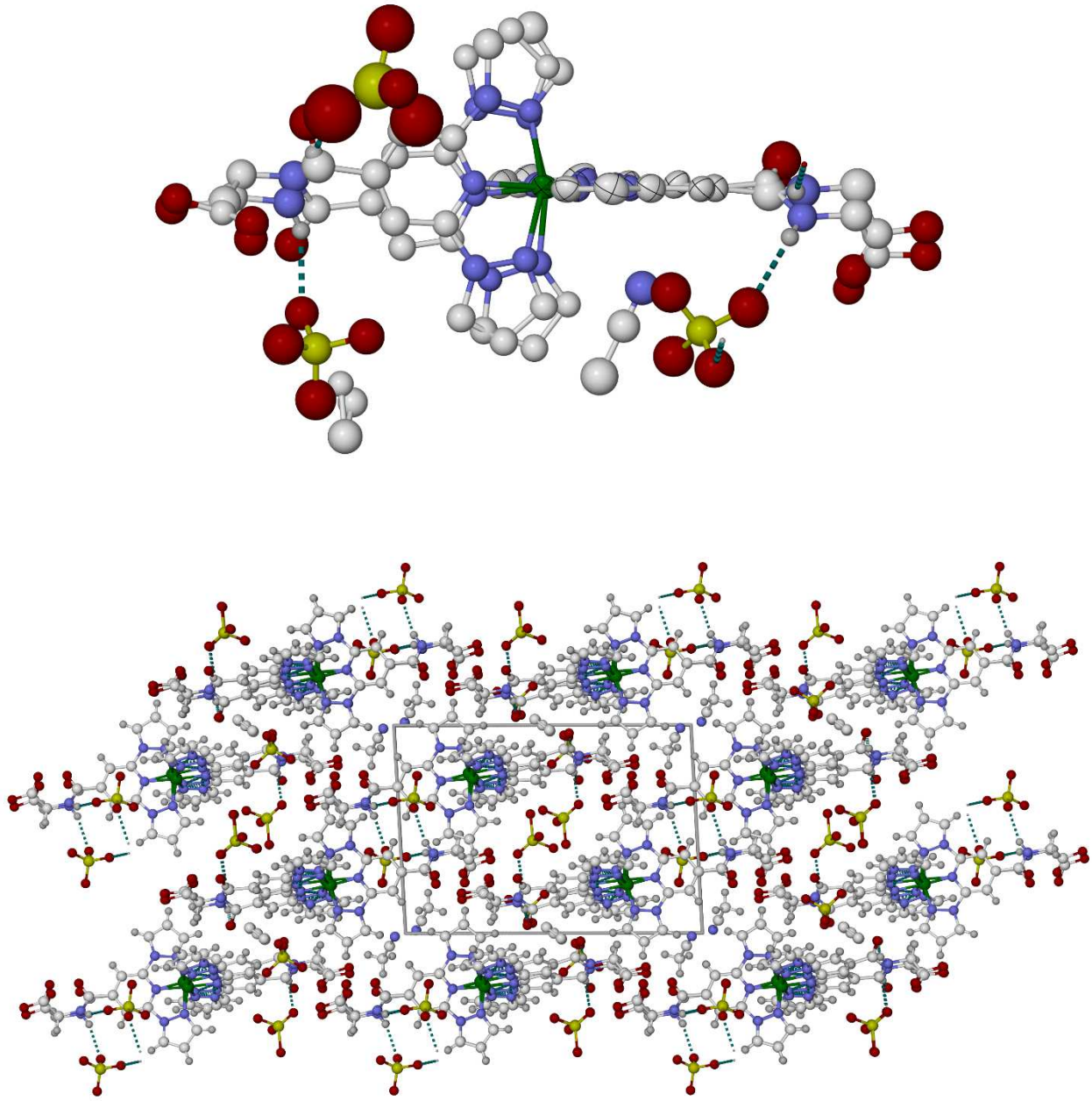

Figure S26 Top: preliminary structure solution of the triclinic form of $[Fe(L^5)_2][ClO_4]_2{\cdot}x$MeCN at 120 K. Displacement ellipsoids are at the 50 % probability level, and C-bound and O-bound H atoms are omitted (the carboxylic acid O−H hydrogen atoms were not unambiguously located in the model). Bottom: packing diagram of the compound, viewed parallel to [100] with the *c* horizontal.

Colour code: C, white; H, pale grey; Cl, yellow; Fe, green; N, blue; O, red.

The only crystallographically ordered residues are the *tris*-heterocyclic core of one L^5 ligand, one ClO_4^- ion and the resolved acetonitrile molecule. All other atoms, including the iron atom and the two remaining anion sites, are half-occupied or disordered over at least two sites. The triangle of C atoms spans the crystallographic inversion centre, and is probably another unresolved half-molecule solvent site. There are no solvent-accessible cavities in the lattice. Rather, the cation disorder reflects the disposition of nearest neighbour hydrogen-bond acceptor residues, which induces disorder in both *N*-carboxamidoacetic acid substituents.

The two half-occupied iron atoms in the model show V_{Oh} = 9.27(3) and 9.72(4) Å^3, confirming that both cation disorder sites are low-spin at this temperature (page S33).

The refinement residuals of the model in the Figure are R_1 [$I > 2\sigma(I)$] = 0.138 and wR_2 [all data] = 0.415, from 7516 reflections. This structure solution was used to generate the powder pattern simulation in Figure S37, but it has not been deposited with the CCDC.

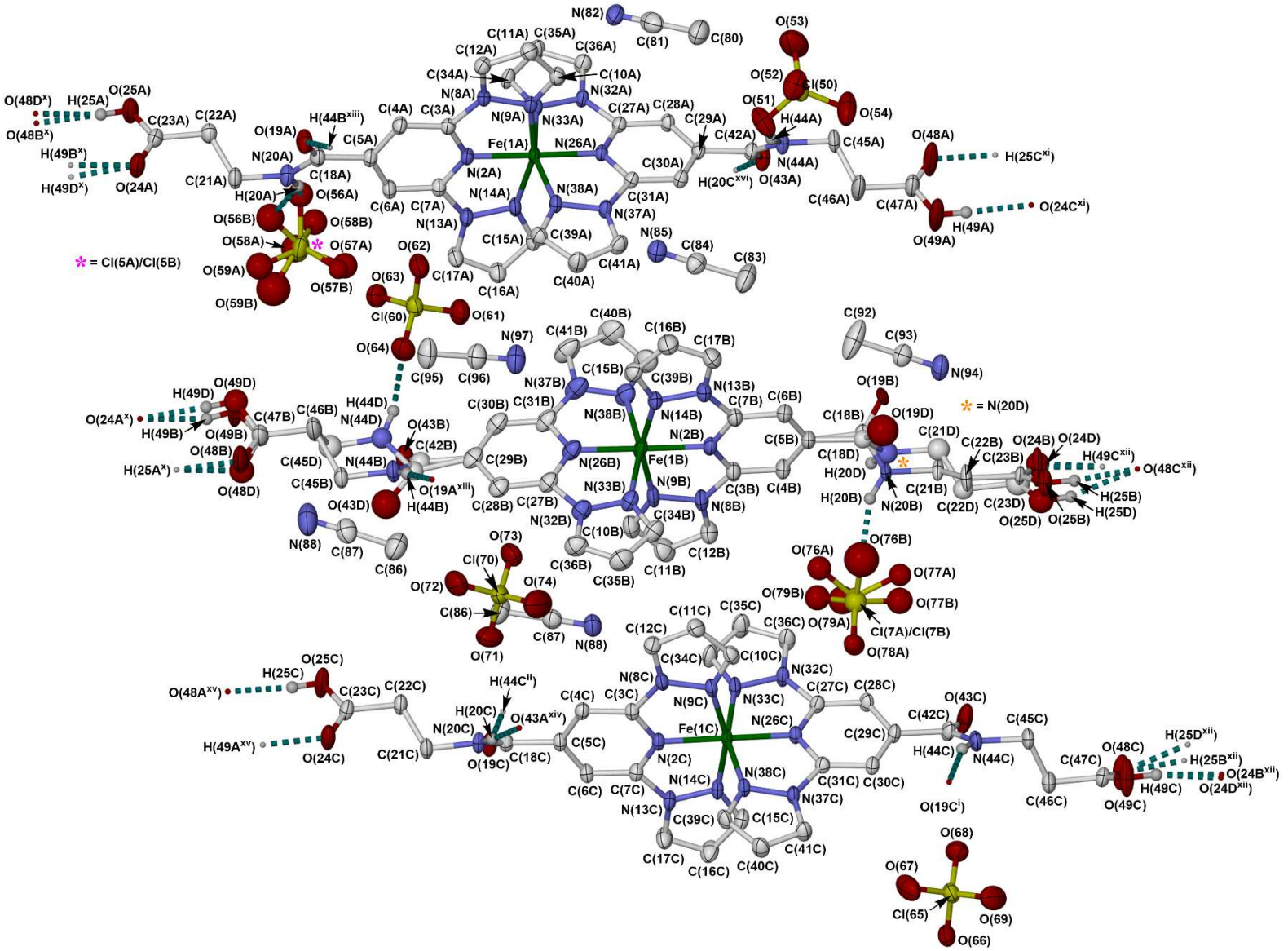

Figure S27 The asymmetric unit of $[Fe(L^6)_2][ClO_4]_2 \cdot 2MeCN$ at 120 K, with the full atom numbering scheme. Displacement ellipsoids are at the 50 % probability level, and C-bound H atoms are omitted. Symmetry codes: (i) 1+*x*, *y*, *z*; (ii) −1+*x*, *y*, *z*; (x) −1−*x*, 1−*y*, 1−*z*; (xi) 1+*x*, 1+*y*, *z*; (xii) 3−*x*, 1−*y*, −*z*; (xiii) −*x*, 1−*y*, 1−*z*; (xiv) *x*, −1+*y*, *z*; (xv) −1+*x*, −1+*y*, *z*; (xvi) *x*, 1+*y*, *z*. Colour code: C, white; H, pale grey; Cl, yellow; Fe, green; N, blue; O, red.

Table S6 Selected bond lengths, angles and other structural parameters (Å , °, Å^3) for [Fe(L^6)$_2$][ClO$_4$]$_2$·2MeCN. See Figure S27 for the atom numbering scheme, while definitions of V_{Oh}, Σ, Θ, φ and θ are given on page S33.

T / K		120 K			290 K	
	Molecule A	Molecule B	Molecule C	Molecule A	Molecule B	Molecule C
Fe(1)–N(2)	1.883(2)	1.927(2)	1.902(2)	1.892(4)	2.044(4)	1.980(4)
Fe(1)–N(9)	1.978(3)	2.003(3)	1.988(3)	1.971(5)	2.109(6)	2.044(5)
Fe(1)–N(14)	1.964(3)	1.991(3)	1.978(3)	1.971(5)	2.099(6)	2.038(5)
Fe(1)–N(26)	1.888(2)	1.903(3)	1.902(2)	1.905(4)	2.040(6)	1.974(4)
Fe(1)–N(33)	1.980(3)	1.988(3)	1.970(3)	1.995(6)	2.084(7)	2.034(5)
Fe(1)–N(38)	1.969(3)	1.995(3)	1.983(3)	1.972(5)	2.130(8)	2.042(5)
N(2)–Fe(1)–N(9)	80.40(10)	79.02(11)	79.77(10)	80.1(2)	75.29(19)	77.50(17)
N(2)–Fe(1)–N(14)	80.45(11)	79.10(11)	80.01(10)	80.2(2)	75.8(2)	77.66(17)
N(2)–Fe(1)–N(26)	179.01(11)	178.49(12)	177.26(11)	179.3(2)	179.5(3)	176.03(18)
N(2)–Fe(1)–N(33)	99.79(10)	101.90(11)	98.40(10)	100.2(2)	104.2(2)	99.30(18)
N(2)–Fe(1)–N(38)	99.48(10)	99.03(12)	101.91(10)	100.16(19)	105.1(2)	105.30(17)
N(9)–Fe(1)–N(14)	160.78(10)	158.11(10)	159.79(10)	160.3(2)	151.07(19)	155.16(17)
N(9)–Fe(1)–N(26)	98.61(10)	100.38(12)	102.37(10)	99.4(2)	104.6(2)	104.97(17)
N(9)–Fe(1)–N(33)	93.18(11)	92.34(12)	89.89(11)	92.5(2)	94.4(3)	90.22(19)
N(9)–Fe(1)–N(38)	91.34(11)	93.67(13)	93.92(11)	92.2(2)	95.6(2)	95.70(19)
N(14)–Fe(1)–N(26)	100.54(10)	101.51(12)	97.83(11)	100.4(2)	104.4(2)	99.82(18)
N(14)–Fe(1)–N(33)	91.67(11)	91.32(12)	93.00(11)	91.8(2)	91.7(3)	93.4(2)
N(14)–Fe(1)–N(38)	90.19(11)	90.58(13)	90.28(11)	90.3(2)	92.8(3)	91.1(2)
N(26)–Fe(1)–N(33)	80.30(10)	79.49(12)	79.97(10)	79.4(2)	76.3(3)	77.69(17)
N(26)–Fe(1)–N(38)	80.46(10)	79.61(12)	79.73(10)	80.23(19)	74.5(3)	77.70(17)
N(33)–Fe(1)–N(38)	160.68(10)	158.97(12)	159.68(10)	159.57(19)	150.6(3)	155.40(17)
V_{Oh}	9.506(10)	9.802(10)	9.620(8)	9.595(17)	11.30(2)	10.443(15)
Σ	83.2(4)	93.5(4)	88.3(4)	84.8(7)	130.8(7)	109.3(6)
Θ	274	307	290	286	429	359
φ	179.01(11)	178.49(12)	177.26(11)	179.3(2)	179.5(3)	176.03(18)
θ	88.78(3)	89.38(4)	85.35(3)	87.50(7)	89.84(9)	84.57(6)

Table S7 Hydrogen bond parameters (Å , °) for $[Fe(L^6)_2][ClO_4]_2 \cdot 2MeCN$. See Figure S27 for the atom numbering scheme. Symmetry codes: (i) 1+*x*, *y*, *z*; (x) −1−*x*, 1−*y*, 1−*z*; (xi) 1+*x*, 1+*y*, *z*; (xii) 3−*x*, 1−*y*, −*z*; (xiii) −*x*, 1−*y*, 1−*z*; (xiv) *x*, −1+*y*, *z*; (xv) −1+*x*, −1+*y*, *z*.

	X−H (X = N or O)	H···O	X···O	X−H···O
T = 120 K				
N(20A)−H(20A)···O(56A)/O(56B)	0.88	2.14/2.11	2.961(5)/2.819(9)	155.8/137.1
O(25A)−H(25A)···O(48B^{x})/O(48D^{x})	0.84	1.80/1.86	2.637(4)/2.693(2)	172.8/170.9
N(44A)−H(44A)···O(51)	0.88	2.10	2.959(3)	165.2
O(49A)−H(49A)···O(24C^{xi})	0.84	1.83	2.666(3)	174.5
N(20B)−H(20B)···O(76B)[a]	0.88	1.70	2.520(12)	153.8
O(25B)−H(25B)···O(48C^{xii})	0.84	1.78	2.610(4)	169.4
O(25D)−H(25D)···O(48C^{xii})	0.84	2.00	2.807(13)	161.2
N(44B)−H(44B)···O(19A^{xiii})	0.88	2.08	2.956(4)	174.6
N(44D)−H(44D)···O(64)	0.88	1.88	2.554(16)	132.5
O(49B)−H(49B)···O(24A^{x})	0.84	1.86	2.680(4)	163.2
O(49D)−H(49D)···O(24A^{x})	0.84	1.86	2.697(2)	174.7
N(20C)−H(20C)···O(43A^{xiv})	0.88	2.03	2.911(3)	175.5
O(25C)−H(25C)···O(48A^{xv})	0.84	1.82	2.653(3)	175.0
N(44C)−H(44C)···O(19C^{i})	0.88	2.10	2.954(4)	162.1
O(49C)−H(49C)···O(24B^{xii})/O(24D^{xii})	0.84	1.82/1.79	2.654(9)/2.62(3)	172.5/167.7
T = 290 K				
N(20A)−H(20A)···O(56A)/O(56B)	0.88	2.13/2.48	2.909(12)/3.133(19)	147.0/131.8
O(25A)−H(25A)···O(48B^{x})	0.84	1.81	2.643(8)	173.2
N(44A)−H(44A)···O(51A)/O(51B)	0.88	2.15/2.15	2.992(13)/2.991(12)	159.7/159.8
O(49A)−H(49A)···O(24C^{xi})	0.84	1.82	2.657(7)	172.8
N(20B)−H(20B)···O(76B)[a]	0.88	2.31	2.843(11)	119.3
O(25B)−H(25B)···O(48C^{xii})	0.84	1.87	2.678(6)	160.3
N(44B)−H(44B)···O(19A^{xiii})	0.88	2.35	3.099(13)	143.7
O(49B)−H(49B)···O(24A^{x})	0.84	2.34[b]	2.650(9)	102.0[b]
N(20C)−H(20C)···O(43A^{xiv})	0.88	2.07	2.945(5)	173.0
O(25C)−H(25C)···O(48A^{xv})	0.84	1.84	2.683(6)	176.2
N(44C)−H(44C)···O(19C^{i})	0.88	2.17	3.038(8)	168.3
O(49C)−H(49C)···O(24B^{xii})	0.84	1.82	2.645(6)	165.9

[a]There is no acceptor within hydrogen bonding distance of the minor disorder site of this carboxamido group, N(20D)−H(20D). [b]The carboxylic acid H atom associated with this interaction did not refine to the optimal position for this hydrogen bond, at this temperature. That could reflect unresolved disorder in this propionic acid substituent.

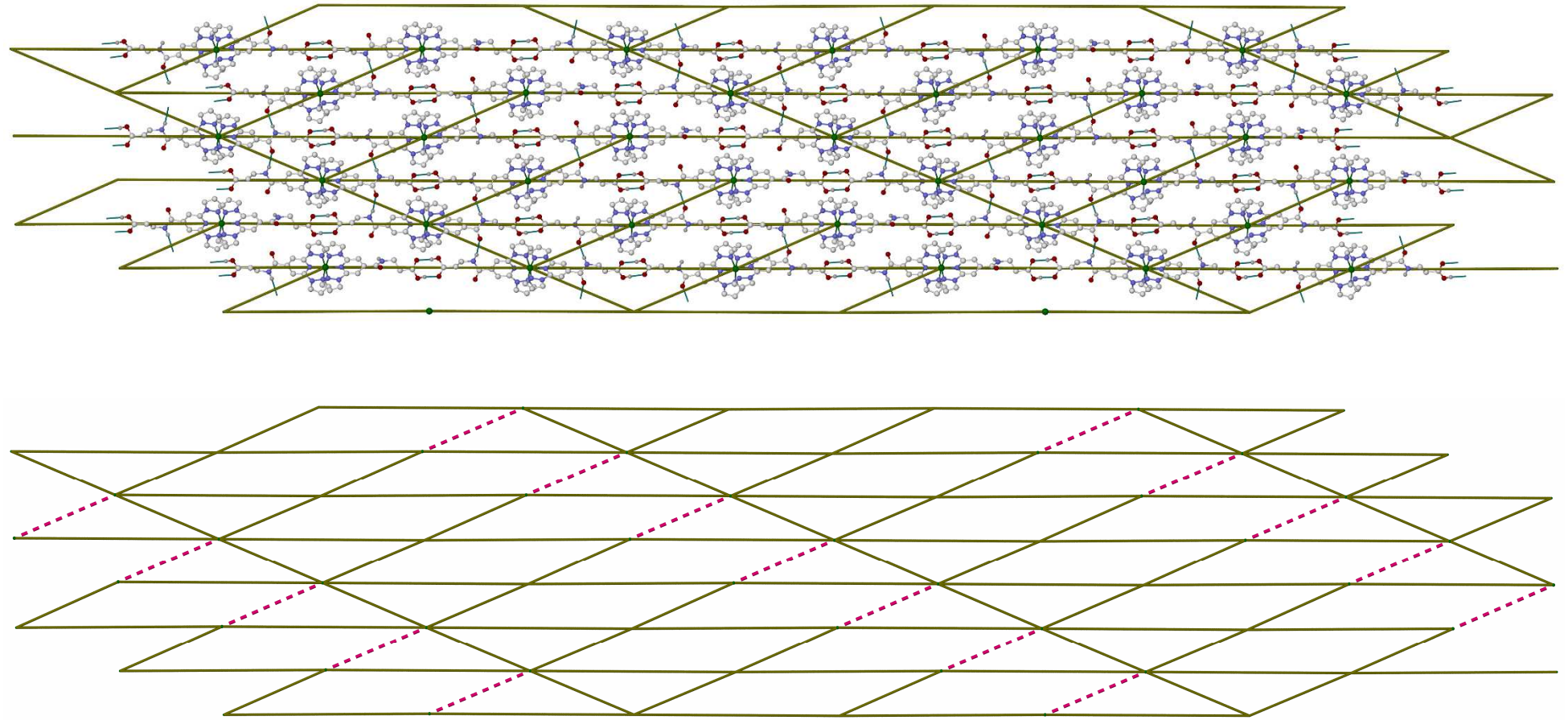

Figure S28 Top: The 2D hydrogen bond network topology in $[Fe(L^6)_2][ClO_4]_2 \cdot 2MeCN$ at 120 K. The view is similar to Figure 4 of the main article, but only the major ligand disorder sites of molecule B are included. Only hydrogen bonds that link cations together are shown, and anions, solvent and C-bound H atoms are omitted from the diagram. Network connections between molecules linked by hydrogen bonds are shown with a gold colouration. Colour code: C, white; H, pale grey; Cl, yellow; Fe, green; N, blue; O, red.

Bottom: the 6,4-connected $(3 \cdot 4^3)^2(3^2 \cdot 4 \cdot 3^2 \cdot 4)$ 2D topology from which the top network is derived, by removal of the dashed connections.

The molecule A sites are connected to four nearest neighbours, molecule B is three-connected and molecule C is five-connected. The resultant topology $(4 \cdot 3 \cdot 4 \cdot 5)(4 \cdot 5^2)(3 \cdot 4 \cdot 3 \cdot 5^2)$ in the short Schläfli notation (top).[32] In the minor disorder of one ligand in molecule B, one intercation hydrogen bond is cleaved so that molecule becomes 2-connected. That disorder site is 16 % occupied at 120 K.

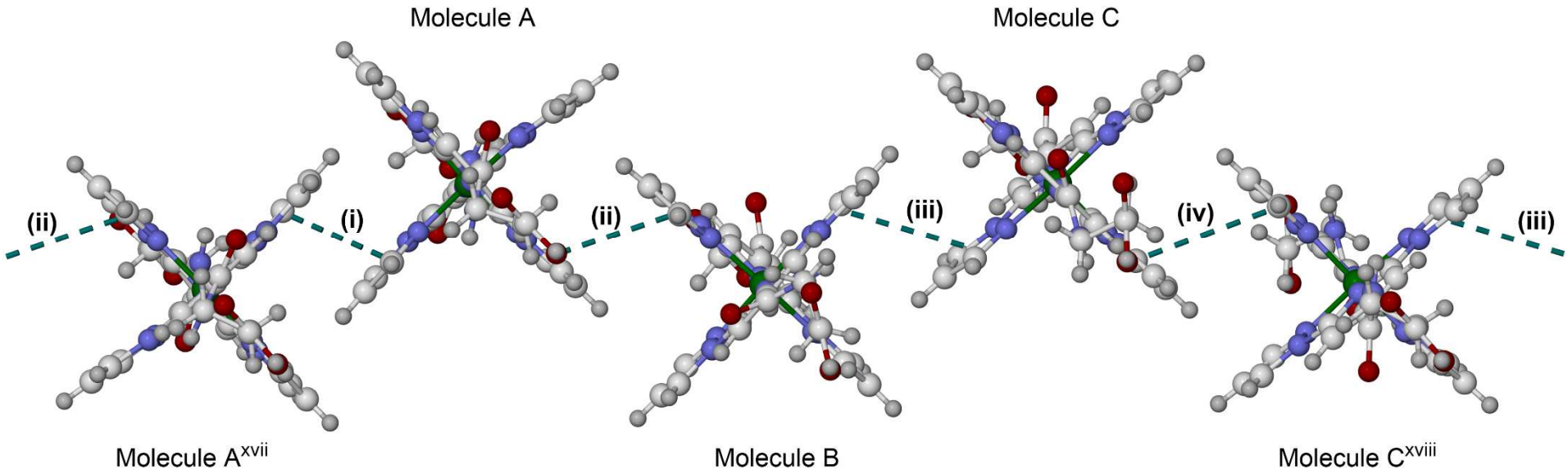

Figure S29 Partial packing diagram of $[Fe(L^6)_2][ClO_4]_2 \cdot 2MeCN$ at 120 K, showing the intermolecular $\pi \cdots \pi$ interactions between the hydrogen bonded molecular chains (Table S8). Only the major ligand disorder orientations of molecule B are included in the view. Symmetry codes: (xvii) $-x$, $2-y$, $1-z$; (xviii) $2-x$, $-y$, $-z$.

Colour code: C, white; H, pale grey; Fe, green; N, blue; O, red.

Interaction **iv** is too long to be considered a $\pi \cdots \pi$ interaction, with an interplanar spacing of 3.81(3) Å at 120 K and 3.72(7) Å at 290 K. It's included in the Figure for comparison with interaction **i** in Figure S30.

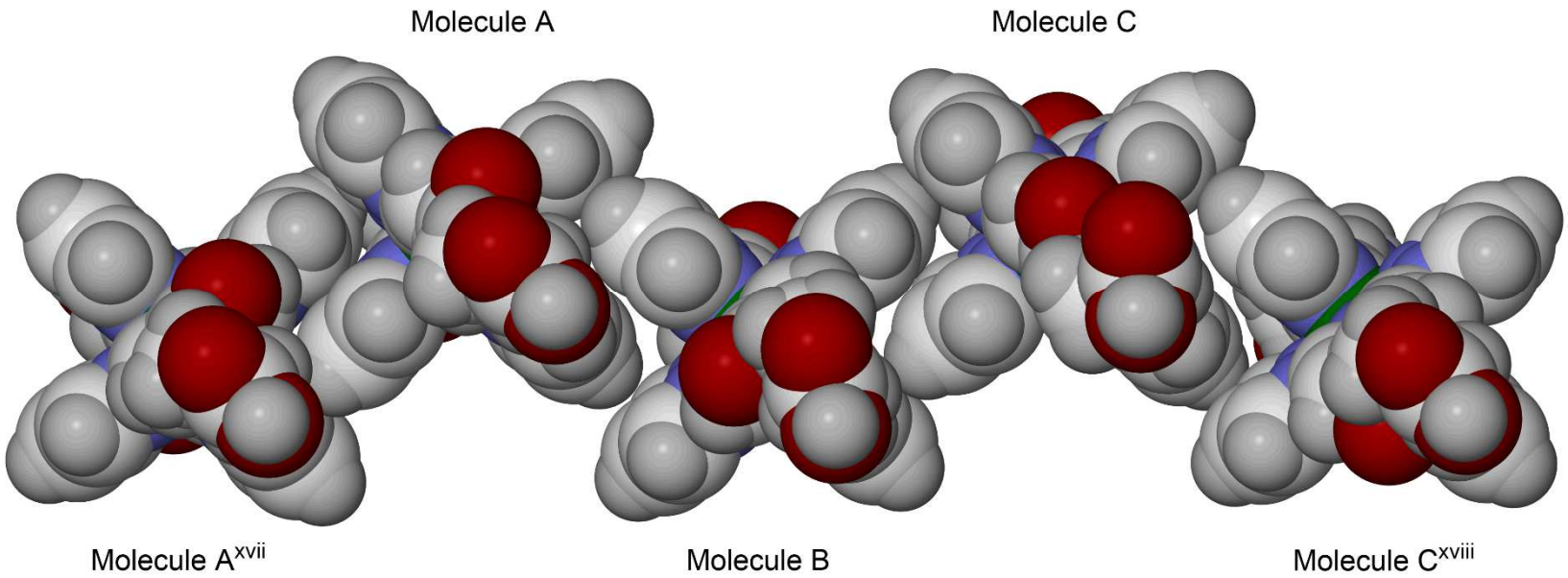

Figure S30 Space-filling view of the partial packing diagram of $[Fe(L^6)_2][ClO_4]_2 \cdot 2MeCN$ in Figure S29. Symmetry codes: (xvii) $-x, 2-y, 1-z$; (xviii) $2-x, -y, -z$.

The more intimate $\pi \cdots \pi$ and C−H$\cdots\pi$ contacts between molecule A and its symmetry equivalent A^{xvii} (interaction **i**, Figure S29) might explain why molecule A remains low-spin when the compound is warmed, while molecules B and C undergo gradual SCO. The close contact between two A cation sites could inhibit SCO to their high-spin form, which would require those two molecules to expand against each other.

The equivalent contact between molecules C and C^{xviii} (interaction **iv**, Figure S29) is more open, allowing molecule C to undergo thermal SCO as observed.

Table S8 Intermolecular $\pi\cdots\pi$ interaction parameters (Å , °) for $[Fe(L^6)_2][ClO_4]_2\cdot 2MeCN$. The Roman number labels refer to the equivalent interactions in Figure S29. Symmetry code: (xvii) $-x$, $2-y$, $1-z$.

	Dihedral angle	Interplanar distance	Horizontal offset
T = 120 K			
[N(8A)−C(12A)]···[N(8A^{xvii})−C(12A^{xvii})] (**i**)	0	3.17(5)	1.52
[N(37A)−C(41A)]···[N(37B)−C(41B)] (**ii**)	5.14(19)	3.461(16)	2.11
[N(8B)−C(12B)]···[N(8C)−C(12C)] (**iii**)	8.4(2)	3.303(11)	2.28
T = 290 K			
[N(8A)−C(12A)]···[N(8A^{xvii})−C(12A^{xvii})] (**i**)	0	3.31(11)	1.66
[N(37A)−C(41A)]···[N(37B)−C(41B)] (**ii**)[a]	6.1(5)	3.65(4)	1.95
[N(8B)−C(12B)]···[N(8C)−C(12C)] (**iii**)	8.5(5)	3.38(2)	2.28

[a]The sum of the Pauling van der Waals radii of two aromatic rings is 3.4 Å.[11] On that basis, this contact is too long to be considered an attractive $\pi\cdots\pi$ interaction at this temperature.

Interaction **iv** in Figure S29 isn't included in the Table, because it is too long to be a significant $\pi\cdots\pi$ interaction.

Introduction to the Hirshfeld surface analyses (Figures S31-S36).

A Hirshfeld surface is the boundary surrounding a molecule in a crystal, where the electron density from the enclosed molecule is equal to that from its nearest neighbours.[12] The surface can be plotted in various ways, including interaction (or fingerprint) maps which show intermolecular distances from each atom inside the surface (d_i, i = internal) and its nearest neighbours in the lattice (d_e, e = external). These are scaled according to their distance from the Hirshfeld surface about the residue of interest.[13] Intermolecular contacts between different elements are plotted separately, chosen to highlight relevant C–H···O, C–H···π, anion···π, or O–H···O hydrogen bonding intermolecular interactions.[14]

Only data points with d_i and d_e less than the relevant Van der Waals radius are significant intermolecular contacts. Strong interactions like O–H···O hydrogen bonds afford characteristic sharp lines on the donor O···H and acceptor O···H maps, extending well below the Van der Waals radii of each element. Weaker interactions like C–H···O or anion···π appear broader in the maps, and extend only slightly below the Van der Waals radii limits. Disorder in one (or both) of the groups involved also broadens the distribution of datapoints associated with an interaction.

Separate Hirshfeld interaction maps are plotted below for cations A, B and C in the 120 K and 290 K structures. The background expansion of the lattice at the higher temperature has little effect on the Hirshfeld maps, other things being equal.[15] Hence, differences between the two temperatures are mostly a consequence of the partial SCO in molecules B and C on warming the crystal.

More detailed interpretations of the intermolecular interactions in each structure are given beside the relevant Figure.

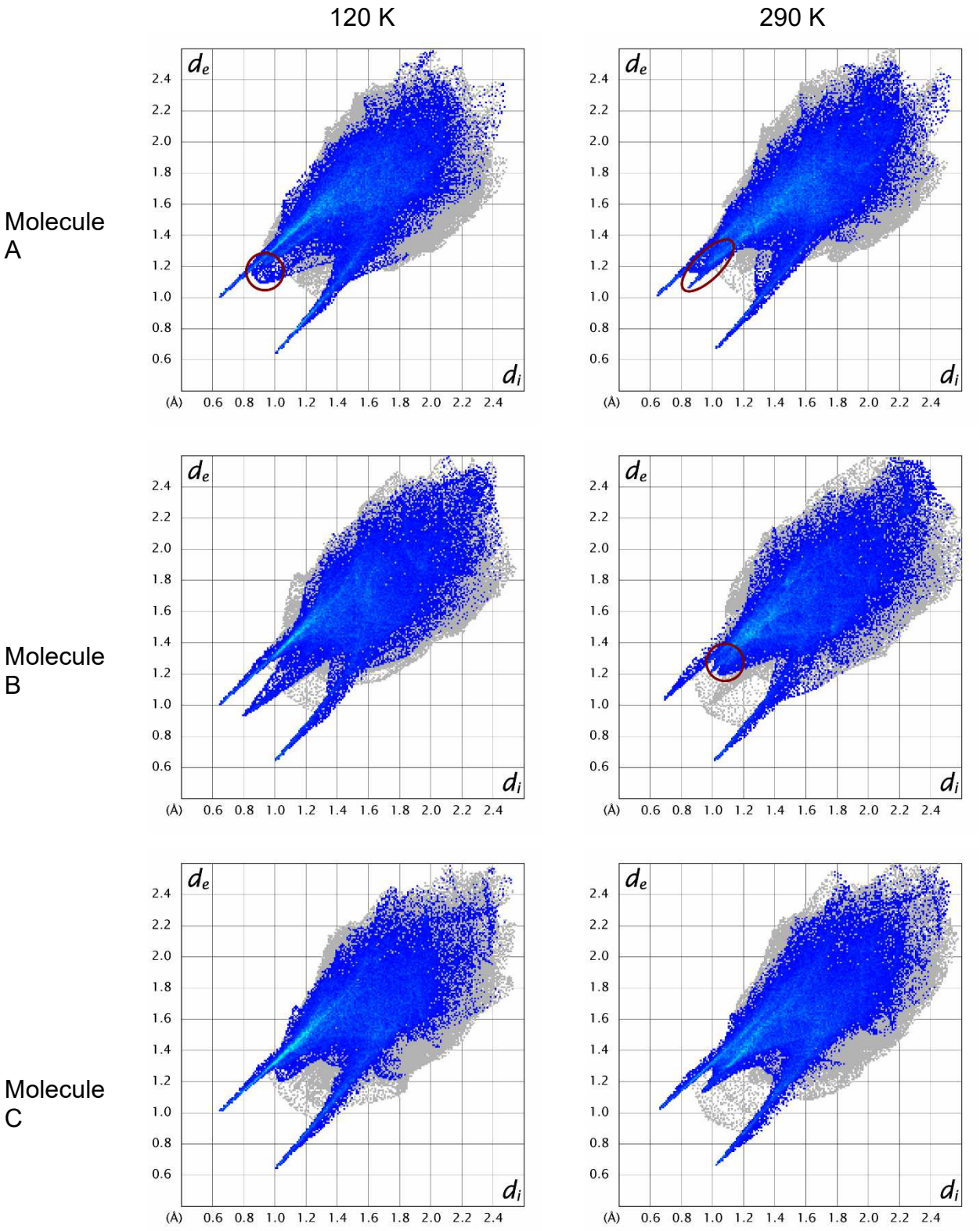

Figure S31 Hirshfeld interaction maps of $[Fe(L^6)_2][ClO_4]_2 \cdot 2MeCN$, showing intermolecular H···O contacts involving the three cation sites.

The strong O–H···O hydrogen bonds between the carboxylic acid substituents are visible as the sharp spikes of datapoints extending to short intermolecular distances. The N–H···O hydrogen bonds to perchlorate ions or ligand carbonyl groups give longer and broader distributions of H···O distances. The circled regions include hydrogen bonds to disordered anions.

Weaker C–H···O contacts between the L^6 pyrazolyl groups and ClO_4^- ions are obscured by the stronger hydrogen bonds.

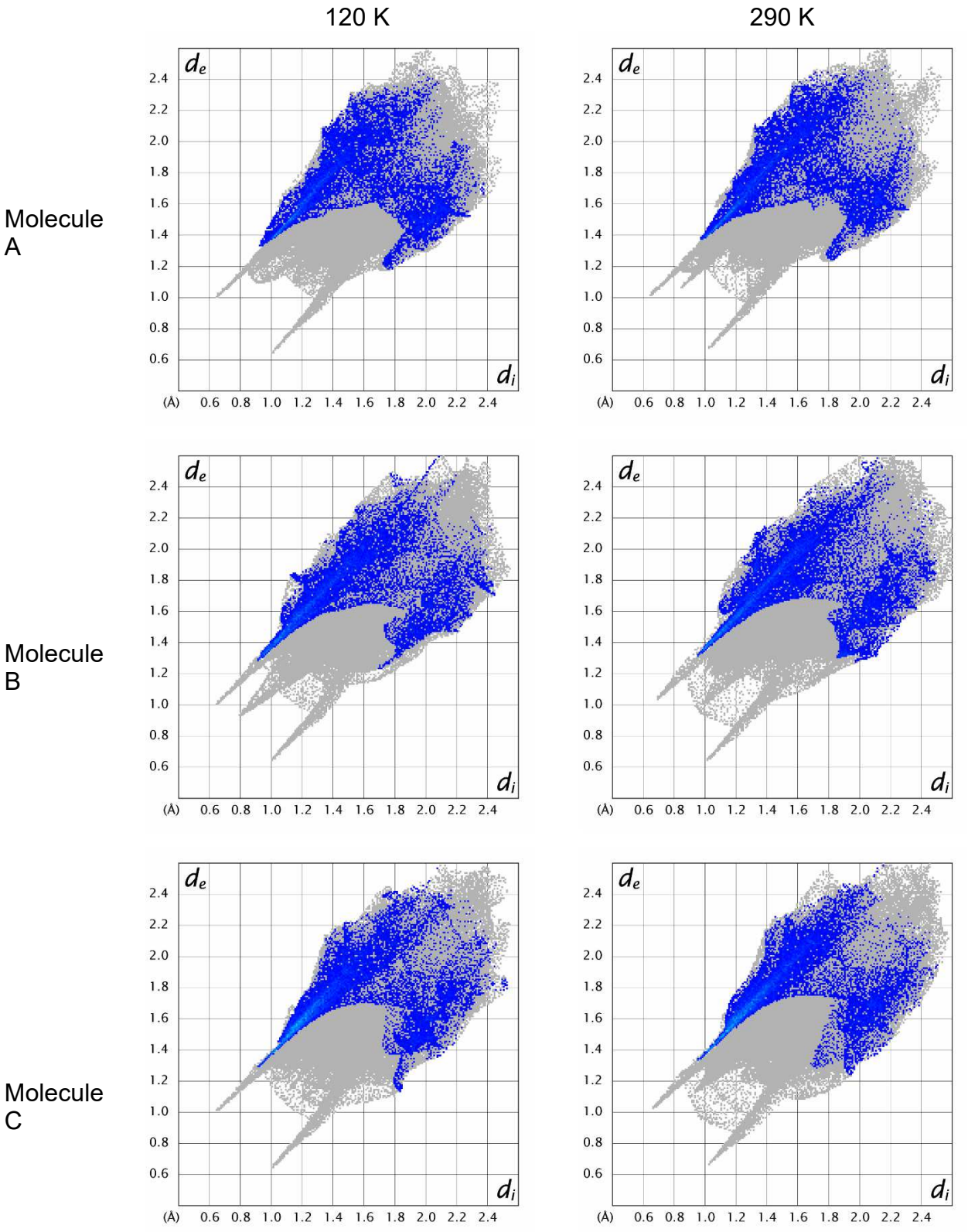

Figure S32 Hirshfeld interaction maps of $[Fe(L^6)_2][ClO_4]_2 \cdot 2MeCN$, showing intermolecular H···N contacts involving the three cation sites.

This plot highlights C–H···N contacts between the L^6 pyrazolyl *C*3 C–H groups and the MeCN molecules. Each cation donates one such interaction, which is evident as a finger of datapoints protruding towards the top left of the plot.

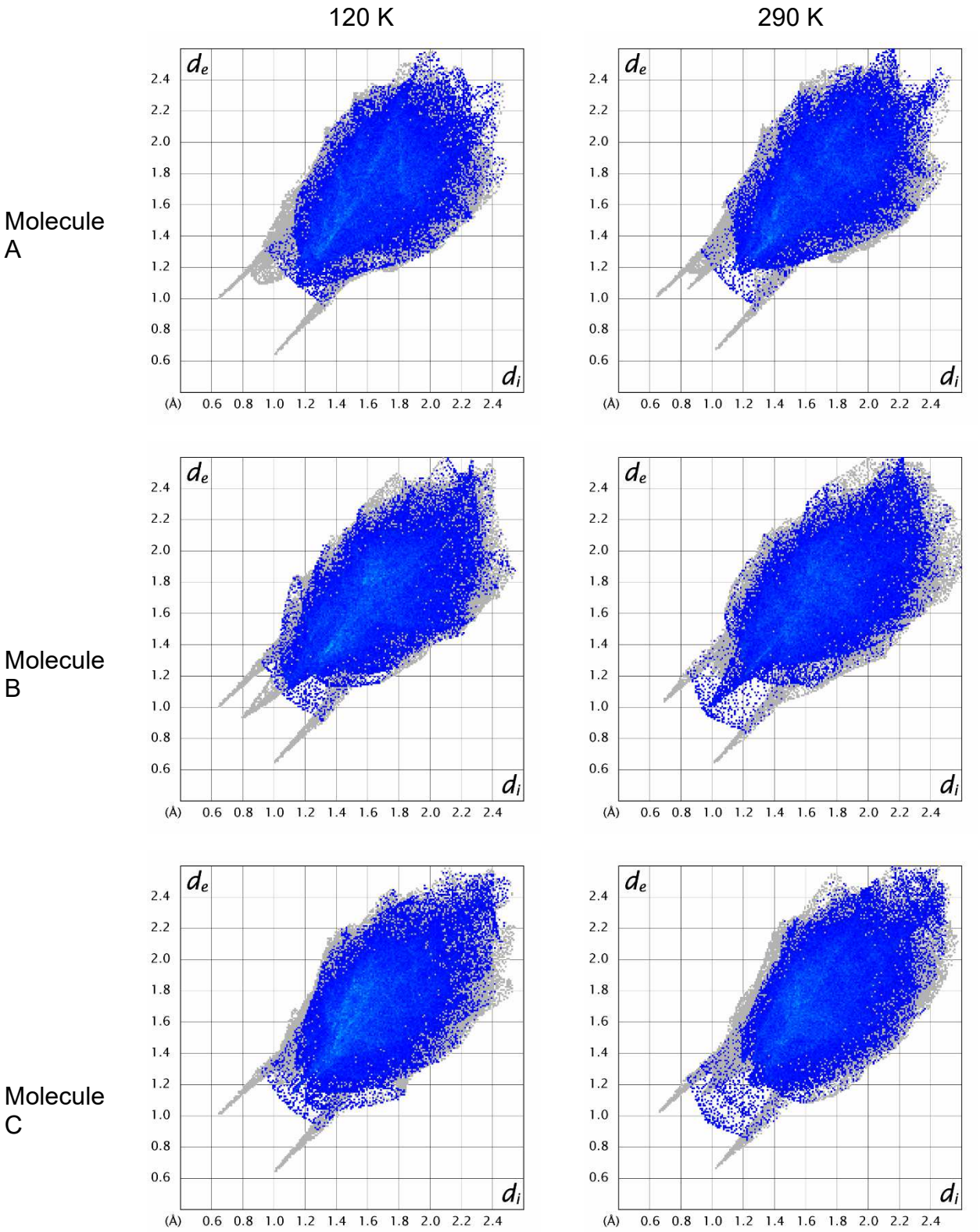

Figure S33 Hirshfeld interaction maps of $[Fe(L^6)_2][ClO_4]_2{\cdot}2MeCN$, showing intermolecular H···H contacts involving the three cation sites.

All the shortest contacts in these plots are between the two H atoms in each cyclic $R_2^2(8)$ O–H···O hydrogen bond motif, between pairs of carboxylic acid groups (Figure 4, main article).[16] That these appear shorter at 290 K simply reflects the different calculated positions for the idealised H atoms in the higher temperature refinement, and is probably an artefact.

When these are discounted, there are no short H···H contacts involving the heterocyclic ligand cores of cations A, B and C, that could obviously influence their different spin state properties.

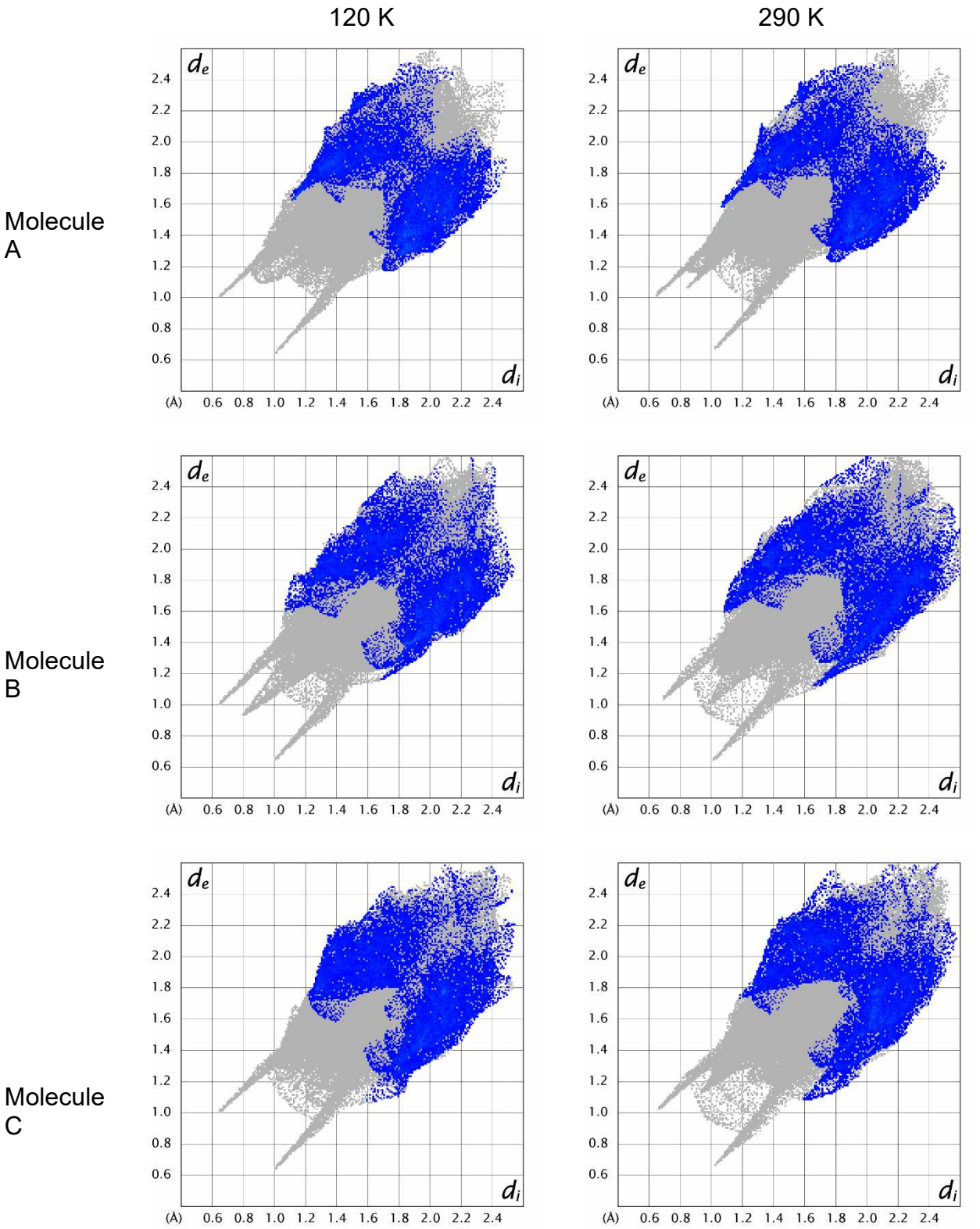

Figure S34 Hirshfeld interaction maps of $[Fe(L^6)_2][ClO_4]_2{\cdot}2MeCN$, showing intermolecular H···C contacts involving the three cation sites.

There are no intermolecular C–H···π contacts in the crystal. Rather, the shortest H···C distances for molecule A involve one of its pyrazolyl C–H groups and a MeCN molecule C atom. This is more pronounced in the 290 K structure, which could be relevant to the inhibition of SCO in this cation.

The shortest intermolecular H···C contacts for molecules B and C involve flexible propionic acid side-chains, and are unlikely to influence their SCO. All three molecules also show signatures of H···C contacts from face-to-face π···π overlap of their pyrazolyl rings.

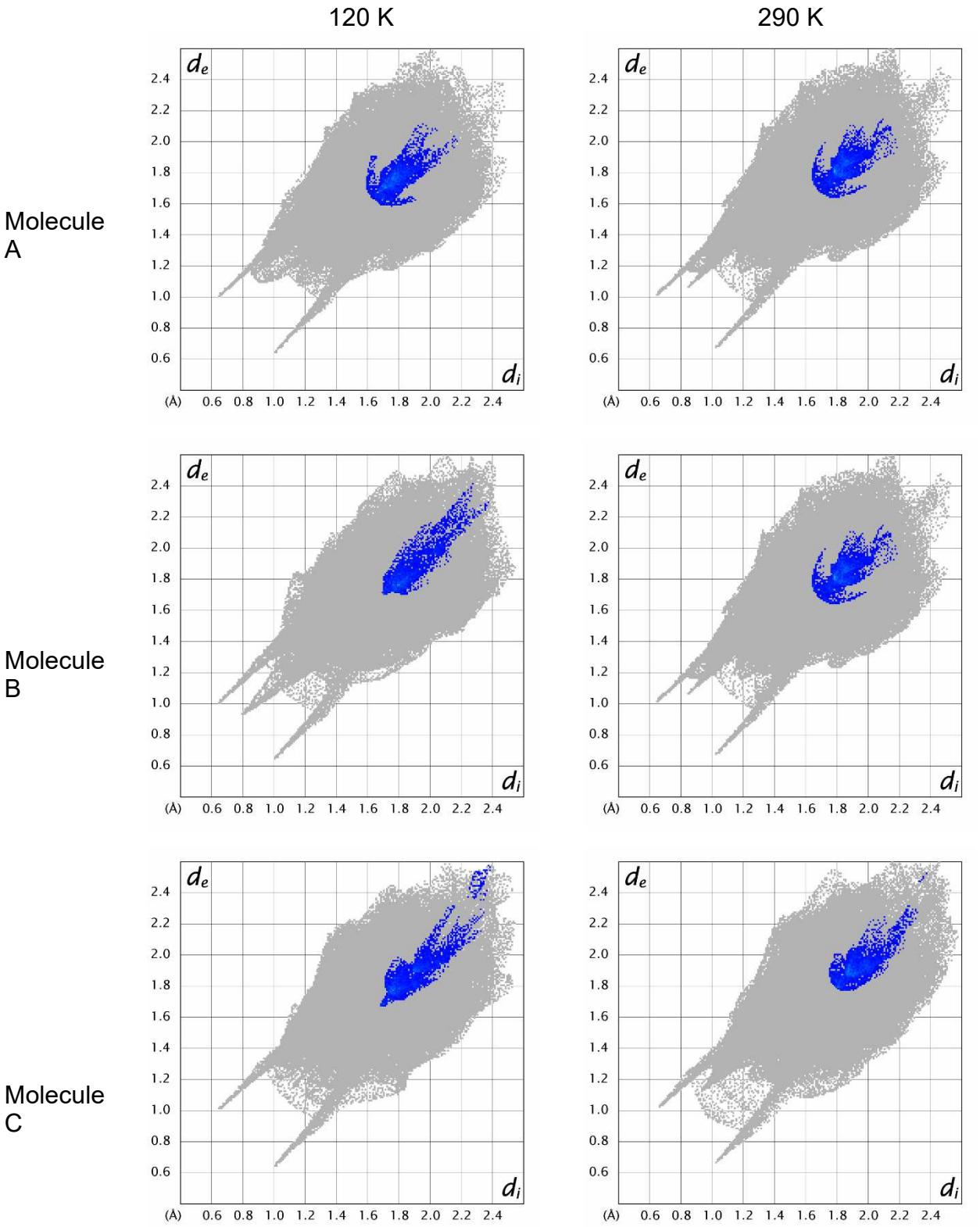

Figure S35 Hirshfeld interaction maps of $[Fe(L^6)_2][ClO_4]_2 \cdot 2MeCN$, showing intermolecular C···C contacts involving the three cation sites.

Two pyrazolyl rings from each cation experience face-to-face $\pi \cdots \pi$ overlap with nearest neighbour cations. However, the maps show these interactions are weak and unexceptional, with the rings simply being in face-to-face van der Waals contact.

One $\pi \cdots \pi$ interaction between molecules B and C is more pronounced in this plot for the low-temperature structure, where a short interplanar distance and a larger lateral offset combine to place the C atoms from the interacting rings closer together (Table S8).

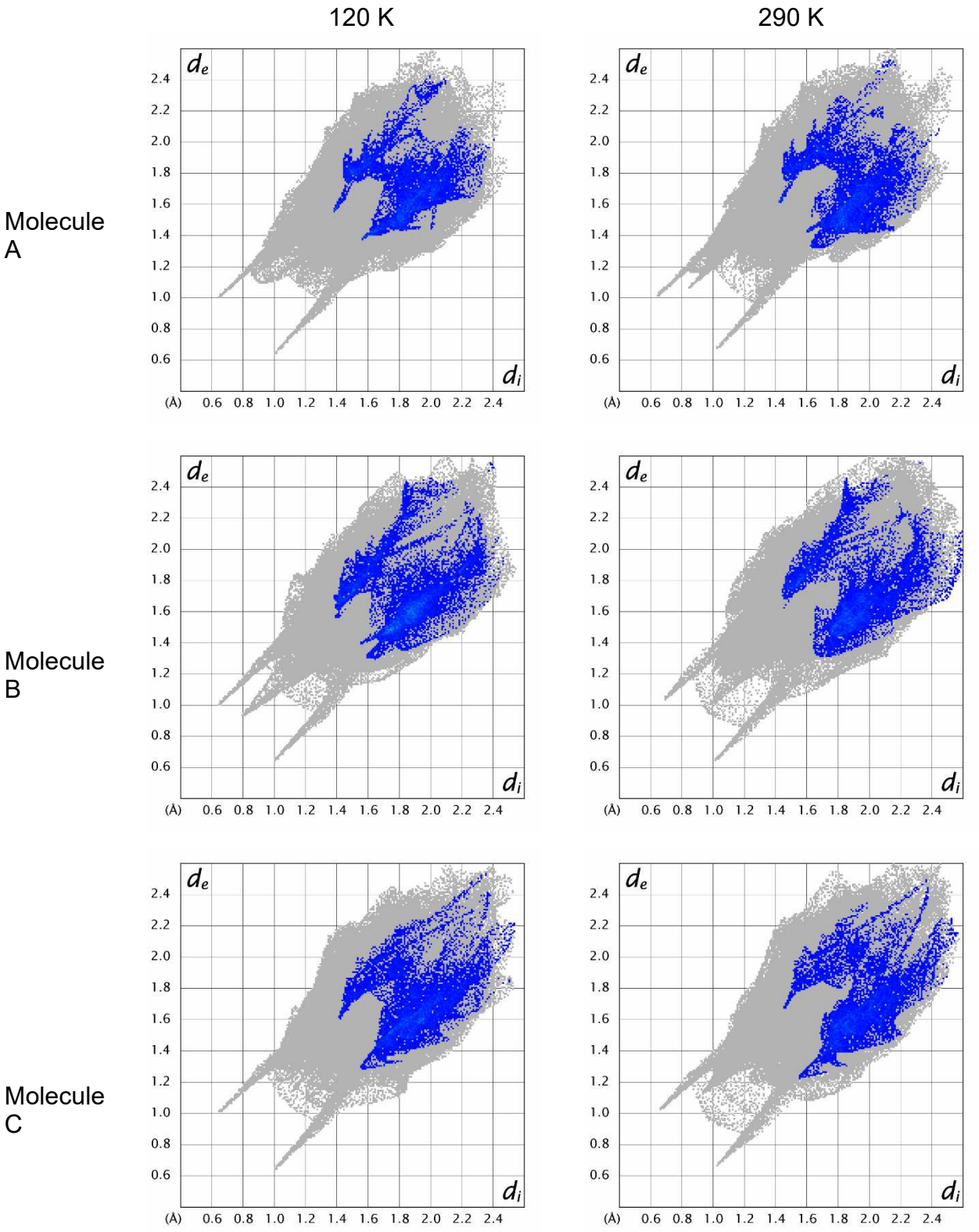

Figure S36 Hirshfeld interaction maps of $[Fe(L^6)_2][ClO_4]_2 \cdot 2MeCN$, showing intermolecular C···O contacts involving the three cation sites.

This plot was generated to highlight any anion···π contacts between cations and anions in the lattice. However, there are no noteworthy C···O contacts in the Figure.

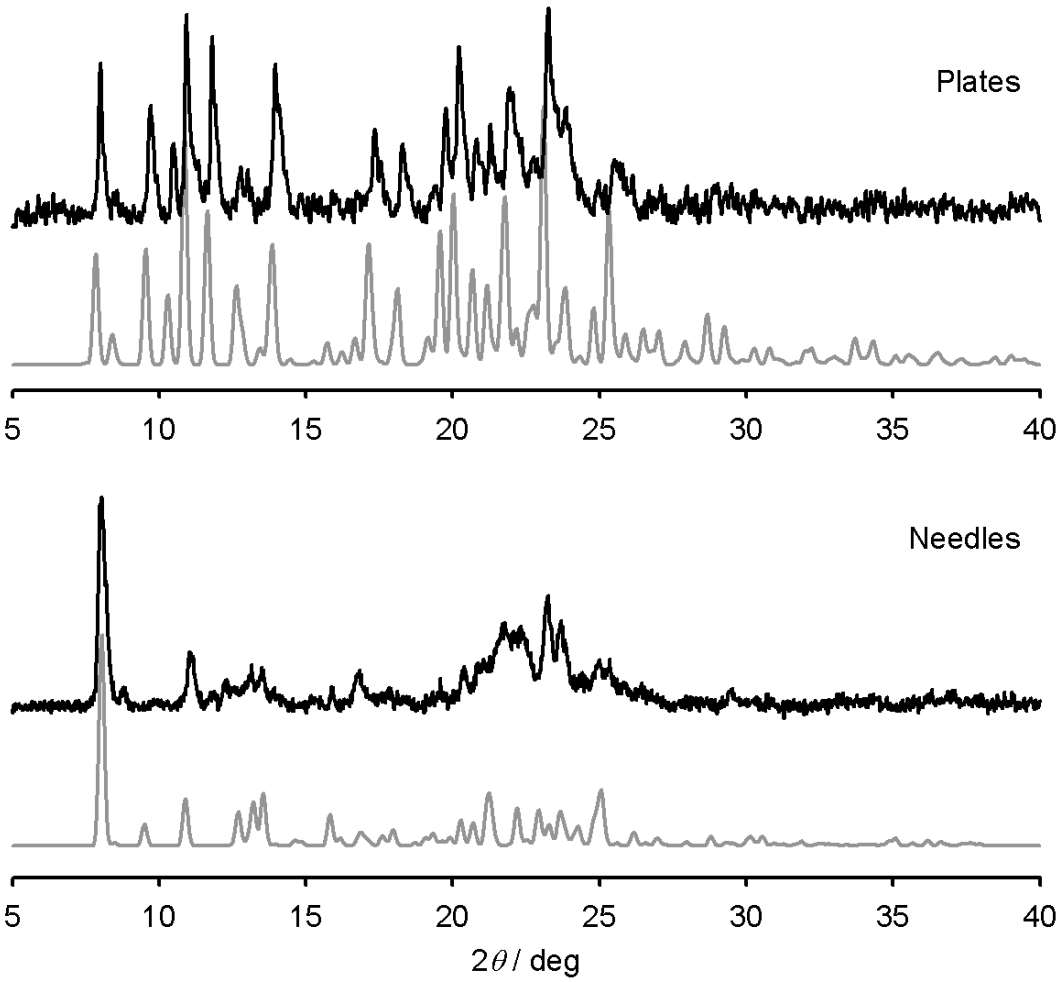

Figure S37 Measured (black) and simulated (grey) powder diffraction data for the pseudopolymorphs $[Fe(L^5)_2][ClO_4]_2$·MeCN (plates, top) and $[Fe(L^5)_2][ClO_4]_2$·*x*MeCN (needles, bottom).

The two morphologies formed together in the crystallisation vials, and were separated manually for this measurement. The simulation of the plate morphology was produced from the 330 K structure determination. The simulated powder pattern of the needle crystals is based on a preliminary structure solution of that compound (Figure S26).

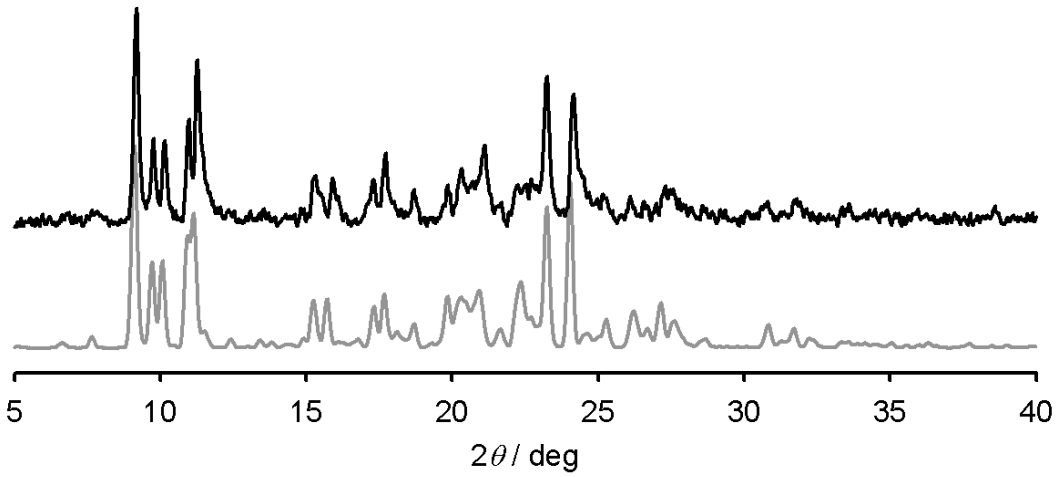

Figure S38 Measured (black) and simulated (grey) powder diffraction data for $[Fe(L^6)_2][ClO_4]_2$·2MeCN. The simulation was produced from the 290 K structure determination.

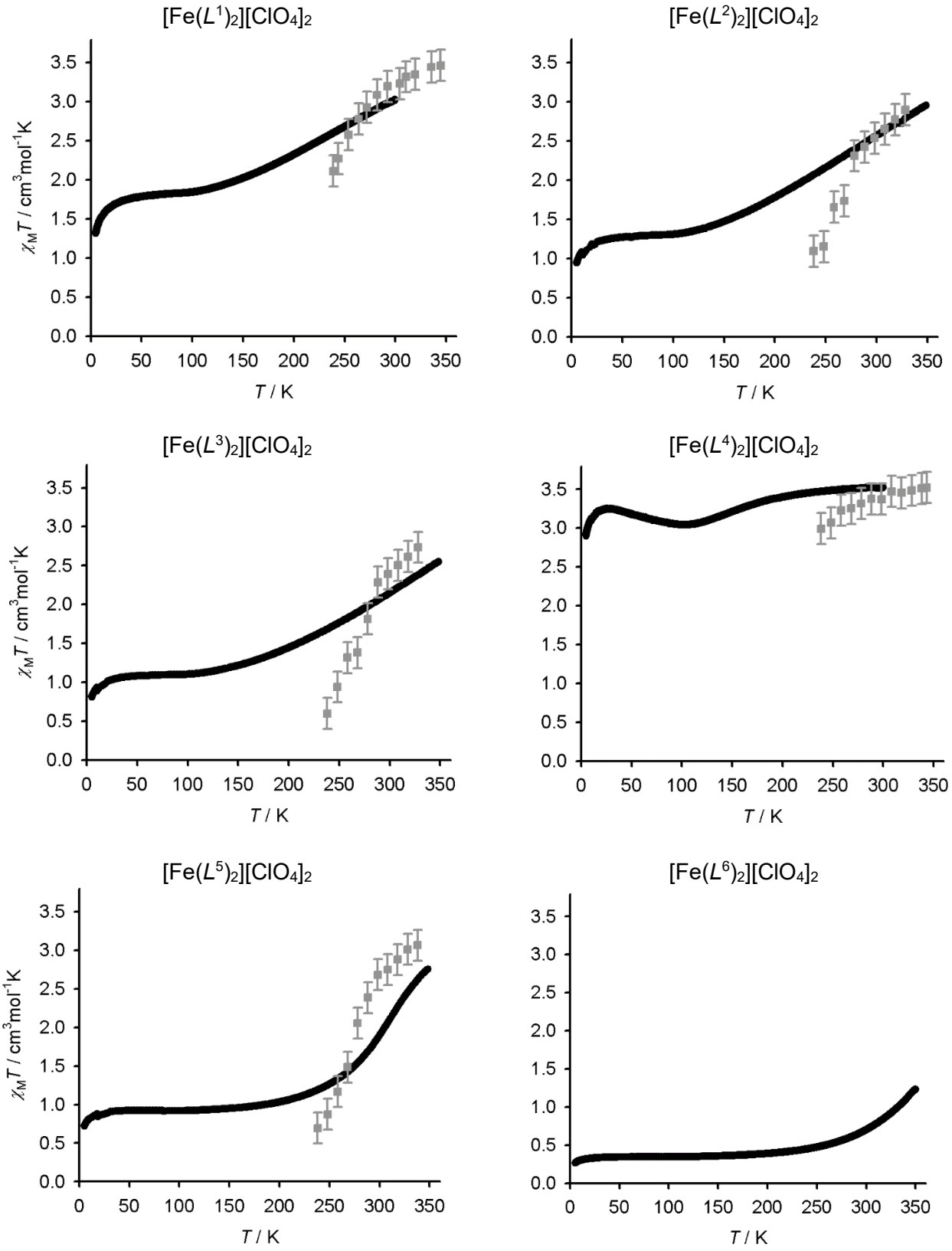

Figure S39 Solid state magnetic susceptibility data for dried samples of the complexes in this work, at a scan rate of 5 K min^{-1} (black circles). The solution magnetic data from Figure 5 (main article) are also included for comparison (grey squares). The sample of $[Fe(L^5)_2][ClO_4]_2$ was the purified, crystallographically characterised $[Fe(L^5)_2][ClO_4]_2$·MeCN pseudopolymorph of that compound (Figure S36).

The decrease in $\chi_M T$ below 30-50 K for each compound is not associated with SCO, but is caused by zero-field splitting of the residual high-spin fraction of the samples.[17] More detailed discussion of these data is given in the main article.

Table S9 Relevant σ_P and σ_P^+ Hammett parameters for the linker group substituents of the complexes in this work, taken from ref. 18. The substituent corresponding to each Hammett parameter is given in square brackets. Solution phase SCO $T_{½}$ values are also included (Figure 5, main article).

	R	σ_P	σ_P^+	$T_{½}$, K
$[Fe(L^1)_2][ClO_4]_2$	$CH_2OC(O)R'$	+0.05 [$CH_2OC(O)CH_3$]	−0.05 [CH_2OCH_3]	234 ±2
$[Fe(L^2)_2][ClO_4]_2$	$C(O)NHR'$	+0.36 [$C(O)NHCH_3$]	–[a]	269 ±3
$[Fe(L^3)_2][ClO_4]_2$	$C(O)OR'$	+0.45 [$C(O)OC_2H_5$]	+0.48 [$C(O)OC_2H_5$]	275 ±2
$[Fe(L^4)_2][ClO_4]_2$	SR'	+0.03 [SC_2H_5]	−0.60 [SCH_3]	208 ±5
$[Fe(L^5)_2][ClO_4]_2$	$C(O)NHR'$	+0.36 [$C(O)NHCH_3$]	–[a]	271 ±1

[a]There is no available σ_P^+ parameter for a carboxamido substituent.

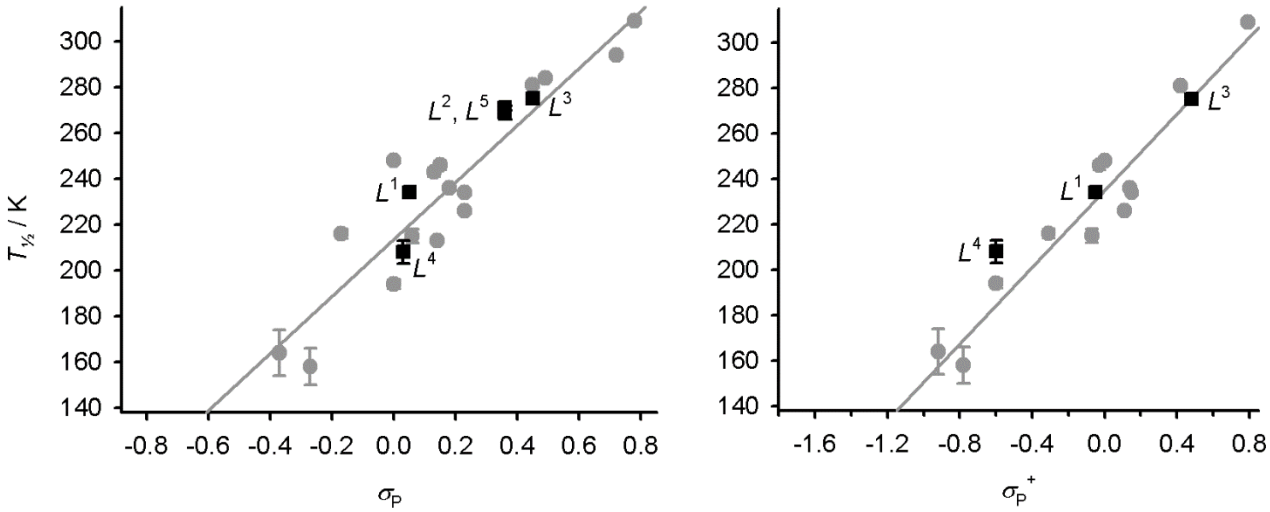

Figure S40 Correlation of the solution phase SCO temperatures with the Hammett parameters of the linker group substituents for the $[FeL_2][ClO_4]_2$ complexes (black ■; Table S9). Our previously published data points and correlations involving these parameters are shown in grey.[19]

We've previously reported a positive linear free energy relationship between $T_{½}$ and the σ_P substituent Hammett parameter in $[Fe(bpp^R)_2]^{2+}$ derivatives (left graph).[19] A significantly better correlation is found using the σ_P^+ parameter, which accounts for conjugation of 'R' with a positively charged reaction centre, in this case the Fe^{2+} ion (right graph).[19] However, σ_P^+ values have been measured for fewer substituents, which impacts this study in two ways.

First, no σ_P^+ parameter is available for carboxamido substituents,[18] so $[Fe(L^2)_2][ClO_4]_2$ and $[Fe(L^5)_2][ClO_4]_2$ can't be included in that correlation.

Second, $T_{½}$ for $[Fe(bpp^R)_2]^{2+}$ bearing sulfanyl 'R' substituents varies significantly for different sulfanyl groups, at $T_{½}$ = 194 K for R = SMe, 215 K for R = S*i*Pr and 241 K for R = S*t*Bu.[20] That couldn't be rationalised by a linear free energy plot, because σ_P^+ is only available for R = SMe (Table S9). Since $T_{½}$ for $[Fe(L^4)_2][ClO_4]_2$ is *ca.* 10 K higher than predicted by this Figure, a SMe substituent may also be a poor model for the L^4 tether group in this analysis.

In fact, $T_{½}$ for $[Fe(L^4)_2][ClO_4]_2$ (208 ±5 K) lies between $T_{½}$ for R = SMe and S*i*Pr, which is reasonable.

References

1 T. Vermonden, D. Branowska, A. T. M. Marcelis and E. J. R. Sudhölter, *Tetrahedron*, 2003, **59**, 5039; C. Klein, E. Baranoff, M. Grätzel and M. K. Nazeeruddin, *Tetrahedron Lett.*, 2011, **52**, 584; N. Bridonneau, L. Rigamonti, G. Poneti, D. Pinkowicz, A. Forni and A. Cornia, *Dalton Trans.*, 2017, **46**, 4075.

2 J. Elhaïk, C. M. Pask, C. A. Kilner and M. A. Halcrow, *Tetrahedron*, 2007, **63**, 291.

3 P. Guionneau, M. Marchivie, G. Bravic, J.-F. Létard and D. Chasseau, *Top. Curr. Chem.*, 2004, **234**, 97.

4 M. A. Halcrow, I. Capel Berdiell and R. Kulmaczewski, *Inorg. Chem.*, 2017, **56**, 8817.

5 J. K. McCusker, A. L. Rheingold and D. N. Hendrickson, *Inorg. Chem.*, 1996, **35**, 2100.

6 M. A. Halcrow, *Coord. Chem. Rev.*, 2009, **253**, 2493.

7 L. J. Kershaw Cook, R. Mohammed, G. Sherborne, T. D. Roberts, S. Alvarez and M. A. Halcrow, *Coord. Chem. Rev.*, 2015, **289–290**, 2.

8 J. M. Holland, J. A. McAllister, C. A. Kilner, M. Thornton-Pett, A. J. Bridgeman and M. A. Halcrow, *J. Chem. Soc., Dalton Trans.*, 2002, 548.

9 S. Vela, J. J. Novoa and J. Ribas-Arino, *Phys. Chem. Chem. Phys.*, 2014, **16**, 27012.

10 L. J. Kershaw Cook, F. L. Thorp-Greenwood, T. P. Comyn, O. Cespedes, G. Chastanet and M. A. Halcrow, *Inorg. Chem.*, 2015, **54**, 6319; K. S. Kumar, B. Heinrich, S. Vela, E. Moreno-Pineda, C. Bailly and M. Ruben, *Dalton Trans.*, 2019, **48**, 3825.

11 L. Pauling, *The Nature of the Chemical Bond*, 3rd edn. Cornell University Press, Ithaca NY, USA, 1960.

12 M. A. Spackman and D. Jayatilaka, *CrystEngComm*, 2009, **11**, 19.

13 J. J. McKinnon, M. A. Spackman and A. S. Mitchell, *Acta Crystallogr., Sect. B*, 2004, **60**, 627.

14 J. J. McKinnon, D. Jayatilaka and M. A. Spackman, *Chem. Commun.*, 2007, 3814.

15 R. Kulmaczewski, E. Trzop, E. Collet, S. Vela and M. A. Halcrow, *J. Mater. Chem. C*, 2020, **8**, 8420.

16 M. C. Etter, *Acc. Chem. Res.*, 1990, **23**, 120.

17 R. Boča, *Coord. Chem. Rev.*, 2004, **248**, 757.

18 C. Hansch, A. Leo and R. W. Taft, *Chem. Rev.*, 1991, **91**, 165.

19 L. J. Kershaw Cook, R. Kulmaczewski, R. Mohammed, S. Dudley, S. A. Barrett, M. A. Little, R. J. Deeth and M. A. Halcrow, *Angew. Chem. Int. Ed.*, 2016, **55**, 4327.

20 R. Kulmaczewski, M. J. Howard and M. A. Halcrow, *Dalton Trans.*, 2021, **50**, 3464.